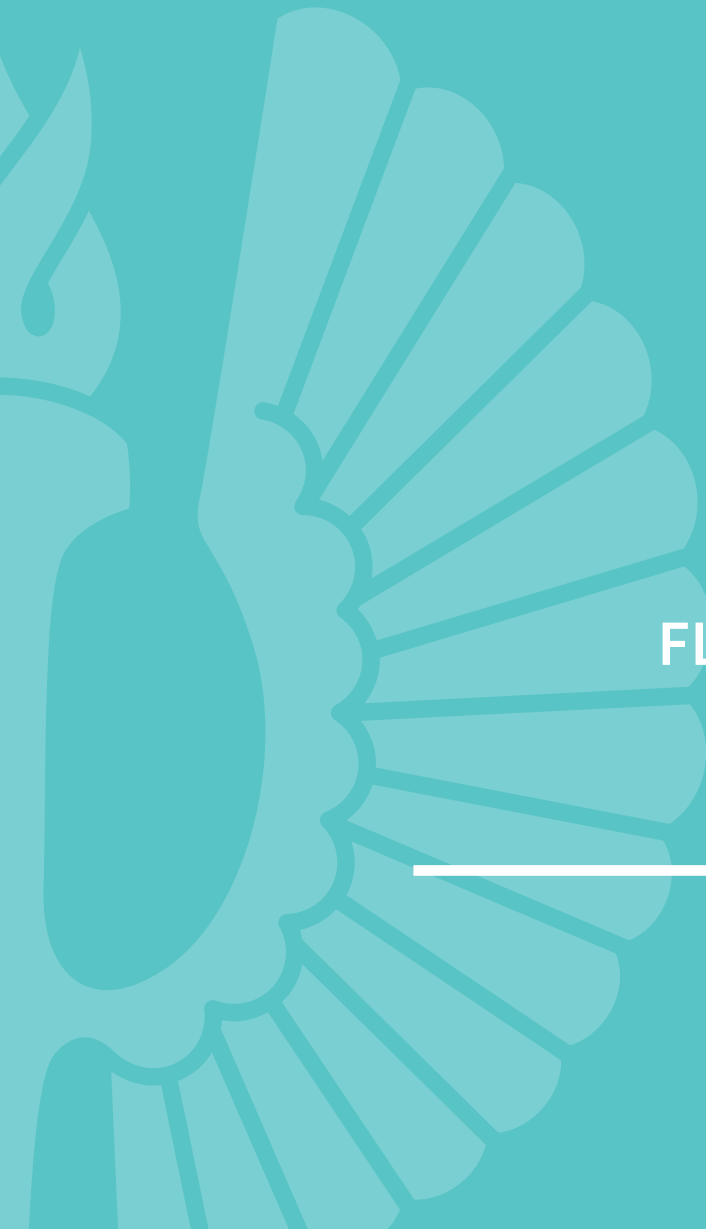




**TURUN
YLIOPISTO**
UNIVERSITY
OF TURKU

A large, stylized sunburst or fan-like graphic in a lighter shade of teal, positioned on the left side of the cover. It consists of a central oval shape with multiple curved, radiating segments extending to the right.

FLUORESCENT AND ¹⁹F PROBES FOR METAL-MEDIATED BASE PAIRING

Asmo Aro-Heinilä



**TURUN
YLIOPISTO**
UNIVERSITY
OF TURKU

FLUORESCENT AND ¹⁹F PROBES FOR METAL-MEDIATED BASE PAIRING

Asmo Aro-Heinilä

University of Turku

Faculty of Science
Department of Chemistry
Laboratory of Organic Chemistry and Chemical Biology
Doctoral programme in Exact Sciences

Supervised by

Assoc. Professor Tuomas Lönnberg
Department of Chemistry
University of Turku
Turku, Finland

Professor Pasi Virta
Department of Chemistry
University of Turku
Turku, Finland

Reviewed by

Professor, Michal Hocek
Institute of Organic Chemistry and
Biochemistry
Academy of Sciences of the Czech
Republic, Prague, Czech Republic

Professor, Frank Seela
Institute für Chemie
University of Osnabrück,
Osnabrück, Germany

Opponent

Professor, Ronald Micura
Department of Organic Chemistry
University of Innsbruck
Innsbruck, Austria

The originality of this publication has been checked in accordance with the University of Turku quality assurance system using the Turnitin OriginalityCheck service.

ISBN 978-951-29-8783-2 (PRINT)
ISBN 978-951-8784-9 (PDF)
ISSN 0082-7002 (Print)
ISSN 2343-3175 (Online)
Painosalama, Turku, Finland 2022

Dedicated to my beloved father

UNIVERSITY OF TURKU
Faculty of Science
Department of Chemistry
Laboratory of Organic Chemistry and Chemical Biology
Bioorganic Chemistry Group
ASMO ARO-HEINILÄ: Fluorescent and ^{19}F NMR Probes for Metal-Mediated Pairing
Doctoral Dissertation, 122 pp.
Doctoral Programme in Exact Sciences
February 2022

ABSTRACT

Research on metal-mediated base pairing has proceeded rapidly during the last decades, and metal-mediated base pairs have become one noteworthy option for developing new DNA-based biological or nanotechnological applications. Many metal ions can bind between specific mismatches and increase thermal stability of the secondary structures of nucleic acids. Metal-mediated base pairs between canonical or artificial nucleobases have been studied extensively. Often, UV or CD spectroscopy techniques have been used to study the global effects of metal-mediated base pairs on secondary structures. More detailed information on the local environment of metal-mediated base pairs can be achieved by ^{15}N NMR or crystallization of metallated oligonucleotides. However, the need for expensive ^{15}N -labeled nucleotides and complex production of the crystals of metallated oligonucleotides are drawbacks of these methods. Instead, fluorescent or ^{19}F -labeled nucleobase analogs would offer an easier way to examine local interactions of metal-mediated base pairs in oligonucleotides.

In the present work, fluorescent and ^{19}F NMR probes were developed. Fluorescent probes were used for screening potential molecules for metal-mediated base pairing and detection of single nucleotide polymorphism. ^{19}F NMR probes were developed to evaluate the local environment of metal-mediated base pairs. Fluorine-labeled nucleobase analogs were synthesized, incorporated into the oligonucleotide and mercurated. Hybridization of the mercurated oligonucleotides were evaluated by ^{19}F NMR spectroscopy and UV melting temperature analysis. Results showed increased stability of the duplexes with different opposite nucleobases, and ^{19}F -labeled analog allowed discrimination of nucleobases by UV and ^{19}F NMR. One ^{19}F -labeled nucleotide was incorporated into fluorescent molecular beacon system for the detection of single nucleotide polymorphism.

KEYWORDS: fluorescent probe, ^{19}F NMR probe, metal-mediated base pairing, single nucleotide polymorphism

TURUN YLIOPISTO

Matemaattis-Luonnontieteellinen tiedekunta

Kemian laitos

Orgaanisen kemian ja kemiallisen biologian laboratorio

Bio-orgaanisen kemian tutkimusryhmä

ASMO ARO-HEINILÄ: Fluoresoivat ja ^{19}F NMR koettimet metallivälitteisen emäspariutumiseen

Väitöskirja, 122 s.

Eksaktien tieteiden tohtoriohjelma

helmikuu 2022

TIIVISTELMÄ

Metallivälitteisen emäspariutumisen tutkimus on ottanut huimia askeleita lähivuosisikymmeninä, ja metallivälitteisistä emäsparista on tullut yksi varteen-otettava vaihtoehto kehittää DNA-pohjaisia biologisia ja nanoteknologian sovelluksia. Monet metalli-ionit kykenevät sitoutumaan tiettyjen nukleoemästen väliin ja kasvattamaan DNA:n sekundaarirakenteiden pysyvyyttä. Metallivälitteistä emäspariutumista on tutkittu sekä luonnollisten että keinotekkoisten nukleoemästen välillä kattavasti. Yleensä metallivälitteisten emäsparien kokonaisvaikutuksia sekundaarirakenteeseen on tutkittu UV-sulamislämpötilamittauksilla ja CD spektroskopiolla. Tarkempaa tietoa metallivälitteisten emäsparien paikallisesta ympäristöstä saadaan ^{15}N -NMR spektroskopiolla ja kiteyttämällä metalloituja oligonukleotideja. Kuitenkin ^{15}N -leimatuiden nukleotidien kallis hinta ja metalloitujen oligonukleotidien haastava kiteyttäminen ovat haittapuolina näillä menetelmillä. Sen sijaan fluoresoivat ja ^{19}F -leimatut nukleoemäsjohtannaiset mahdollistavat helpomman tavan tutkia metallivälitteisten emäsparien paikallisia vuorovaikutuksia.

Väitöskirjatyössä kehitettiin fluoresoivia ja ^{19}F -NMR koettimia. Fluoresoivia koettimia käytettiin metallivälitteiseen emäspariutumiseen kykenevien molekyylien seulomiseen ja yksittäisen nukleoemästen monimuotoisuuden tunnistamiseen. ^{19}F -NMR koettimia kehitettiin metallivälitteisten emäsparien lähiympäristön tutkimiseen. Fluorileimattuja nukleoemäsjohtannaiset syntetisoitiin, liitettiin oligonukleotideihin ja merkuroitiin. Merkuroitujen oligonukleotidien hybridisaatiota arvioitiin ^{19}F -NMR spektroskopiolla ja UV sulamislämpötilamittauksilla. Tuloksista havaittiin kasvaneet dupleksien pysyvyydet eri vastinemäksillä, ja ^{19}F -leimatut koettimet mahdollistivat nukleoemästen tunnistamisen sulamisprofiileista UV:lla ja ^{19}F -NMR:llä. Yksi ^{19}F -leimattu nukleotidijohdannainen liitettiin fluoresoivaan molekulaariseen beacon systeemiin yksittäisten emästen monimuotoisuuden tunnistamista varten.

ASIASANAT: Fluoresoiva koetin, ^{19}F NMR koetin, metallivälitteinen emäspariutuminen, yhden emäksen monimuotoisuus

Table of Contents

Abbreviations	8
List of Original Publications	10
1 Introduction.....	11
1.1 Metal-mediated base pairs between canonical nucleobases ..	13
1.1.1 T-Hg ^{II} -T base pairing	13
1.1.2 C-Ag ^I -C base pairing	18
1.1.3 Other Hg ^{II} - and Ag ^I -mediated base pairs between canonical nucleobases	21
1.2 Nucleobase analogs for metal-mediated base pairing with canonical nucleobases	25
1.2.1 Fluorescent nucleobase analogs for the metal- mediated base pairs	25
1.2.2 Organometallic nucleobases for the metal-mediated base pairing	27
1.2.3 Nucleobase analogs discriminating canonical nucleobases via metal-mediated base pairing	30
1.3 Incorporation of metal-mediated base pairs into oligonucleotides	31
1.4 Applications and potential of the metal-mediated base pairs ..	33
1.4.1 Construction of nucleic acid structures via metal- mediated base pairing	33
1.4.2 Detection of single nucleotide polymorphisms	36
1.4.3 Therapeutic and diagnostic potential of metal- mediated base pairing	38
2 Aims of thesis	39
3 Results and Discussion	41
3.1 Probing molecules capable of metal-mediated base pairing at monomer level.....	41
3.1.1 Synthesis of the fluorescent oligonucleotide probes	42
3.1.2 Fluorescence measurements	42
3.2 Recognition of metal-mediated base pairing by ¹⁹ F NMR	45
3.2.1 Synthesis of the mercurated oligonucleotides	47
3.2.1.1 Synthesis of the Phosphoramidite building block F and F3	47
3.2.1.2 Oligonucleotide synthesis	47

3.2.2	Hybridization studies of the mercurated oligonucleotides.....	52
3.2.2.1	Melting temperature analysis of ON(F-Hg) and ON(F3-Hg).....	52
3.2.2.2	Evaluation of thermodynamic parameters.....	55
3.2.3	CD spectropolarimetric analysis of ON(F-Hg) and ON(F3-Hg)	56
3.2.4	¹⁹ F NMR measurements.....	57
3.2.4.1	¹⁹ F NMR of ON(F-Hg) and ON(F3-Hg) duplexes.....	57
3.2.4.2	Temperature elevated measurements.....	62
3.3	Recognition of SNPs by F-Hg.....	64
3.3.1	Synthesis of Beacon(F).....	64
3.3.2	Evaluating the potential of F-Hg as an SNP probe.....	66
3.3.3	Fluorescence measurements of B(F-Hg).....	67
3.3.4	Temperature-elevated fluorescence measurements.....	69
4	Conclusions	72
5	Experimental methods.....	74
5.1	General methods.....	74
5.2	Oligonucleotide synthesis.....	74
5.3	UV melting temperature studies.....	75
5.4	¹⁹ F NMR measurements.....	75
5.5	CD spectropolarimetric measurements.....	76
5.6	Fluorescence measurements.....	76
5.7	Enzymatic digestion.....	76
	Acknowledgements	77
	References	79

Abbreviations

A	adenine
ATP	adenosine triphosphate
C	cytosine
CD	circular dichroism
CTP	cytidine triphosphate
DCM	dichloromethane
DBCO	dibenzocyclooctyne
DMF	<i>N,N</i> -dimethylformamide
DNA	deoxyribonucleic acid
EDTA	ethylenediaminetetraacetic acid
ESI-MS	electrospray ionization mass spectrometry
FAM	fluorescein
G	guanine
GTP	guanosine triphosphate
HPLC	high performance liquid chromatography
ITC	isothermal titration calorimetry
KF	Klenow fragment
KF ^{exo} -	3'→5' exonuclease deficient Klenow fragment
MeC	5-methylcytosine
MeCTP	5-methylcytidine triphosphate
miRNA	microRNA
NHS	<i>N</i> -hydroxysuccinimide
NMR	nuclear magnetic resonance
NOE	nuclear overhauser effect
NOESY	nuclear overhauser effect spectroscopy
NTP	nucleoside triphosphate
ON	oligonucleotide
PCR	polymerase chain reaction
PNA	peptide nucleic acid
PyC	pyrrolo-C
RNA	ribonucleic acid

RP-HPLC	reversed-phase high performance liquid chromatography
SNP	single nucleotide polymorphism
SPAAC	strain-promoted azide-alkyne cycloaddition
T	thymine
T_m	melting temperature
Taq	a thermostable DNA polymerase I
TBDMS	<i>tert</i> -butyldimethylsilyl
TEAA	triethylammonium acetate
THF	tetrahydrofuran
TOF	time-of-flight
TTP	thymidine triphosphate
UV	ultraviolet
WC	Watson-Crick

List of Original Publications

This dissertation is based on the following original publications, which are referred to in the text by their Roman numerals:

- I Aro-Heinilä, A., Lönnberg, T., Fluorescent Oligonucleotide Probes for Screening High-Affinity Nucleobase Surrogates, *Chemistry – A European Journal*, 2017, 5, 1028–1031.
- II Aro-Heinilä, A., Lönnberg, T., Virta, P., 3-Fluoro-2-mercuri-6-methylaniline Nucleotide as a High-Affinity Nucleobase-Specific Hybridization Probe, *Bioconjugate Chemistry*, 2019, 8, 2183–2190.
- III Aro-Heinilä, A., Lönnberg, T., Virta, P., Covalently Mercuroated Molecular Beacon for Discriminating the Canonical Nucleobases, *ChemBioChem*, 2021, 22, 354–358.
- IV Aro-Heinilä, A., Lepistö, A., Äärelä, A., Lönnberg, T., Virta, P., 2-trifluoromethyl-6-mercurianiline nucleotide; a sensitive ¹⁹F NMR probe for Hg(II)-mediated base pairing, *J. Org. Chem*, 2022, 1, 137–146.

The original publications have been reproduced with the permission of the copyright holders.

1 Introduction

Many cellular biochemical processes depend on the presence of metal ions such as K^+ , Na^+ and Mg^{2+} .^[1,2] For example, metal ions participate in biochemical processes such as replication, transcription and translation, steps that are essential for the transfer of genetic information. Typically, the concentrations of many other metals like transition metals are very low in the cells, causing only minor effects on nucleic acid structures and functions. On the other hand, an increased amount of metal ions can lead to errors in the biochemical processes by crosslinking, degradation, stabilization or destabilization and replacing the hydrogen bonding of Watson–Crick (WC) base pairing in nucleic acid structures. Thus, the diverse interactions of metal ions with nucleic acids make them an important target of study.

A starting point was the revealing of the structure of the double-helical DNA in 1953.^[3] Actually, even before in the same decade, in 1952, the first evidence of interactions between nucleobases and mercury ions^[4,5] was discovered. Ten years later, similar interactions were observed in DNA duplex^[6], and the interactions with other metal ions (Ag^I , Cu^{II} , Zn^{II} , etc.) were examined in the 1960s.^[7–10] However, detailed knowledge of the coordination of metal ions in DNA structures remained still unknown in DNA structures.

Polynucleotides offer multiple attractive binding positions for metal ions, such as the negatively charged phosphate backbone and the nitrogen and oxygen atoms of nucleobases.^[11–14] Indeed, the backbone of the double-helical DNA is stabilized by metal ions.^[2,11] The binding of metal ions on the phosphate backbone is unspecific, but it stabilizes the double-helical oligonucleotide by neutralizing negatively charged oxygens of the phosphate groups. Metal ions can also coordinate to more specific binding sites in nucleobases such as endocyclic and exocyclic nitrogen atoms and exocyclic oxygen atoms.^[11,14–17] Depending on metal preferences, the binding positions vary. According to Hard and Soft Acid and Base (HSAB) theory, soft metal ions prefer binding to softer donors as nitrogens of nucleobases, and hard metal ions tend to bind to harder donors as phosphates or oxygens of nucleobase. Possible binding sites are N1 or N7 of purine and N3 of pyrimidine nucleosides, but also the exocyclic amino and carbonyl groups. C5 carbons of cytidine and uridine are prone to mercurate and are thus possible binding sites (Figure 1).^[18]

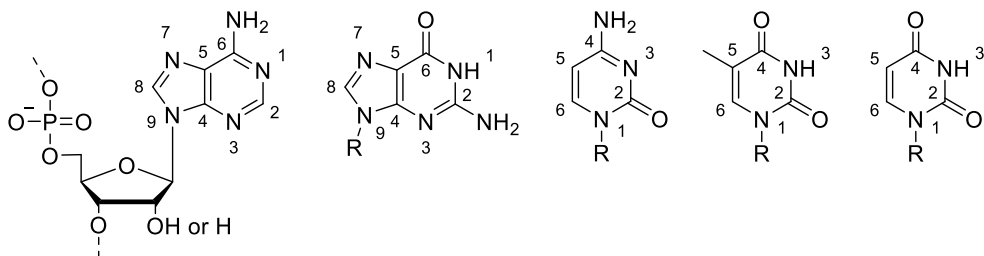


Figure 1. Canonical nucleotides: adenosine, guanosine, cytidine, thymidine and uridine. R denotes ribose or deoxyribose.

Normally, canonical nucleobases pair with each other by obeying the rules of Watson-Crick base pairing; adenine pairs with thymine, and cytosine pairs with guanine. Instead, in metal-mediated base pairing, a metal ion coordinates between two nucleobases through a coordination bond (Figure 2). Early studies of the interactions between mercury ions and nucleic acids were most likely associated with the mercury-mediated base pairing. The mercury ion was supposed to coordinate between thymines,^[4–6,19–24] but in oligonucleotides the direct evidence of exact mercury coordination between thymines was lacking. It took more than 50 years before the first direct evidence of the coordination sphere was revealed by Tanaka *et al.* Mercury ion was coordinated between N3s of thymines to form a T(N3)-Hg-T(N3) basepair.^[25] The discovery of the “extraordinary” formation of T-Hg^{II}-T and C-Ag^I-C base pairs started the hype around the field, and these two are, without doubt, the most extensively studied metal-mediated base pairs.^[26–36] Also, many artificial nucleobases have been developed to enhance metal-mediated base pairing with natural or artificial nucleobases.^[37–43] In an optimal scenario, the geometry of a metal-base pair would mimic that of normal WC pairs, thus not disturbing the normal secondary structure of nucleic acids. As for the double-helical system, the optimal coordination geometry of the formed metal-mediated base pair should be either linear or planar to not to disrupt the helical structure of nucleic acid. However, in some cases, other types of geometries/topologies are possible, and actually, metal-mediated pairs can induce the formation of different higher-order structures (see chapter 1.4.1). The site-specific formation of metal-mediated base pairs offers possibilities to develop applications such as sensors, nanowires, nanodevices, expanding genetic code, different DNA-based structures and biological applications such as detecting single nucleotide polymorphisms (SNPs).^[28,32]

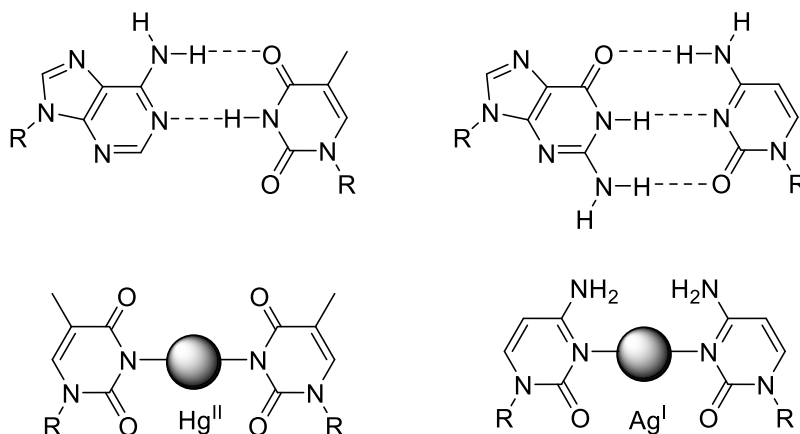


Figure 2. Watson-Crick base pairing and Hg^{II} - and Ag^{I} -mediated base pairing. R denotes deoxyribose or ribose.

1.1 Metal-mediated base pairs between canonical nucleobases

Metal-mediated base pairing in oligonucleotides containing only canonical nucleotides is the easiest way to examine the effects of metal ions in nucleic acids. The advantages are well-known and straightforward oligonucleotide synthesis protocols and commercial availability compared to artificial nucleosides. The most studied metal pairs are T- Hg^{II} -T and C- Ag^{I} -C, forming between the mismatches of two thymines and two cytosines, respectively (Figure 2). In addition to these two, other metal pairs are possible between different canonical nucleobases (*e.g.* C- Hg^{II} -T, G- Ag^{I} -G and G- Ag^{I} -C pairs) but are not as comprehensively studied. Therefore, other base pairs are described briefly to underline the versatility and potential of metal-mediated base pairs in nucleic acid structures.

1.1.1 T- Hg^{II} -T base pairing

The most studied metal ion in respect of metal-mediated base pairing is Hg^{II} . The first pieces of evidence of interactions of Hg^{II} with thymine were observed at a monomer level in the 1950s^[5] and a decade later, T- Hg^{II} -T base pairs were suggested to form in an A-T rich double-helical DNA by a strand slippage mechanism.^[6] Crystal structure of 1:2 Hg^{II} -1-methylthymine complex was determined to support the binding of mercury ion between N3s.^[44] NMR studies of the binding site indicated similar binding as the resonance signals of imino protons in the ^1H NMR spectrum disappeared after adding Hg^{II} ions, and carbon resonance signals of carbonyls C2 and C4 of thymine were shifted $\sim 2,5$ ppm downfield in the ^{13}C NMR spectrum.^[22] In an oligomer, the first direct confirmation of T- Hg^{II} -T base pair

formation between N3s was observed by ^{15}N NMR using ^{15}N 3 labeled thymines. ^{15}N - ^{15}N J-coupling through N3-Hg^{II}-N3 bond was detected, and the J_{NN} coupling constant was much smaller (2.4 Hz) compared to A-T Watson-Crick pair ($\sim 7\text{--}6$ Hz) (Figure 3).^[25] Significant changes in chemical shifts were observed by ^{15}N NMR, which showed approximately 30 ppm downfield shift for N3 of thymine.^[25,45] This binding mode in oligomers was also supported by Raman spectroscopy^[46] and theoretical calculations.^[46]

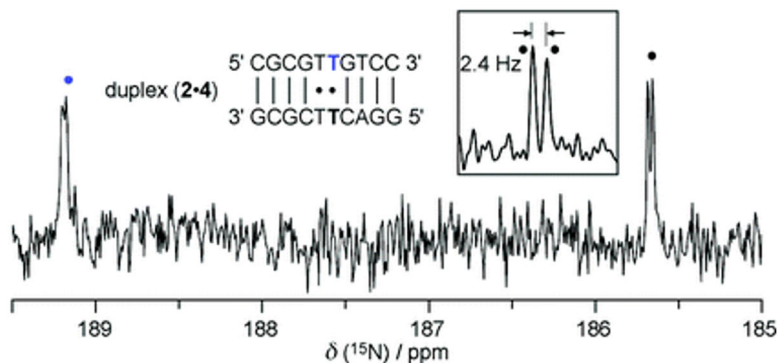


Figure 3. ^{15}N NMR spectrum of the duplex containing two T-Hg^{II}-T pairs. Reprinted with permission from *J. Am. Chem. Soc.* 2007, 129, 2, 244–245. Copyright 2007 American Chemical Society.^[25]

The three-dimensional solution^[47] and crystal structures^[48] of short metallo-oligonucleotides, containing two consecutive T-Hg^{II}-T pairs, have been determined by NMR spectroscopy and X-ray crystallography, respectively (Figure 4). Based on the constraints of interatomic distances from the NOESY spectra, the geometry of the solution structure was optimized, and the lowest energy structure maintained the B-type helix.^[47] From the crystal structure, the distance of N3s and Hg^{II} was determined to be 2.0 Å, suggesting the removal of the imino protons of N3. Similar distance has been observed by experimental and theoretical methods with the 1:2 thymidine: mercury complexes.^[44,49,50] Considerable twist angles between thymidines through N3-Hg^{II}-N3 bonds were observed (-22° and -20°) compared to WC pairs which are almost planar (-1°).^[48] A larger twist angle can occur because only one bond is formed between nucleobases, and repulsion between carbonyl groups can be minimized. Crystal and solution structures both showed ~ 1 Å shorter distance between the anomeric carbons of the sugar moieties than in typical B-type duplexes.^[47,48] Despite these minor differences, the global conformation of the metallated duplex was close to that of a corresponding oligonucleotide containing only WC base pairs. In addition, the short distance between mercury ions (3.3 Å in

crystal structure and ~ 4 Å in solution structure) inside the DNA duplex suggests stabilizing metallophilic attraction.^[49,51] Metallophilic interactions between closed d-shell ions/atoms such as Hg^{II}, Ag^I, Au^I, Pt^{II} and Tl^I have been distinguished in many previous studies.^[52–54] As a conclusion of structure determination, the results on crystal and solution structures corroborate each other, giving a solid background of understanding these structures. Detailed data from the three-dimensional structures obtained by NMR and X-ray crystallography is essential for applications and the development of metallo-DNAs.

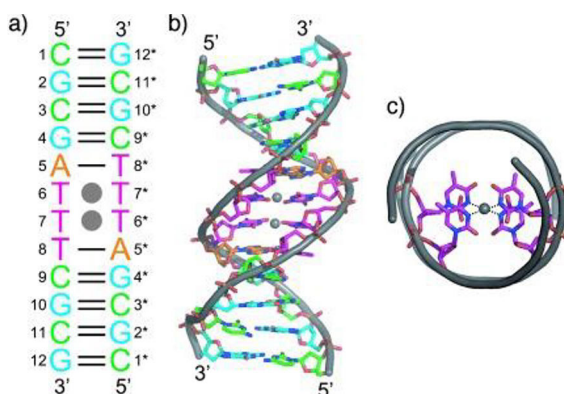


Figure 4. Crystal structure of the 12mer DNA duplex containing two consecutive T-Hg^{II}-T pairs. Reprinted with permission from J. Kondo, T. Yamada, C. Hirose, I. Okamoto, Y. Tanaka, A. Ono, *Angew. Chemie - Int. Ed.* 2014, 53, 2385–2388. Copyright © 2014 WILEY-VCH Verlag GmbH & Co. KGaA, Weinheim.^[48]

The formation mechanism of the T-Hg^{II}-T base pair has been proposed based on many experimental and computational results.^[29,46,47,55–58] It requires deprotonation of the N3 imino protons of thymine moieties (pK_a 9.8). Based on theoretical calculations, a detailed mechanism of the Hg^{II}-mediated pair formation has been proposed by Šebera *et al.* (Figure 5).^[56] The results suggest that the formation occurs in two separate steps, where the second Hg-N bond formation is the rate-limiting step. In aqueous solution, the mercury ion forms an aqua complex, and due to the high acidity of the aqua ligand, a hydroxo ligand might be present (Hg(H₂O)₄OH)⁺. In the first step, a hydroxo ligand of the Hg^{II}-aqua complex captures the first imino proton from the N3 of thymine, forming a Hg^{II}-N3 bond. The first step happens with a relatively low activation energy barrier. The second Hg-N bond formation, in turn, is energetically more demanding, and it has been proposed to occur either by tautomerization of the other thymine residue or by deprotonation by the hydroxo ligand of the Hg^{II}-aqua complex, which is already bound to thymine.^[56] Actually, another high-resolution X-ray crystallographic study revealed the flexibility of the T-Hg^{II}-T pair in which either an O4-Hg^{II}-N3 or an O2-Hg-N3 bridge is formed.^[59]

Indeed this form has been proposed based on theoretical calculations to be a stable intermediate before formation of the N3-Hg^{II}-N3 bridge.^[56] Minor tautomer (oxo, hydroxo) of thymine forms an O4-Hg^{II}-N3 bridge and a water-mediated hydrogen bond with other thymine. Eventually, the more stable N3-Hg-N3 bridge is formed after releasing a proton to bulk solvent.

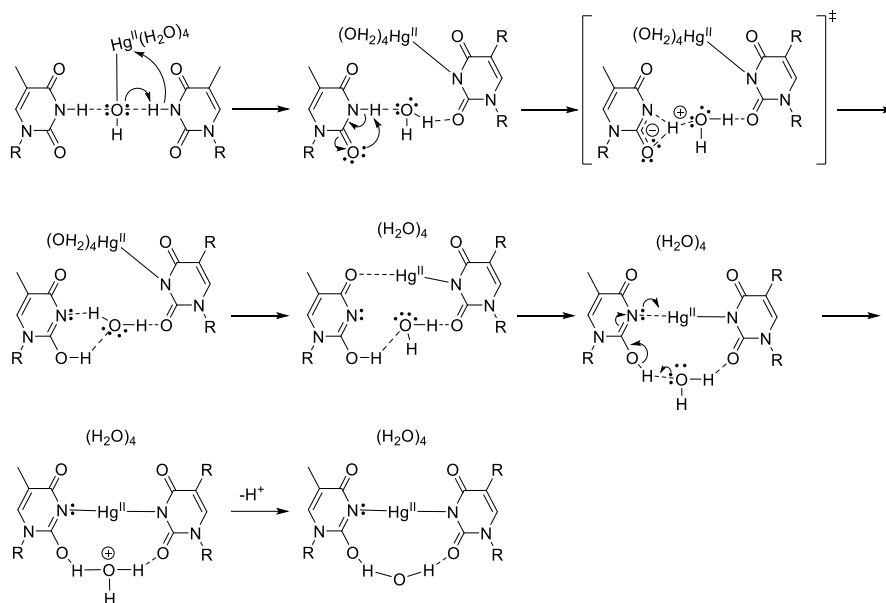


Figure 5. Proposed reaction mechanism for the T-Hg^{II}-T pair by Šebera et al.,^[56] reproduced from reference 56.

The nature of the T-Hg^{II}-T bond has been investigated in more detail, and it has been considered to have a low covalency and a relatively high ionic nature. A few key findings support this hypothesis. The first is the cleavability of the bond under 100 °C.^[46,60] Another is the huge downfield shift observed by ¹⁵N NMR which suggests, that the nitrogen of N-Hg bond has a large negative partial charge.^[25,45] In ¹⁵N NMR, metal coordination to nitrogen shifts the ¹⁵N resonance signal upfield. In contrast, proton-metal exchange shifts the signal downfield, which is observed in the case of the T-Hg^{II}-T base pair. In addition, the upfield shift in the ¹⁹⁹Hg NMR spectrum of the T-Hg^{II}-T pair is similar to other linear mercurated N-Hg^{II}-N crosslinked compounds like $(\text{Me}_3\text{Si})_2\text{N-Hg}^{\text{II}}\text{-N}(\text{Me}_3\text{Si})_2$.^[61] Also, Raman spectroscopy showed an exceptionally low wavenumber of carbonyl stretching ($\text{C}=\text{O}$, 1586 cm^{-1} and 1570 cm^{-1} for ¹⁸O labeled), which suggests partial enolization due to the deprotonation of imino proton and resonance structures transferred

through the system. However, the slow formation and very slow dissociation of the T-Hg^{II}-T pair are in line with the partially covalent nature of the bond.^[40]

UV melting experiments and isothermal titration calorimetry have been used to examine the effects of mercury-mediated base pairing on duplex stability and thermodynamical properties.^[55,62–64] Based on the UV melting temperature measurements of duplexes containing T-T mismatches, a T-Hg^{II}-T base pair stabilizes the duplex to an extent comparable to A-T or T-A Watson-Crick base pairs.^[62] Addition of Hg^{II} ions results in significant thermal stabilization only with the T-T mismatch containing duplex. Even though stabilization was not observed with a perfectly matched DNA duplex, the formation of T-Hg^{II}-T crosslinking is still possible by a strand displacement but it would cause conformational changes such as bulges and other large deviations from a typical B-type duplex.^[6,65] Other metal ions such as Ag^I, Cu^{II}, Ni^{II}, Pd^{II}, Co^{II}, Mn^{II}, Zn^{II}, Pb^{II}, Cd^{II}, Mg^{II}, Ca^{II}, Fe^{II}, Fe^{III}, and Ru^{III} did not stabilize the T-T mispair. The stabilization of the duplex by Hg^{II} ions was observed over a wide pH range (~3–10), but the most stable duplexes were observed between pH 5.5–8.5.^[62] The substituents of 5-position of thymine affect the pH dependence of the thermal stability of duplexes as the pK_a of N3 is lowered (Br = 8.4, F = 7.7 and CN = 6.5). An acidic medium favors a Hg^{II}-mediated pair, whereas a basic medium Ag^I-mediated pair. In lower proton concentration, silver ions are favored over protons and coordinate to N3.^[63]

Isothermal titration calorimetry (ITC) measurements of a 25mer duplex containing one T-T mismatch revealed the expected 1:1 molar ratio for the binding of the Hg^{II} ion, and the measured binding constant was approximately 10⁶ M⁻¹.^[55] The magnitude of the binding constant is considerably larger than observed for nonspecific metal-DNA interactions (10³–10⁵ M⁻¹).^[66–69] Interestingly, in the duplex containing two consecutive T-T mispairs, the affinity of the second binding Hg^{II} ion was significantly higher than the binding of the first metal ion, which indicates a positive cooperation effect between Hg^{II} ions.^[47,58] A similar effect was observed even with a duplex containing one Watson-Crick base pair between the T-Hg^{II}-T pairs. One suggested hypothesis is based on conformational changes observed by CD spectroscopy as a small distortion in secondary structure could make binding of the second mercury ion easier.^[58] CD spectroscopy offers a way to determine helicity, and it has been used to evaluate a double-helical structure containing the T-Hg^{II}-T pair. The structure was not markedly distorted by Hg^{II} ion binding, and CD spectra were similar to unmetallated duplexes.^[55,62]

Thermodynamical parameters, enthalpy, entropy and Gibb's free energy can be extracted from ITC results, which showed negative enthalpy and positive entropy changes upon the binding of Hg^{II}.^[55,58] Positive entropy can be explained by a huge positive dehydration entropy of the Hg^{II} aqua complex when pairing occurs. Indeed, the three-dimensional structures of oligomers show complete dehydration of the Hg^{II}

ion in the metal-mediated base pair.^[47,48] The effect of conformational entropy can be assumed negligible since no significant changes were observed in the double-helical structure. The favorable negative enthalpy is likely a consequence of the N-Hg^{II}-N bond formation because the dehydration of the Hg^{II} aqua complex, deprotonation of thymines and protonation of cacodylate buffer are all associated with positive enthalpy changes.^[55] These observations were in line with theoretical calculations.^[47,56] All in all, the formation of a T-Hg^{II}-T base pair is driven by the positive desolvation entropy of the Hg^{II} aqua complex and negative enthalpy of N3-Hg^{II}-N3 bond formation.

1.1.2 C-Ag^I-C base pairing

As the T-Hg^{II}-T metal pair is the most studied metallo pair, the C-Ag^I-C pair is next in second place. A hint of this kind of a metallo pair was observed first with pyridine nucleobases in a double-helical structure as the thermal stability increased in the presence of silver ions.^[70] Ag^I ion is considered as a soft Lewis acid, which prefers to coordinate linearly between two monodentate ligands such as nitrogen donors. In contrast to Hg^{II} ions, the ligands of the Ag^I aqua complex are only slightly acidic, preferring coordination to unprotonated sites. A stabilizing C-Ag^I-C metal pair was found where Ag^I coordinates between two cytosines^[71-73], but stabilization was not observed with other metals ions (Mg^{II}, Ca^{II}, Mn^{II}, Fe^{II}, Fe^{III}, Co^{II}, Ni^{II}, Cu^{II}, Zn^{II}, Ru^{III}, Pd^{II}, Cd^{II} and Pb^{II}).^[71] Detailed information of the binding and structural data have been collected by ¹H and ¹⁵N NMR, X-ray crystallography, UV and CD spectroscopy, ESI-MS and ITC.^[71,72,74]

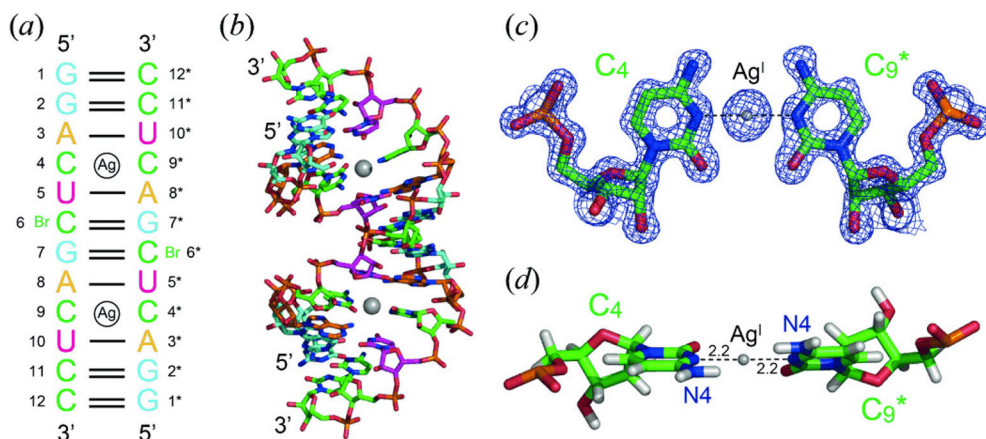


Figure 6. Crystal structure of 12mer RNA duplex containing two C-Ag^I-C pairs. Reprinted with permission from J. Kondo, Y. Tada, T. Dairaku, H. Saneyoshi, I. Okamoto, Y. Tanaka, A. Ono, *Angew. Chemie - Int. Ed.* **2015**, *54*, 13323–13326. © 2015 WILEY-VCH Verlag GmbH & Co. KGaA, Weinheim.^[74]

Crystal structure of a short RNA duplex containing two C-C mismatches revealed evidence of Ag^{I} -mediated base pairing between N3s of cytosines, as a short distance between N3 and Ag^{I} ion was measured (2.2–2.3 Å) (Figure 6).^[74] Also, ^{15}N NMR and ^1H NMR-based 3D solution structure of a DNA duplex supported these observations.^[75] Duplexes containing ^{15}N labeled cytosines showed a doublet of 1-bond coupling of $J(^{15}\text{N}, ^{109}\text{Ag})$ at 83–84 Hz coupling constant value. The value were in line with the theoretically predicted ones. A huge upfield shift of ^{15}N 3s (21.8 ppm) with labeled cytosine indicates the binding between N3s.^[73] In ^1H NMR spectra of a duplex, imino and methyl proton regions showed clear differences without and with one equivalent. of Ag^{I} ions. Also, ^1H shifts of H5 and H6 protons were similar with duplex and cytosine monomers suggesting similar binding of Ag^{I} between cytosines.^[71,73] The observed slow proton exchange rate compared to typical fast metal ion association/dissociation rates in nucleic acid structures in NMR time scale^[76] suggested binding to the inner N3 rather than to the exocyclic oxygens or nitrogens of the cytosines. Similar slow exchange rates were observed with T-Hg^{II}-T pairing.^[62] Interestingly, monomer crystals showed a different geometry, where two 1-methylcytosines formed an O2- Ag^{I} -N3 pair,^[77–80] and similar results were observed from molecular dynamics simulation of the dimer, where a suitable binding pocket for the metal ion was observed.^[81,82] However, in the NMR studies on an oligonucleotide duplex, no signs of a plausible N3- Ag -O2 metal bond, which would be observable as a smaller 3-bond coupling constant from other N3 to Ag^{I} ion, were detected.^[75]

In the crystal structure (Figure 6), the A-type RNA duplex was maintained after the addition of Ag^{I} ions.^[74] In line with corresponding results on the T-Hg^{II}-T base pair,^[48] twist angles between cytosines were much greater than with WC pairing in an A-type RNA duplex (-29° and -27° vs. -12°), likely to diminish the repulsion between the exocyclic amino groups of the cytosines. The solution structure of the DNA duplex containing the C- Ag^{I} -C pair was determined in the same way as Im- Ag^{I} -Im^[83] and T-Hg^{II}-T^[47] structures using NOE results to optimize the structure. The solution structure showed similar results as the twist angle was $-18.3 \pm 3^\circ$ and the distance between protons of the amino groups was 2.2 Å.^[75] Unfortunately, the resolution of the X-ray measurement was not sufficient to determine precisely if the exocyclic nitrogens of both cytosines are in amino form or if one is in the deprotonated imino form.^[75] ^{15}N NMR, on the other hand, revealed a triplet signal from both amino groups, thus confirming their amino nature. So, diminished repulsion of the amino groups cannot be explained by the tautomerization as was proposed earlier,^[75] which is supported by the observation that the stability of a duplex was highly increased when the C- Ag^{I} -C pair was in transoid orientation.^[84] Also, the most stable structures of the C- Ag^{I} -C base pairs are in transoid orientation based on theoretical optimization.^[85–87] Larger twist angles might also allow the

formation of intermolecular hydrogen bonds with other nucleobases^[88,89], which seems to bring additional stability at least in more complex metal–nucleobase constructs, such as silver nanowires.^[88]

The effect of Ag^{I} on thermal stabilities of oligonucleotide duplexes was examined by UV melting temperature experiments. An equimolar amount of Ag^{I} ions increased the T_m -value by 4.8–8 °C compared to the corresponding oligonucleotides in the absence of silver ions, depending on the sequence and neighboring nucleobases.^[71–73] At a pH range of 5–9, the stabilization was highest, and at the lower end of the range, protonation of cytosine and formation of a protonated CH⁺-C pair also competes with metal-mediated base pairing.^[71] From ITC measurements, binding constants of 10^6 M^{-1} ^[72,73] were determined, which was much larger than unspecific DNA-metal interactions (10^3 – 10^5 M^{-1}).^[67–69,90,91] Also, thermodynamical parameters (enthalpy, entropy and Gibbs energy) were extracted from the ITC results. Negative enthalpy and positive entropy were observed, supporting the site-specific formation of a single C- Ag^{I} -C pair. Total positive entropy was similar in magnitude to the dehydration enthalpy of the Ag^{I} aqua complex. Conformational entropy was assumed to be small because only minor conformational changes were observed in the CD spectra. These observations suggest that the positive dehydration entropy mostly causes the positive entropy as water molecules are released from the Ag^{I} aqua complex due to the specific binding into the C-C mismatch.^[72,73] Total negative enthalpy is likely a consequence of combining the positive dehydration enthalpy of Ag^{I} ions and greater negative enthalpy from the formation of N- Ag^{I} -N bonds. When two silver ions were bound into a duplex containing either consecutive or interrupted C-C mismatches, similar binding constants were observed. In other words, the positive cooperation effect observed with consecutive T- Hg^{II} -T pairs and Im- Ag^{I} -Im pairs was not detected.^[58,92] Interestingly, however, more negative enthalpy and a sign change of entropy from positive to negative was observed for the second binding. More significant changes in helical structure were also observed in CD spectra after binding of the second Ag^{I} ion, but an exact reason for the changes in the thermodynamical parameters was unclear. Metallophilic interactions have been proposed to lead to increased stabilization of the double-helical structure with Ag^{I} ions.^[83,88,93] However, those alone might not be enough to stabilize the structure, as was observed from the results of theoretical calculations of a C_{20} - Ag_{20} - C_{20} homoduplex. This duplex was stable only in parallel (rather than antiparallel) chain orientation.^[86] Indeed, hydrogen bonding between stacked nucleobases has also been suggested to be a key contributor for additional stability.^[86,88,89,94]

1.1.3 Other Hg^{II}- and Ag^I-mediated base pairs between canonical nucleobases

In addition to the most commonly recognized and studied T-Hg^{II}-T and C-Ag^I-C metal pairs, many other metal-mediated base pairs between natural nucleobases have been observed (Figure 7–9). Competing binding modes between N1 and N7 of purines and deprotonation of N3 of thymine and N1 of guanine opens more options for metal-mediated pairing. DNA structures cause limitations for metal-mediated base pairs; for example, linear and square planar geometries fit within the base stack to maintain the duplex structure. However, larger DNA constructions in different orientations might find stable conformations induced by the metal ions. Also, an increased number of the metal pairs might overcome an effect of the traditional WC pairs and the normal formation of the duplex. Indeed, the larger structures add much more variables, and “unexpected” pairs can be formed.

Intuitively, it could be proposed that a G-Hg^{II}-G pair is formed similarly as the T-Hg^{II}-T pair via deprotonation of N1s because of similar pK_a values of N3 of T and N1 of G (Figure 7). However, G-Hg^{II}-G pair formation has not been observed in a double-helical oligonucleotide, albeit at monomer level it seems to be stable.^[21,22,95] Instead, a T-Hg^{II}-G pair increased the thermal stability of the duplex^[96], and it has also been found in a crystallized oligonucleotide^[97]. Longer purine-purine pairs do not fit into the base stack, which might strain the helical structure, whereas pyrimidine-purine pairs such as the T-Hg^{II}-G pair might fit better into at least some sequences. Also, the repulsion between exocyclic amino substituents of guanine in cisoid orientation might affect stability. However, these pairs have not been widely studied in oligonucleotide structures, so it is hard to draw firm conclusions. Instead, the C-T mismatch has been studied in more detail. The C-T mismatch is moderately stabilized by both Ag^I and Hg^{II} ions,^[31,59,98] although the latter effect is not observed in all sequences.^[55] As in this case and on some other occasions, the metal-binding might only reflect on thermal stability minimally or by decreasing it.^[55,99,100] At first, a coordination sphere was suggested to mimic the T-Hg^{II}-T pair where the metal ion sets up between the N3s of cytosine and thymine. Later studies support the formation of a different coordination sphere for the C-Hg^{II}-T (Figure 7).^[59,101] Based on the crystal structure of short 8mer DNA duplexes, Hg^{II} ion coordinates between N3 of T and exocyclic N4 of cytosine, including one water-mediated hydrogen bond to form an A-type duplex.^[59] Also, ¹H NMR and fluorescence results of a duplex suggested the formation of a stoichiometric Hg^{II}-mediated base pair between C and T. Binding affinity was similar to that of a duplex containing T-Hg^{II}-T base pair.^[40,101] The rates of association and dissociation of the duplex containing C-Hg^{II}-T pair were about ten times faster than those of the corresponding duplex containing T-Hg^{II}-T pair, which supports kinetically less stable and more solvent-exposed coordination into the exocyclic amine.^[101] Indeed, the proposed formation of the T-Hg^{II}-T base pair

goes through the T(O2)-Hg^{II}-T(N3) form, isosteric with the C(N4)-Hg^{II}-T(N3) base pair.^[56] Flanking nucleobases^[31] and solvent interactions have been suggested to stabilize the C-Hg^{II}-T pair significantly.^[59]

The crystal structures of the 8mer duplexes supported the formation of A-type duplexes, and changes in the level of compression and stretch along the helical axis were observed.^[59] Different results were obtained from the CD spectra of longer duplexes (14-21mer), which suggested the formation of a B-type duplex with no significant changes in the conformation.^[101,102] Indeed, an NMR study of the 14mer duplex containing well-separated C-Hg^{II}-T pairs showed two sets of signals representing different conformations.^[102] Interestingly, the major conformer (more B-type) contains the T(N3)-Hg^{II}-C(N3) pair, and the minor one (more A-type) the T(N3)-Hg^{II}-C(N4) pair. In the latter one, metal-nucleobase interactions were stronger, but structural perturbations of the DNA structure were also more significant. The opposite was observed with the T(N3)-Hg^{II}-C(N3) coordination. In these duplexes, higher overall stability was observed in the B-type duplex containing the T(N3)-Hg^{II}-C(N3) base pair, which overcomes the stronger metal-nucleobase interaction of the T(N3)-Hg^{II}-C(N4) base pair in the A-type duplex.

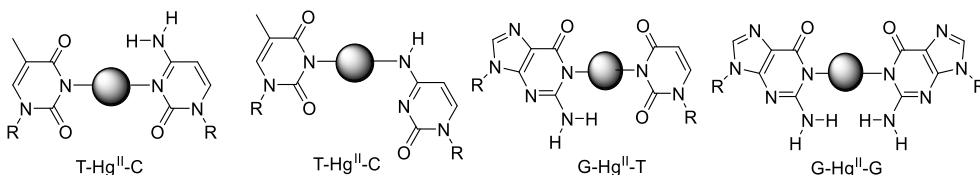


Figure 7. Proposed Hg^{II}-mediated pairs with other canonical nucleobases.

Silver ions were observed to stabilize also C-A and C-T mismatches in some sequences^[103–105], but as T_m -values are highly dependent on neighboring nucleobases minor changes are harder to distinguish.^[31,98] Theoretical calculations suggest that the C-Ag^I-A pair can have multiple binding modes, energetically close to each other, such as WC and Hoogsteen forms, in both antiparallel and parallel orientations.^[85] Not all of these forms have been observed in the solution, which might result from competition between binding to N7 or N1 of purines. Slight modifications on the natural nucleobases have been used to control the binding mode. For example, adenine and guanine analogs, where the endocyclic nitrogens have been replaced with a carbon atom, give limited options for metal-mediated base pairing (Figure 8). 7-deaza-adenine nucleobase and its 7-substituted analogs allow the formation of A-Ag^I-T^[39] and A-Ag^I-C as well as A-Ag^I-G^[106] base pairs. A lack of the endocyclic N7 forces pairing into the WC face via N1. On the other hand, 1-deaza-adenine forces binding to N7 through Hoogsteen face and, hence, formation of an N7(A)-

Ag^{I} -N3(T) pair.^[107] Even though Ag^{I} ions or the Ag^{I} aqua complex are not as acidic as the Hg^{II} aqua complex, they can still deprotonate the N3 of uridine or thymine which would allow the formation of a plausible A- Ag^{I} -T pair.^[7] Similarly, 7-deazaguanine allows the formation of a G- Ag^{I} -C pair.^[108] A different guanine analog, 5-aza-7-deazaguanine, lacks a proton at N1 position which should allow easier binding with Ag^{I} .^[104] Also, a notable stability difference between metallated and unmetallated duplex is observed as only two hydrogen bonds are involved in the WC pairing of 5-aza-7-deazaguanine.

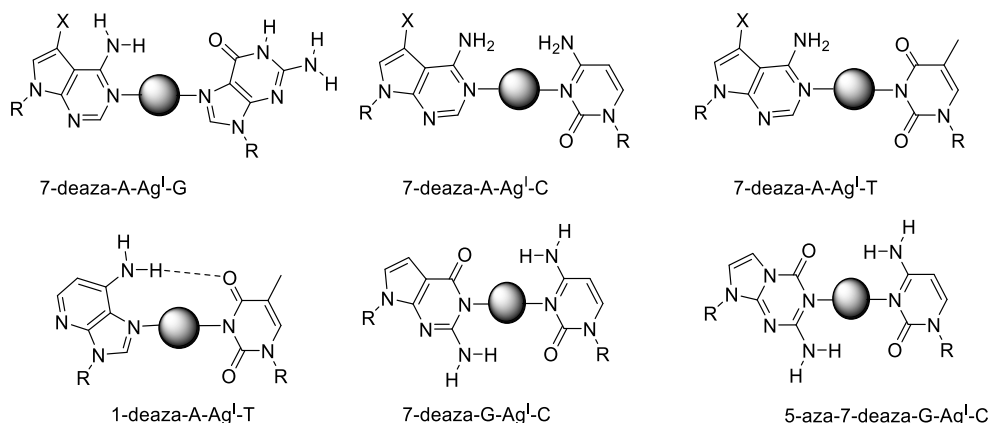


Figure 8. Deaza-analogs of adenine and guanine, and proposed Ag^{I} -mediated metal pairs. R represents ribose or deoxyribose and X represents H, I or cyclopropyl substituents.

Silver ions seem to be more versatile compared to mercury ions, and many different pairs have been observed, such as C- Ag^{I} -C, G- Ag^{I} -G, G- Ag^{I} -C and T- Ag^{I} -T (Figure 9). The formation of the G- Ag^{I} -G pair was first observed by ESI-MS when mixing C_{11} and G_{11} homostrands and Ag^{I} ions. After the addition of Ag^{I} ions, only C_{11} - Ag_x , G_{11} - Ag_x and homoduplexes containing Ag^{I} ions were observed. The G_{11} - Ag_{11} - G_{11} duplex showed to be much more stable than a respective duplex consisting of Watson-Crick base pairs.^[109] In addition, the G- Ag^{I} -G base pair has been observed in a non-helical DNA structure formed by two 8mer oligonucleotides.^[110] The structure is stabilized by G- Ag^{I} -G and C- Ag^{I} -C base pairs and mimicks a pyramid from one and a cylinder shape from another orientation. The crystal structure of a non-helical structure and theoretical optimizations suggest that the binding occurs between N7s of guanine.^[109,110] An extreme example of the complexity of metal pairs is the formation of consecutive different metal-mediated base pairs along the DNA duplex, forming metallo-DNA nanowires (Figure 10).^[88,97,111] In a silver-DNA nanowire, dodecamer units of a pre-designed single-stranded DNA can form a long polymer containing multiple natural metal pairs such

as C-Ag^I-C, G-Ag^I-G, G-Ag^I-C and T-Ag^I-T.^[88] Adenine residues are bulged out of the structure, but those also contribute to crystal packing by forming A-T-Ag^I-T triplets and adenine-adenine stacks between duplexes. Interestingly, the dodecamers could form a duplex containing both WC base pairs and C-Ag^I-C pairs, which actually is the case with the corresponding RNA sequence, but only the polymer mentioned above crystallized.^[74] Distances between the silver ions are short, which might suggest significant metallophilic interactions, previously observed between consecutive T-Hg^{II}-T^[47,48] and Im-Ag-Im^[83,93] metal pairs. Also, intermolecular hydrogen bonding between nucleobases due to large twist angles of the metal pairs (-28 – -44°) might stabilize the structure.^[88,89] Similarly, in a Hg^{II}-DNA nanowire, pentamer units could form three consecutive T-Hg^{II}-T pairs and GC-overhangs pair with WC hydrogen bonds to form a higher-order polymer structure.^[97] Instead, two T-Hg^{II}-T and one T-Hg^{II}-G pair are formed per one pentamer unit. Interestingly, the T-Hg^{II}-T pairs are formed in the same plane, and crosslinks are formed between T2s and T3s (Figure 10). In addition, water-mediated C-C mismatches bind pentamer units to each other. The structure is similar to the Ag^I-DNA -nanowire, but the Hg^{II} ions are not arranged in a line but instead in a spiral form.

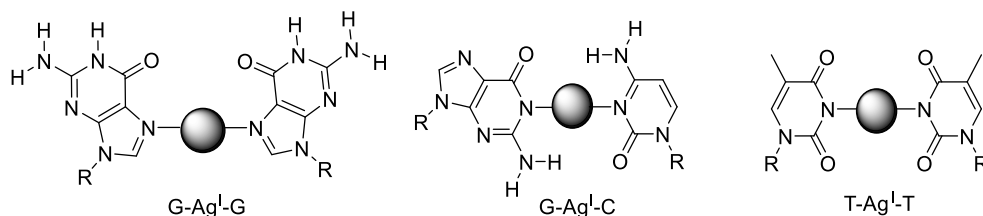


Figure 9. Proposed silver-mediated base pairs between canonical nucleobases. R represents ribose or deoxyribose

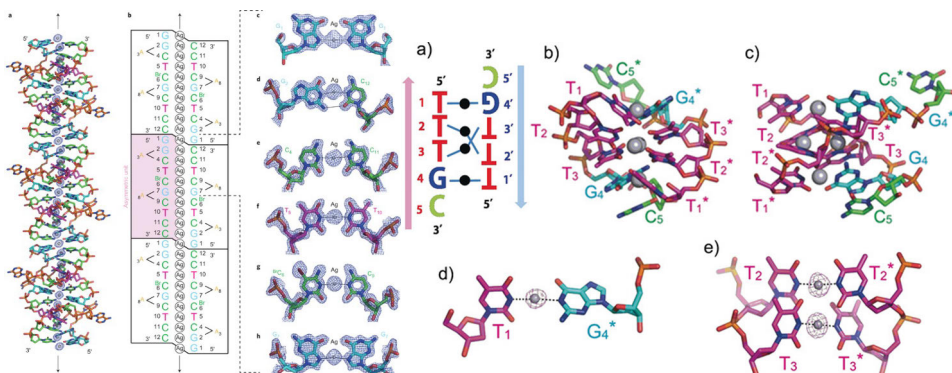


Figure 10. Crystal structures of silver and mercury nanowires. Reprinted with permission from J. Kondo, Y. Tada, T. Dairaku, Y. Hattori, H. Saneyoshi, A. Ono, Y. Tanaka, *Nat. Chem.* **2017**, *9*, 956–960. Copyright © 2017, Nature Publishing Group.^[88] Reprinted with permission from A. Ono, H. Kanazawa, H. Ito, M. Goto, K. Nakamura, H. Saneyoshi, J. Kondo, *Angew. Chemie - Int. Ed.* **2019**, *58*, 16835–16838. © 2019 Wiley-VCH Verlag GmbH & Co. KGaA, Weinheim.^[97]

As these extreme examples show, different metal pairs need to be considered carefully as many of those might be stable only in certain circumstances, and other interactions such as the metallophilic and intermolecular hydrogen bonding might play a considerable role in the stability of the structures.^[88,89] However, this also underlines the versatility of metal ions, which opens multiple options for applications.

1.2 Nucleobase analogs for metal-mediated base pairing with canonical nucleobases

1.2.1 Fluorescent nucleobase analogs for the metal-mediated base pairs

Fluorescent nucleobase analogs have been developed for many purposes to study nucleic acid structures and interactions.^[112–114] These would be useful for detailed studies of metal binding and changes in the local environment of the fluorescent probe. Indeed, the fluorescence intensity of analogs is highly sensitive to the surrounding environment. Free fluorescent nucleosides often show the highest fluorescence, and the intensity drops in a single-stranded oligonucleotide and even further in a double-stranded oligonucleotide due to stacking and base-pairing interactions.^[115–118] Many of these analogs used for the metal-mediated base pairing mimic thymine^[40,119,120] or cytosine^[121–124], where the conjugated system has been expanded by attaching aromatic moieties into the nucleobase (Figure 11).

^{DMA}T and ^{DMA}C (Figure 11a & 11b), where dimethylaniline rings are fused to uridine or cytosine, work as fluorescent thymine and cytosine analogs, respectively.^[119] In ^{DMA}T , the binding face stays intact, and also the pK_a of N3 proton (9.5) is close to that of thymine and uracil (9.7).^[125] The stability of ^{DMA}T -A pairs is comparable to that of T-A base pair. ^{DMA}C pairs with guanine with an affinity comparable to that of cytosine.^[126] ^{DMA}T has been used as a probe for the site-specific binding of Hg^{II} ions into the T-T mispair. The binding caused a considerable decrease in fluorescence intensity (95%), not observed with C and G. With this analog, a detailed kinetic analysis of the T- Hg^{II} -T pair formation was carried out, which revealed slow association and very slow dissociation rate constants ($k_{on} \approx 10^4$ – 10^5 M^{-1} s^{-1} and $k_{off} \approx 10^{-4}$ – 10^{-3} at 25 °C) within double-helical DNA.^[40] In addition, both analogs, ^{DMA}T and ^{DMA}C , have been used for the detailed kinetic study of the T- Hg^{II} -C base pair, as discussed in the earlier chapter.^[40] Another thymine analog is ^{diox}T , where a dioxoquinazoline ring is fused to thymine (Figure 11c).^[120] It forms a Hg^{II} -mediated base pair with thymine and cytosine. Fluorescence quenching efficiency was high (~90 and ~70 %) when pairing with T or C, respectively, in the presence of Hg^{II} ions. Also, Ag^I ions suppressed fluorescence but only 30 % in the case of a ^{diox}T -C mismatch. Another thymine analog, 5-methoxybenzofuranuridine, was used for site-specific Hg^{II} -mediated pairing with uridine and thymine in hybrid RNA/DNA duplexes and RNA duplexes (Figure 11d).^[127]

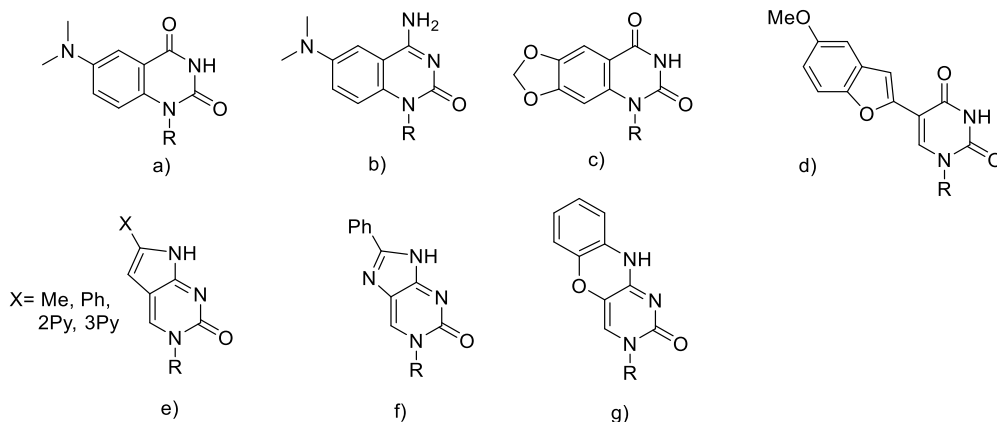


Figure 11. Fluorescent nucleobase analog used for the metal-mediated base pairing a) ^{DMA}T , b) ^{DMA}C , c) ^{diox}T , d) 5-methoxybenzofuranuridine, e) PyC and its analogs, f) 8-Phenylimidazolo-dC and g) 1,3-diaza-2-oxophenoxazine. R denotes deoxyribose.

Fluorescent pyrrolo-C has been used widely for studies of nucleic acid interactions.^[128–133] It pairs similarly as cytosine and is also capable of silver-mediated base pairing with cytosine.^[122] Fluorescence quenches only when a PyC-G

or a PyC-Ag^I-C pair is formed. Neighboring nucleobases in the oligonucleotide strands significantly affect the quenching efficiency as smaller surrounding pyrimidine bases lead to weaker stacking than larger purine bases. Indeed, two Pyrrolo-C analogs can bind two silver ions between each other, causing a considerable increase in the thermal stabilities of duplexes.^[134] PyC has been used as an indirect probe for the metal-mediated base pairing as a part of the duplex to examine the duplex stabilization by metal ion binding.^[135] Pyrrolo C has been developed further by extending the structure with phenyl or pyridine ring at the 6th position of PyC to enhance binding and fluorescence properties (Figure 11e).^[123,132,134,136] Fluorescent 1,3-diaza-2-oxophenoxazine nucleoside behaved differently from the fluorescent nucleobases discussed earlier (Figure 11g).^[121] It forms a strongly fluorescent metal pair when pairing with itself or cytosine. Interestingly, fluorescence does not quench after forming Ag^I-mediated metal pair with cytosine. Indeed, in the case of cytosine, fluorescence even increases, which might be caused by the different electronic configuration of the metal-mediated pair. On pairing with another 1,3-diaza-2-oxophenoxazine base, the fluorescence is quenched but only modestly. A redshift of the emission maximum from 448 to 460 nm was observed when pairing with both targets.

1.2.2 Organometallic nucleobases for the metal-mediated base pairing

Metal-mediated base pairs can also be formed between an organometallic nucleobase and a canonical nucleobase. In organometallic nucleobases, a metal ion is covalently coupled to a nucleobase or a nucleobase analog via a metal-carbon bond. The advantages of organometallic compounds are their superior stability in a metal-deficient environment compared to many metal-coordination compounds. Organometallic bonds can resist dissociation even at low concentrations within human cells, which is required for therapeutic applications. Metal ions can be coupled to a specific position in the nucleobases/nucleobase analogs. With organometallic Hg- and Pd-compounds, stable complexes can be achieved in metal deficient conditions.

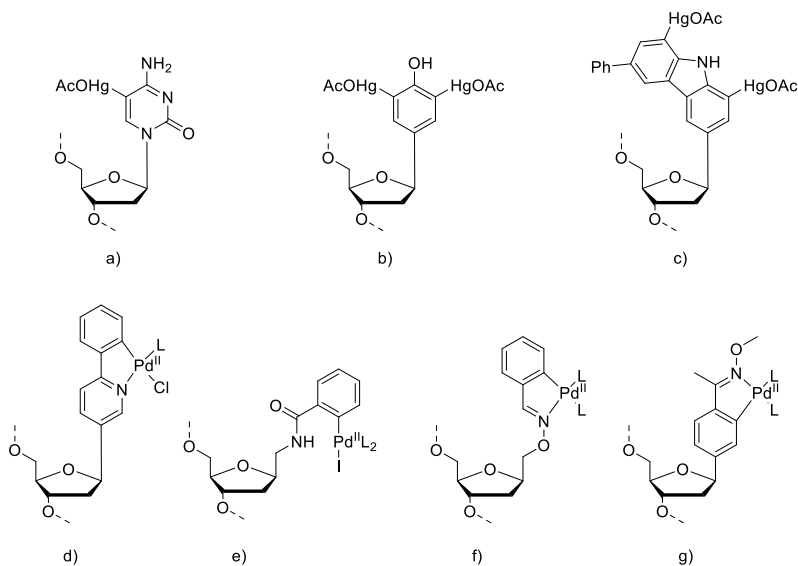


Figure 12. Mercurated and palladated nucleobase analogs a) 5-mercuricytosine, b) 2,6-dimercuriphenol, c) 1,8-dimercuri-6-phenyl-1*H*-carbazole, d) palladated 2-phenylpyridine, e) (2-palladabenzoyl-amino)methylbase surrogate, f) and g) benzaldoxime palladacycles used for the metal-mediated base pairing. L represents an exchangeable ligand.

Mercury is one promising candidate because of its simple linear coordination, and mercurated nucleoside analogs are readily accessible compounds from the synthetic perspective. The linear coordination of the mercury ion allows organomercury compounds to fit easily into double-helical DNA. Canonical nucleobases, cytosine and uridine, are prone to mercurate at the C5 position of the pyrimidine ring.^[96,137–140] Limited binding sites for mercuration have led to the development of artificial organomercury nucleobase analogs. Indeed, mercuration by an electrophilic aromatic substitution has been known for a very long time, and numerous aryl mercury compounds have been synthesized.^[141–147] However, the potential of these compounds has been utilized for the Hg^{II}-mediated base pairing only recently (Figure 12).^[96,137,148–150] Hybridization properties, like thermal stabilities of duplexes and the pairing between different canonical nucleobases, have been studied with various mercurated oligonucleotides. One candidate, 5-mercuricytosine, is easily prepared from cytosine by treating with Hg(OAc)₂ in an aqueous solution (Figure 12a). Similarly, cytosine residues can be mercurated within an oligonucleotide. 5-mercuricytosine can form base pairs via both *syn*- and *anti*-conformations, the *anti*-conformation hybridizes via WC hydrogen bonds similar to cytosine, and the *syn*-conformation via a mercury-mediated bond.^[96,137] Rotation around the glycosidic bond allows either face to bind with the opposite strand. Duplex formation was examined with complementary oligonucleotides, where the

nucleobase opposite to 5-mercuricytosine varied (A, C, G, T). The thermal stability of the duplex was significantly increased when thymine was opposite to the mercuricytosine, which indicates mercury-mediated base-pairing (Figure 13a). Instead, when 5-mercuricytosine was placed opposite to guanine, the T_m value decreased but was restored after the addition of mercaptoethanol, a compound that strongly coordinates Hg^{II} ions, causing the dissociation of the metal-mediated pair.^[151] A metal-mediated pair is likely formed also with guanine, but it is not as strong as the WC pairing of the *syn*-face. Also, 5-mercuricytosine was able to stabilize a triple-helical oligonucleotide opposite to A-T or T-A pairs in the duplex, whereas other base combinations destabilized the triplex.^[137]

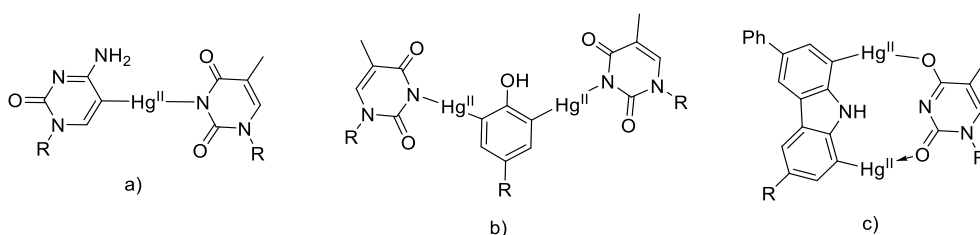


Figure 13. Proposed binding modes between thymine and a) 5-mercuricytosine, b) 2,6-dimercuriphenol and c) 1,8-dimercuri-6-phenyl-1*H*-carbazole. R represents ribose or deoxyribose.

The artificial dinuclear nucleoside analog 2,6-dimercuriphenol (Figure 12b) can bind with both faces via Hg^{II} -mediated base-pairing. When incorporated into the middle strand of an A•T•A triple helix, it formed stable Hg^{II} -mediated base triples with the thymines, adenines or cytosines of the other strands (Figure 13b).^[148] Both faces were stabilized equally compared to corresponding unmercurated triple-helical oligonucleotide, but due to low stabilization of Hoogsteen face, instead of a clear biphasic profile, more gradual melting profile was observed. Another dinuclear but monofacial nucleobase analog, 1,8-dimercuri-6-phenyl-1*H*-carbazole (Figure 12c), showed a slightly smaller T_m value than 5-mercuricytosine placed opposite to thymine within a double helix.^[148] In other words, the second mercury ion in the binding face did not significantly affect the thermal stability, which might be associated with the restrictions in geometry. Structure optimization by DFT calculations suggested that the dinuclear mercury-mediated pair is formed through coordination of the two Hg^{II} ions to the two carbonyl oxygens of thymine (Figure 13c).

In addition to mercurated oligonucleotides, also palladated oligonucleotides containing organopalladium nucleobase surrogates could for duplexes through the metal-mediated base pairing (Figure 12).^[135,149,152–163] Palladated oligonucleotides

can be prepared by oxidative addition^[158], ligand-directed metallation^[156,157,160,161] or post-synthetic coupling of a prefabricated organopalladium compound.^[156,159] Indeed, methods that allow coupling of a metallated nucleobase analog to an oligonucleotide would be desirable as those allow easier purification protocols. Some organometallic palladacyclic compounds have been found to bind with a high affinity to canonical nucleotides^[164,165], thus having the potential to act as anti-cancer drugs.^[166] A few palladacyclic nucleobase analogs have been incorporated into oligonucleotide sequences, and their thermal stabilities have been studied.^[160,161] However, most likely due to the square planar coordination chemistry, the analogs are not easily fitted into duplexes, as the highest thermal stabilities have been observed at the terminus of the oligonucleotides. Also, palladated molecules coupled via a flexible linker at the oligonucleotide terminus have provided stronger binding than corresponding nucleotide analogs. Hybridization studies on palladated oligonucleotides are not as straightforward as those on mercurated oligonucleotides due to the slower ligand exchange of Pd^{II} compared to Hg^{II}. The slow ligand exchange affects the melting profiles that usually contain a wider transition between structures as well as significant hysteresis between the heating and the cooling curve. Thus, the T_m -experiments do not necessarily give reliable picture of the affinity how these metallated oligonucleotides would behave in constant temperature e.g. at 25°C or 37°C. In addition to the presented examples, many different organometallic complexes with nucleobase analogs have been synthesized, but most have not been incorporated into oligonucleotides.^[167]

1.2.3 Nucleobase analogs discriminating canonical nucleobases via metal-mediated base pairing

Usually, metal-mediated pairing of nucleobases or nucleobase analogs has been studied in detail with one specific opposite nucleobase, typically the one forming the most stable base pair in the presence of a given metal ion. Binding with different nucleobases is, however, possible because of different binding modes and orientations of metal pairs. All mismatches can behave very differently from each other in double-helical oligonucleotides, allowing the discrimination of canonical nucleobases. However, not many analogs have been studied in this context (Figure 14). Different orientation of α - and β -anomers of cytosine in the presence of Ag^I ions influences differently to T_m values for every opposite nucleobase.^[84] The binding mode changes as the orientation of the nucleobase changes from cisoid to transoid. The impact of silver-mediated base pairing by α -C on the melting temperature of a DNA duplex was increasing with cytosine, decreasing with adenine, and negligible with thymine, compared to the corresponding duplex in the absence of silver ions. In the presence of Ag^I ions, α -C can, hence, recognize three of the four canonical

nucleobases (adenine, cytosine and thymine), the T_m values of the respective duplexes varying by at least 9 °C. Watson-Crick pairing in the absence of silver ions is still needed to distinguish between guanine and thymine. Different binding affinities for two canonical nucleobases have been observed with a metal-specific approach. 1*H*-imidazo[4,5-*f*][1,10]phenanthroline (**P**) (Figure 14b) pairs with thymine in the presence of mercury ions and with cytosine in the presence of silver ions.^[168–171] At first, **P** was found to bind with itself via silver ions^[172] and later via copper ions^[168]. Another nucleobase analog that shows metal-dependent discrimination between canonical nucleobases is picolinamide (Figure 14c).^[152] In the presence of Pd^{II} ions, base pairing with guanine was promoted, while with Ag^I ions the pairing with adenine was retarded. All metal ions tested (Ag^I, Cu^{II}, Hg^{II}, Pd^{II}, Zn^{II} and Ni^{II}) retarded binding with cytosine.

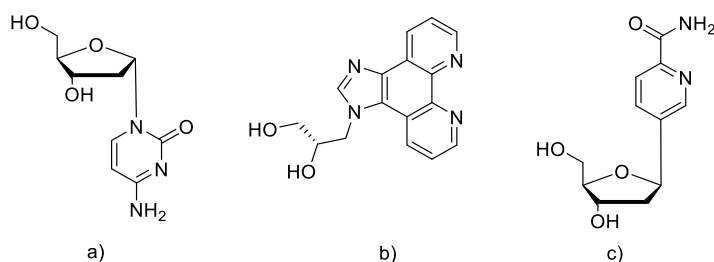


Figure 14. Nucleobase analogs a) α -cytosine, b) 1*H*-imidazo[4,5-*f*][1,10]phenanthroline GNA block and c) picolinamide C-nucleoside discriminating canonical nucleobases via metal-mediated base pairing.

1.3 Incorporation of metal-mediated base pairs into oligonucleotides

Usually, the formation of metal-mediated base pairs at the oligonucleotide level begins with synthesizing a suitable oligonucleotide, which contains a specific binding site for a metal ion. Conventional methods for oligonucleotide synthesis using an automated solid-phase oligonucleotide synthesizer can be used. Afterward, metal ions are introduced, and the heating and cooling cycles allow the metal ions to find the specific binding site between the two strands forming the duplex. This approach has been widely used, and it is efficient for short oligonucleotides. For longer oligonucleotides, overall synthesis yield drops step by step even though coupling yield stays high, and using an excess of phosphoramidites and other reagents is not profitable in the long run. In addition, some functionalities of artificial nucleobases, such as aldehydes, are not compatible with automated solid-phase synthesis protocols, and require orthogonal protection.^[173] Also, forming longer metallated oligonucleotides containing multiple metal ions is problematic.^[31,174]

Added metal ions increase the stability of duplexes, but can also increase the stability of undesirable structures such as hairpin structures.

Another option is enzymatic construction of metal pairs, which would allow the site-specific formation of metal pairs into longer oligonucleotide sequences. DNA polymerases have been found to tolerate nonstandard base pairs, such as those based on other types of hydrogen bonding or shape complementary, in the replication.^[175-184] Metal-mediated base pairs such as T-Hg^{II}-T and C-Ag^I-C pairs do not significantly disrupt the double-helical secondary structure and would, hence, be possible candidates for enzymatic formation.^[47,74] The first example of enzymatic formation of a metal-mediated base pair was described by Urata *et al.* for a primer extension reaction catalyzed by the Klenow fragment (KF) (Figure 15a).^[177] The presence of low to moderate concentrations of mercury ions (10–100 μ M) and TTP, CTP and GTP allowed the T-Hg^{II}-T pair to form. A higher mercury concentration (>100 μ M) inhibited the reaction, while the scarcity of TTP or ATP halted the reaction at the site of T in the template. A combination of different polymerase enzymes (Terminator DNA polymerase and 3'→5' exonuclease deficient KF (KF^{exo-})) allowed the formation of ten consecutive T-Hg^{II}-T pairs (Figure 15d).^[185] However, the construction of consecutive T-Hg^{II}-T pairs still involves careful balancing between enzyme specificity and efficiency.

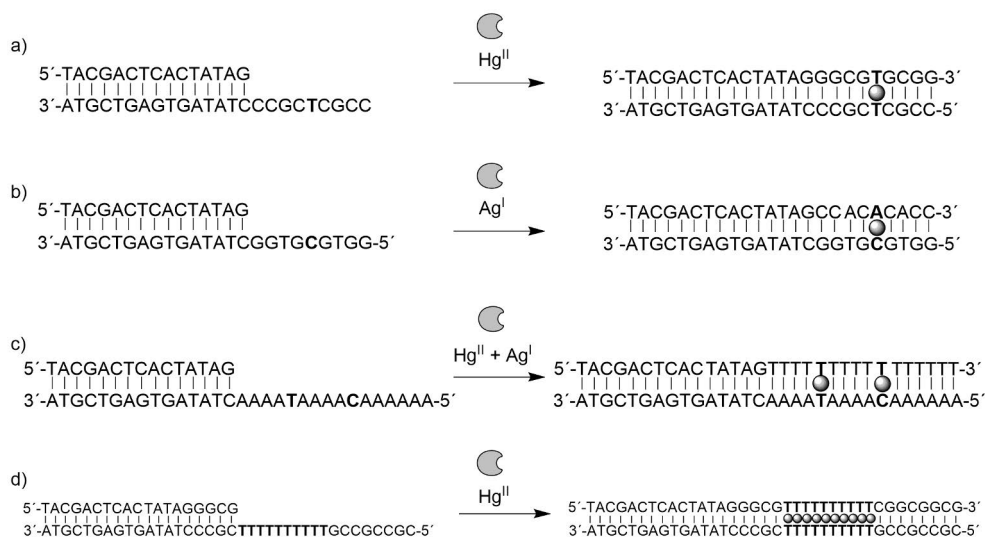


Figure 15. Principle of enzymatic formation of different metal-mediated base pairs.

One exciting application that uses metal-mediated base pairs is logic gates for enzymes.^[186,187] The 3'-terminal of the primer forms either a T-T or a C-C mispair with the template, which prevents Taq polymerase from advancing. The addition of

mercury or silver ions causes the formation of T-Hg^{II}-T and C-Ag^I-C metal pairs, respectively, which in turn allows the polymerase to proceed. Park *et al.* applied metal-mediated base pairs as logic gates in enzymatic polymerase reactions to control PCR amplification. The formation of the T-Hg^{II}-T and the C-Ag^I-C pairs controlled the enzyme activity.^[186,187] Interestingly, formation of the thermally stable C-Ag^I-C pair has not been observed in the primer extension reactions using KF or KF *exo*⁻.^[175,188] Detailed analysis of the products, including mass spectrometric analysis, showed that formation of the product oligonucleotides propagates via C-Ag^I-A or C-Ag^I-T pairs rather than the expected C-Ag^I-C pair (Figure 15b & 15c). The C-Ag^I-A pair was formed only when cytosine was incorporated into the template and not the opposite way, whereas C-Ag^I-T formed in both ways. KF *exo*⁻ is susceptible to formation of purine-purine mispairs by rotating NTP to *syn* conformation to maintain the distances of C1 sugar carbons in double-helical DNA.^[189] Similar conformational restrictions support the formation of a C(N3)-Ag^I-A(N7) pair.^[107] Interestingly, also with KF *exo*⁻, differences in the chain elongation were observed when using MeCTP and ATP instead of CTP and ATP substrates with a template sequence containing cytosines. The first combination produced a much more fully elongated sequence than the latter, which suggests the polymerase goes through the formation of a MeC-Ag^I-C pair.^[190] With the mixture of ATP and CTP, a small amount of the fully elongated product was observed, which might have also proceeded via the C-Ag^I-A pair as was earlier observed. Methylcytosines worked also for the chain elongation when attached in the template sequence.^[190] Higher electron-donating property of MeCTP compared to CTP was proposed to facilitate the formation of the MeC-Ag^I-C pair. Another explanation might be improved base stacking of MeC compared to C. Differences between thermal stabilities and progression of enzymatic polymerization have been noticed in studies before.^[191,192] The polymerase reaction might be affected by shape complementarity and the stability of base pairs without a metal ion,^[105] as well as a positive net charge, which seems to hinder the polymerase efficiency.^[175,188,190] These factors seem to be more crucial for polymerases than the thermal stability of base pairs.

1.4 Applications and potential of the metal-mediated base pairs

1.4.1 Construction of nucleic acid structures via metal-mediated base pairing

The ability of nucleobases to form metal-mediated pairs with specific metal ions can be used for many applications, *i.e.*, the construction and adjustment of different higher-order oligonucleotide structures. Typically, natural DNA and RNA duplexes

obey an antiparallel arrangement.^[193–195] The parallel alignment of these duplexes is less stable owing to the lower stabilities of reverse Watson-Crick base pairs.^[194] While the transoid A-T base pair is relatively stable, the transoid G-C pair is somewhat unstable, because only one hydrogen bond is formed and opposite amino groups repel each other.^[196–199] One interesting feature of metal-mediated base pairs is their ability to exist in either cisoid or transoid orientation. At the oligonucleotide level, this also allows the formation of duplexes with parallel strand orientation (Figure 16). As the T-Hg^{II}-T pair is symmetric, base pairing in either alignment stabilizes the T-T mismatch.^[200] Also, the C-Ag^I-C pair was stabilizing in both orientations.^[200] A transoid C-Ag^I-C pair could form additional stabilizing hydrogen bonds between amino and carbonyl groups. Transoid orientation also diminishes the repulsion between amino groups compared to cisoid orientation. Indeed, the α -anomer of cytosine formed a transoid α -C-Ag^I-C pair, which stabilized duplex much more than the cisoid pair.^[84] Also, computational optimizations suggest that the transoid form of the C-Ag^I-C pair is the most stable conformation,^[85] and that the homoduplex C₂₀-Ag₂₀-C₂₀ is stable in the parallel but not in the antiparallel strand orientation.^[86]

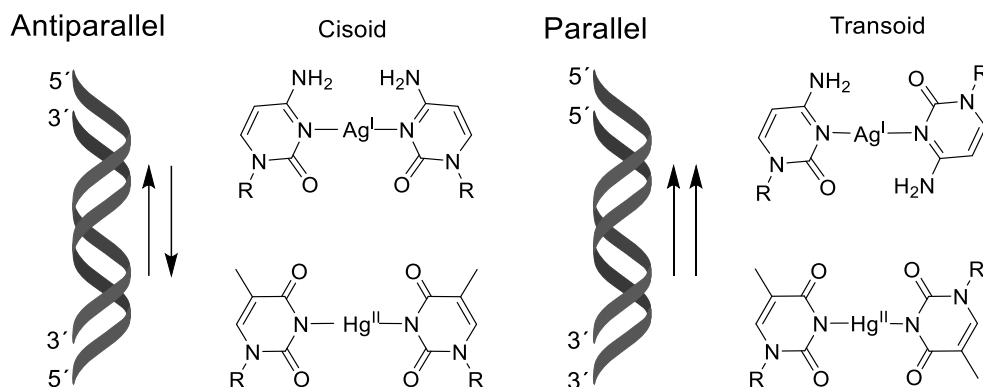


Figure 16. Different orientations of oligonucleotide strands and T-Hg^{II}-T and C-Ag^I-C pairs.

With purine-rich sequences, a parallel duplex can form through metal-mediated base pairing at the Hoogsteen face. A metal-mediated pair between artificial 6-furynylpurine nucleobases^[201] can support formation of both antiparallel and parallel duplexes when Ag^I ions coordinate between N1s, and parallel duplexes when coordination occurs between N7s.^[202] Also, 1-deazaadenine pairing to thymine via one silver ion^[107] and 1,3-dideaza-adenine pairing to thymine via two silver ions^[203] occur through the Hoogsteen face and could form a parallel duplex in theory, but the orientation of the duplexes remained unknown in these studies. Hoogsteen pairing

can also facilitate the formation of a triple-helical oligonucleotide. Normally, stable Hoogsteen pairs occur between A and T, and pairing between C and G requires protonation of N3 of cytosine, so a slightly acidic medium is needed. Proton can be replaced by a metal ion, such as a silver ion, to pair through the Hoogsteen face to form a triplex.^[204] So far, triplex stabilization with the natural nucleobases by metal-mediated pairing has been limited to C-Ag^I-G-C and C-Cu^{II}-G-C base triples.^[204,205] Among artificial nucleobases, pyridine nucleobases^[70], 5-mercuricytosine^[137] and 2,6-dimercuriphenol^[148] have been found to stabilize triple-helical oligonucleotides. Also, a sequence containing only hydroxypyridone nucleobases can form a triple helical structure stabilized by octahedral Fe^{III}-mediated triples.^[206] Within a PNA structure, 2,2'-bipyridine can stabilize the triple-helical structure via Ni^{II}- or Fe^{II}-mediated base pairing^[207]

The formation of more complicated DNA structures such as i-motifs and G-quadruplexes can also be induced by metal ions (Figure 17). i-motifs can be formed in cytosine-rich sequences with parallel-oriented duplexes, which are stabilized by CH⁺-C base pairs.^[208] Silver ions were suggested to replace protons and thus stabilize the i-motif structure.^[209] Interestingly, later studies have shown that spectroscopic signals that was characterized to the i-motif structure might be caused of intermolecular hydrogen bonding.^[89,109] Cu^I ions were also observed to replace protons and to form C-Cu^I-C pairs in the i-motif structure. As Cu^I and Cu^{II} ions have different coordination geometries, the secondary structure can be controlled by oxidation, reduction, pH, or the presence of copper ion or a copper ion chelator (Figure 17).^[210] G-quadruplexes are formed from two or more planar guanine tetrads, where four guanines hydrogen bond via WC and Hoogsteen faces stabilized by a central metal ion, usually K⁺ or Na^I.^[208] In the first example of a G-quadruplex stabilized by other metal ions, four G-rich oligonucleotides containing a 1,2,4-triazole moiety at the terminus were able to form a stable G-quadruplex containing the metal tetrads stabilized by Cu^{II} or Ni^{II} ions (Figure 17).^[211,212] The T-Hg^{II}-T pair was also introduced in the loop section of the G-quadruplex to increase thermal stability and decrease the flexibility of the structure.^[213] As discussed previously, metal nanowires can be formed by lining up consecutive Hg^{II}- or Ag^I-mediated pairs.^[88,97] but similar can be achieved by many artificial metal-mediated pairs such as S-Cu^{II}-S pairs.^[111,214] Those all have the potential to act as molecular wires or magnets, and magnetic and charge transfer properties across metal-DNA duplexes have been the subject of many studies.^[215-219]

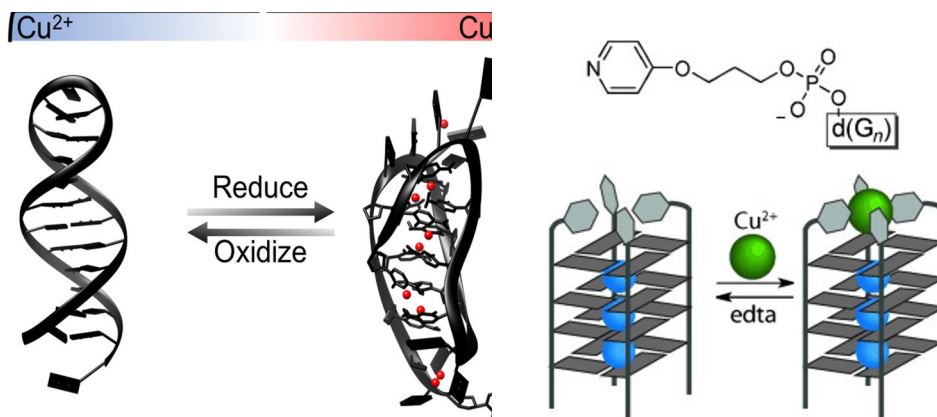


Figure 17. Formation of i-motif by copper ions, reproduced from ref. 210, and copper ion stabilized G-quadruplex. Reprinted with permission from D. M. Engelhard, R. Pievo, G. H. Clever, *Angew. Chemie - Int. Ed.* **2013**, 52, 12843–12847. © 2013 WILEY-VCH Verlag GmbH & Co. KGaA, Weinheim.^[212]

Different oligonucleotide structures can be controlled in more detail with oligonucleotide “devices” or “switches,” where metal ions could reversibly change the conformations of the oligonucleotide. As a simple example, cytosine- or thymine-rich oligonucleotides can change their conformation between single-stranded and hairpin structures depending on the presence of Hg^{II} - or Ag^{I} -ions.^[64,71] One fascinating application of this is the on-off switch controlling Taq DNA polymerase activity.^[220] A hairpin-forming aptamer inhibits polymerase activity, but Hg^{II} -ions can induce a conformation change by forming the T- Hg^{II} -T pair. The conformation change releases the aptamer from the enzyme allowing polymerase reaction to proceed. The addition of cysteine that binds Hg^{II} -ions restores the aptamer and its inhibition function.

1.4.2 Detection of single nucleotide polymorphisms

One potential application for metal-mediated base pairs is the detection of a single nucleotide polymorphism (SNP) in genetic code. Those differences can be used as biomarkers for diseases, and the differences affect the response of drug treatments.^[221–224] Hence, the concept of personalized medicine has been proposed based on the single mutations in the genetic code. One method used for SNP detection is oligonucleotide hybridization probes^[225–229], for example fluorescent molecular beacons.^[230–237] Lately, metal ions have been applied for these probes and used to recognize SNPs.

The most studied metal pairs, T- Hg^{II} -T and C- Ag^{I} -C, have been introduced to detect SNPs by Torigoe *et al.*^[238] Double-stranded oligonucleotides, where one

strand contains a fluorophore and the other strand a quencher close to each other, were examined with perfectly matched and mismatched target strands by both UV melting temperature and fluorescence measurements. Reasonable differences in both the T_m value and the fluorescence intensity of the DNA duplex in the presence and absence of Hg^{II} - and Ag^{I} -ions were observed. The T_m values increased because a stable metal pair was formed when silver or mercury ions were coordinated into C-C and T-T mismatches, respectively. Similarly, the fluorescence quenches as stable duplexes are formed, and the fluorophore and the quencher end up closer to each other, allowing the detection of T-T and C-C mismatches.

Molecular beacons containing metal-mediated base pairs have also been developed (Figure 18).^[171,239–241] In principle, the molecular beacon consists of a hairpin forming oligonucleotide containing a fluorophore at one and a quencher at another terminus. When a complementary strand binds into the hairpin, a duplex is formed, and fluorescence is observed as the quencher and the fluorophore are separated. The approach of Jash *et al.* is capable of discriminating the pyrimidine nucleobases cytosine and thymidine.^[171,240] It relies on the discrimination power of the artificial nucleobase **P** in the presence of silver ions. The metal-mediated pair formed between cytosine and **P** is highly stabilized, which causes the opening of the hairpin and thus a higher fluorescence signal. The thymine- Ag^{I} -**P** pair is not as stable, and the hairpin form is favored over the duplex.

Similar beacon systems with different approaches were proposed by Yang *et al.* and Lin *et al.* (Figure 18).^[239,241] In those, metal-mediated base pairs are formed into the stem section of the hairpin. Both stems contain multiple thymine mismatches, and the hairpin can be formed only in the presence of Hg^{II} ions. If a fully complementary target sequence with the hairpin is available, a duplex can be formed. Depending on the stability of duplex versus hairpin, equilibrium moves towards either form, which is observed from the fluorescence intensity. In other words, a mismatched target strand leads to the retention of the hairpin and quenching of fluorescence, whereas the presence of the perfectly matched target strand leads to the formation of fluorescent duplex form. As the hairpin and the duplex are in equilibrium, changing the Hg^{II} -ion concentration allows to control the hybridization kinetics and thermodynamics.^[239]

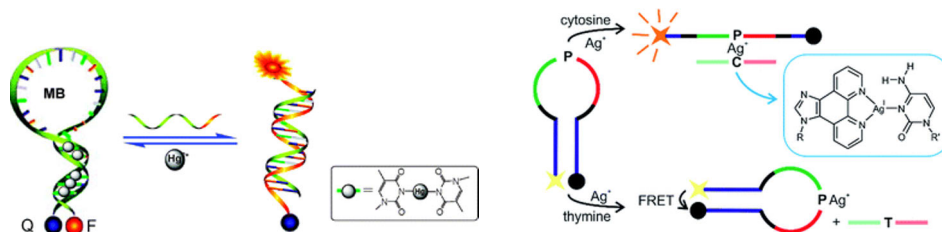


Figure 18. Principle of molecular beacons using metal-mediated pairs. In the left picture, T-Hg^{II}-T pairs are formed in the stem of the beacon. Reproduced from Ref. 239 with permission from the Royal Society of Chemistry. In the right picture, **P** nucleobase is discriminating complementary strands based on opposite nucleobase. Reproduced from Ref. 171 with permission from the Royal Society of Chemistry.

1.4.3 Therapeutic and diagnostic potential of metal-mediated base pairing

High hybridization affinity promoted by the metal ions would make metallated oligonucleotides useful for the selective targeting of biological structures in diagnostic or therapeutic applications. Oligonucleotides containing organopalladium or -mercury components are stable in metal-deficient and dilute conditions and hold the potential to work as high-affinity probes for biological structures. High thermal stabilities of duplexes have been observed with organometallic analogs (discussed in chapter 1.2.2), which would be beneficial when targeting short biologically relevant nucleic acid structures such as miRNAs.^[242] Therapeutic applications of these organometallic oligonucleotides are still scarce, but recently for the first time, palladated oligonucleotide has been utilized as a splice correcting agent.^[157] The delivery of palladated oligonucleotides into cells was possible *in vitro* using standard protocols, and the metallated oligonucleotide worked as a splice-correcting agent more efficiently than the corresponding unmetalled oligonucleotide.

2 Aims of thesis

Increasing interest in metal-mediated base pairing has emerged in the last decades leading to possible applications for nanotechnology, therapeutics and diagnostics. Numerous different metal-mediated base pairs have been developed, where usually a metal ion is coordinated between nucleobases. One drawback is a low stability in metal-deficient conditions. This can be overcome with covalently metallated nucleobases or kinetically inert metal-coordination complexes. Stable metallated oligonucleotides could be used for targeting nucleic acid structures such as miRNAs. Metal-mediated base pairs have been studied by various methods. Typically, easy methods like UV and CD spectroscopy are used, but those only produce information of the global effects on nucleic acid structures, leaving detailed local environment unknown. Most reliable information on metal-mediated base pairing in oligonucleotide structures is achieved by crystallizing the metallated oligonucleotides or labeling nitrogen atoms of nucleobases with ^{15}N , which allows detailed NMR studies of metal-mediated base pairing. However, crystallization of metallated oligonucleotides is not a trivial task, and isotope labeling is a costly method for general use. Also, some artificial nucleobase analogs are only achieved after a long and complicated synthesis before the potential properties are known. Therefore, more straightforward methods for screening potential nucleobase analogs and investigating their properties are needed. Local properties of metal-mediated base pairs can be investigated by fluorescence nucleobase analogs^[40,101] or sensitive ^{19}F NMR nucleobase analogs^[243,244].

For these goals, we have developed a fluorescent probe for screening purposes and ^{19}F -labeled nucleobase analogs for detailed ^{19}F NMR studies of double-helical oligonucleotides. ^{19}F NMR is sensitive to the changes in the electrical and environmental structure around the fluorine label, and would offer a new way to detect and study metal-mediated base pairs, and allow gathering more knowledge of the conformations and the binding modes of metal pairs in double-helical structures.

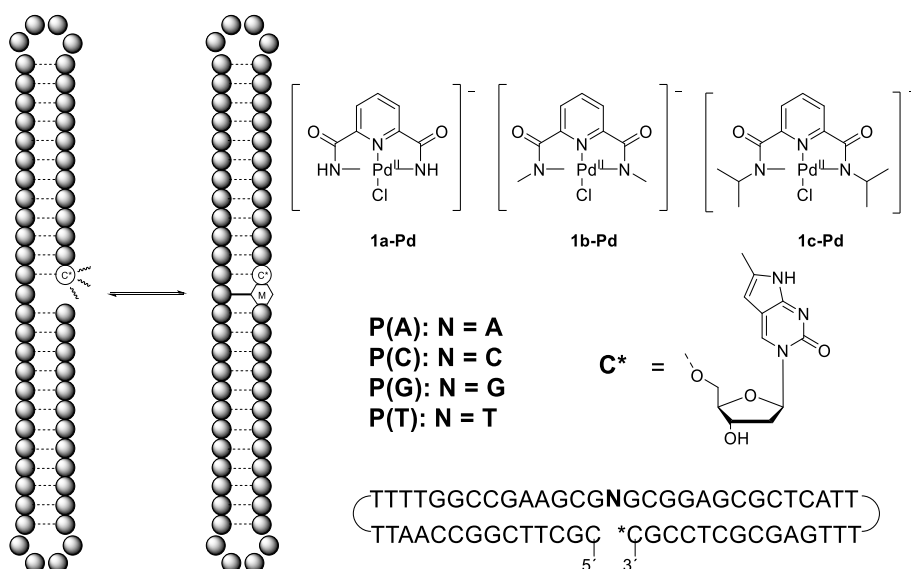
The aims of the thesis can be summarized as follows:

- I Develop a method for screening metallated nucleobase analogs
- II Synthesize fluorine-containing nucleobases that are capable of metal-mediated base pairing.
- III Evaluate local base pairing of the ^{19}F NMR probes towards canonical nucleobases

3 Results and Discussion

3.1 Probing molecules capable of metal-mediated base pairing at monomer level

In the first part of the thesis, the goal was to develop a fluorescent probe to estimate the potential of different small molecules for metal-mediated base pairing. The aim was to get preliminary information on binding before a laborious and time-consuming synthesis. In other words, the affinity and selectivity of small molecules towards different canonical nucleobases were evaluated without incorporating the nucleobase analogs into an oligonucleotide structure. Monomer level studies by NMR have given important information on binding properties.^[153] However, monomer studies are unable to reveal the effects of the binding in secondary structures of oligonucleotides. For this purpose, self-complementary oligonucleotide probes based on fluorescence quenching of a fluorescent nucleoside analog, pyrrolo-C (Scheme 1), were synthesized. Pd^{II} chelates (**1a-c-Pd**), studied previously at monomer level by NMR, were used as model compounds.^[153] Fluorescence titrations with these compounds were conducted. From titration results, the association and dissociation constants were calculated and compared to those from the monomer studies.



Scheme 1. Principle of developed oligonucleotide probe and used Pd^{II}-chelates.

3.1.1 Synthesis of the fluorescent oligonucleotide probes

The oligonucleotide sequence was planned to form a self-complementary structure, leaving one nucleotide gap between the terminuses (Scheme 1). The double hairpin structure was used to ensure effective and concentration-independent hybridization of the stem regions. The single-nucleotide gap was flanked by the fluorescent nucleobase analog pyrrolo-C. It emits higher wavelengths (c.a. 450 nm), and fluorescence is quenched by the stacking effect of neighbor nucleobases.^[245,246] The binding of a planar aromatic molecule to the target nucleobase should, hence, be detectable through changes in fluorescence intensity. Four different probes, **P(A)**, **P(C)**, **P(G)** and **P(T)**, where only the unpaired nucleotide opposite to the gap varies (A, C, G or T), were synthesized by automated oligonucleotide synthesis. Oligonucleotides were cleaved from the solid support by standard ammonolysis and purified by RP-HPLC. An increased temperature of 70 °C was used to prevent the hybridization of the oligonucleotide during purification. Purified oligonucleotides were characterized by ESI-TOF MS.

3.1.2 Fluorescence measurements

Fluorescence emission spectra were recorded between 420 and 480 nm, the excitation wavelength being 350 nm. Sample composition was 3 μM fluorescent oligonucleotide in 20 mM cacodylate buffer (pH = 7.4; $I(\text{NaClO}_4) = 50 \text{ mM}$) and the concentration of metal chelates varied from 0 to 5 μM. Every sample was heated to 90 °C and allowed to cool slowly to 25 °C before starting measurements. Oligonucleotides were titrated using 0.33, 0.66, 1, 2 and 5 μM concentrations of dipicolinamide and its N², N⁶-dialkylated derivatives and Pd^{II} chelates of the same compounds. Emission of pyrrolo-C behaved as expected, showing a broad emission with a maximum at approximately 450 nm that decreased, as in previous studies,^[245,246] after the addition of the metal chelates (Figure 19). However, with the reference compounds (uncomplexed ligands and nucleosides), fluorescence intensity remained unchanged even at a high concentration (0.1 M), indicating weaker or nonspecific binding. The average of three measurements in every ligand concentration was used to construct titration curves. All probes behaved similarly with **1a-Pd** chelates, and one equivalent was almost enough to decrease fluorescence to saturation level. The highest fluorescence decreases were observed with the purine probes **P(A)** and **P(G)** where the position of the metal surrogate might be deeper in the nucleobase stack leading to stronger quenching of pyrrolo-C. Results with the more sterically demanding chelates **1b-Pd** and **1c-Pd** showed a lower, but in most cases detectable, decrease of fluorescence intensity. With **1b-Pd** and **1c-Pd**, saturation was not reached in this range of concentrations and quite linear curves were observed. Fluorescence results suggest that the Pd^{II}- complexes are most likely

bound into the gap in the middle of the oligonucleotide. Also results from sterically more restricted Pd-chelates support this since fluorescence was decreasing. Other metal ions (Cu^{II} , Ag^{I} , Ni^{II} , Zn^{II} , Cd^{II} and Hg^{II}) were also tested in the presence of ligands **1a-c**. Cu^{II} showed affinity one magnitude lower than the Pd-chelates, whereas changes caused by the other metal ions were too small for reliable detection.

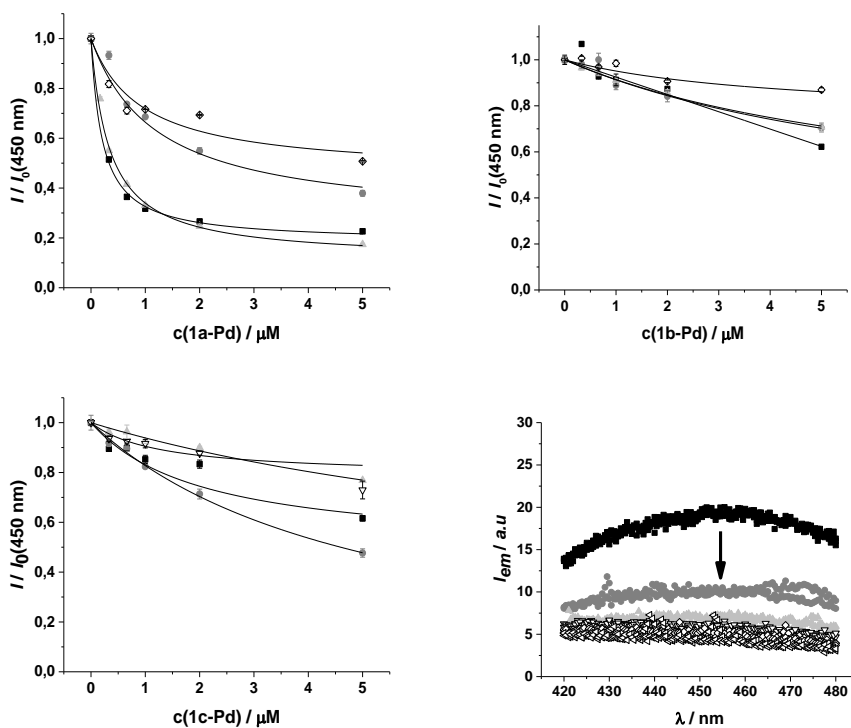


Figure 19. Fluorescence intensity at 450 nm as a function of Pd-chelate concentrations. Black squares = **P(A)**, grey circles = **P(C)**, light grey triangles = **P(G)** and white diamonds = **P(T)** Example of fluorescence behavior after addition of metal chelates.

Dissociation constants (K_d) were calculated from normalized titration curves using Equation 1, where I_∞ is fluorescence intensity at infinite chelate concentration. Dissociation constants were then converted to stability constants (Table 1).

Equation 1.
$$\frac{I}{I_0} = (I_\infty - 1) \frac{c(\text{chelate})}{K_d + c(\text{chelate})} \quad (1)$$

Table 1. Stability constants of the ternary complexes formed by the metal chelates **1a-Pd**, **1b-Pd** and **1c-Pd** with the oligonucleotide probes P(A), P(C), P(G) and P(T); pH 7.4 (20 mM cacodylate buffer); $I(\text{NaClO}_4) = 50 \text{ mM}$; $T = 25^\circ\text{C}$.

PROBE	K [10^5 M^{-1}]		
	1a-Pd	1b-Pd	1c-Pd
P(A)	48 ± 5	n.a ^a	5 ± 3
P(C)	6 ± 1	1.0 ± 0.7	1.9 ± 0.3
P(G)	27 ± 2	1.4 ± 0.3	0.9 ± 0.5
P(T)	15 ± 6	2 ± 1	8 ± 4

a) Could not be determined reliably

Fluorescence results on base pairing within the double-helical oligonucleotide were compared to NMR results of the same compounds at the monomer level (Figure 20).^[153] In the oligonucleotide, all Pd^{II}-mediated base pairs were stabilized, most likely due to base stacking. However, the effect of the metal was crucial because stabilization was not observed when using metal-free ligands. The binding modes detected by NMR at the monomer level most probably prevail also within a double-helical structure. In other words, the less bulky chelate **1a-Pd** binds to N1 and the bulkier chelates **1b-Pd** and **1c-Pd** to N7 of purine bases, while in the case of pyrimidines the binding site is N3 regardless of the chelate. In any of these binding modes, base stacking and hydrophobic interactions may provide additional stabilization. At the monomer level, the bulkiest chelate **1c-Pd** has the highest affinity for adenine, cytosine and uracil, whereas in the oligonucleotide, less bulky chelates showed the highest affinities. The different affinities for monomer and oligomer targets are, hence, associated with the constrained environment of the binding gap. A rotation around the N-Pd bond decreases the steric hindrance of alkyl groups in monomeric Pd^{II}-mediated base pairs. However, in the double-helical oligonucleotide, rotation around the N-Pd bond is not possible, as it would disrupt the structure. However, the net effect even with bulky chelates is favorable compared to monomer level, which suggests that oligonucleotide probes are more suitable to evaluate base-pairing properties before incorporating candidates into a double-helical oligonucleotide.

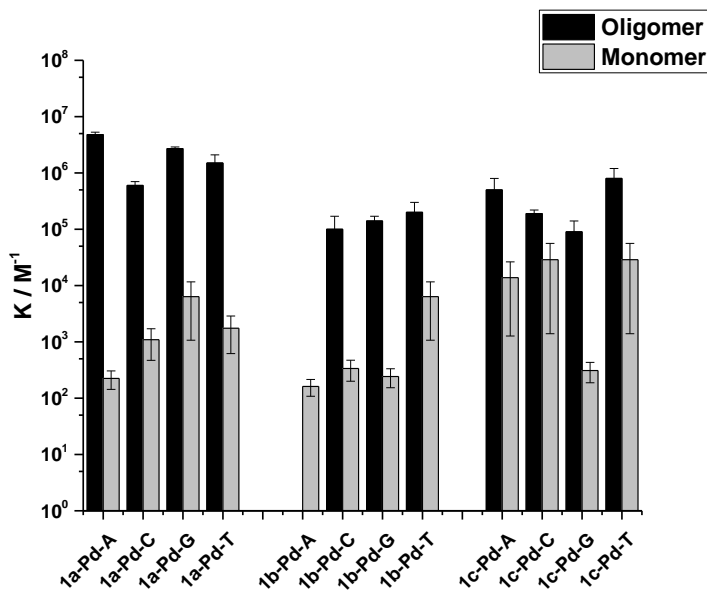


Figure 20. Stability constants for Pd^{II}-mediated base pairs between **1a**, **1b** and **1c** and the canonical nucleobases in the oligonucleotide probes (black columns) and in solution (grey columns); pH 7.4 (20 mM cacodylate buffer) / 7.2 (120 mM phosphate buffer). The error bars represent the standard deviations of the non-linear least-squares fits of the experimental data to Equation 1.

3.2 Recognition of metal-mediated base pairing by ¹⁹F NMR

In the second part of the thesis, ¹⁹F NMR was applied to detect metal-mediated base pairing and to get more detailed information on the immediate surroundings of the metal-mediated base pair. Firstly, two different fluorine-containing C-nucleoside analogs were synthesized and incorporated into oligonucleotides (**ON(F)** and **ON(F3)**) (Table 2 & Figure 21). The oligonucleotides were covalently mercurated and the mercuration reactions were monitored by ¹⁹F NMR spectroscopy. The attached mercury atom had a massive impact on the fluorine shift in the case of **ON(F-Hg)** but a much smaller effect in the case of **ON(F3-Hg)**. Melting temperature studies were conducted with mercurated **ON(F-Hg)** and **ON(F3-Hg)** and unmercurated **ON(F)** and **ON(F3)** to evaluate the effect of the metal ion on stabilities of double-helical oligonucleotides. Four different complementary oligonucleotides, where only the nucleobase opposite to the fluoroprobes varied (A, C, G or T), were tested to evaluate the discrimination power of the probe. ¹⁹F NMR studies were applied to gain detailed information on the local environment of the nucleobase analogs. Also, discrimination between canonical nucleobases was evaluated.

Table 2. Oligonucleotide sequences used in the study.

OLIGONUCLEOTIDE	SEQUENCE
ON F	5'-C ^m GAGC ^m FC ^m TGGC ^m -3'
ON F-Hg	5'-C ^m GAGC ^m F ^{Hg} C ^m TGGC ^m -3'
ON F3	5'-C ^m GAGC ^m F ₃ C ^m TGGC ^m -3'
ON F3-Hg	5'-C ^m GAGC ^m F ₃ ^{Hg} C ^m TGGC ^m -3'
ON X	5'-GCCAGXGCTCG-3'

[a] F refers to 5-fluoro-2-methylaniline, F^{Hg} to 3-fluoro-2-mercuri-6-methylaniline, F₃ to 2-trifluoromethylaniline, F₃^{Hg} 2-trifluoromethyl-6-mercurianiline and C^m to 5-methylcytosine. X refers to A,C,G,T.

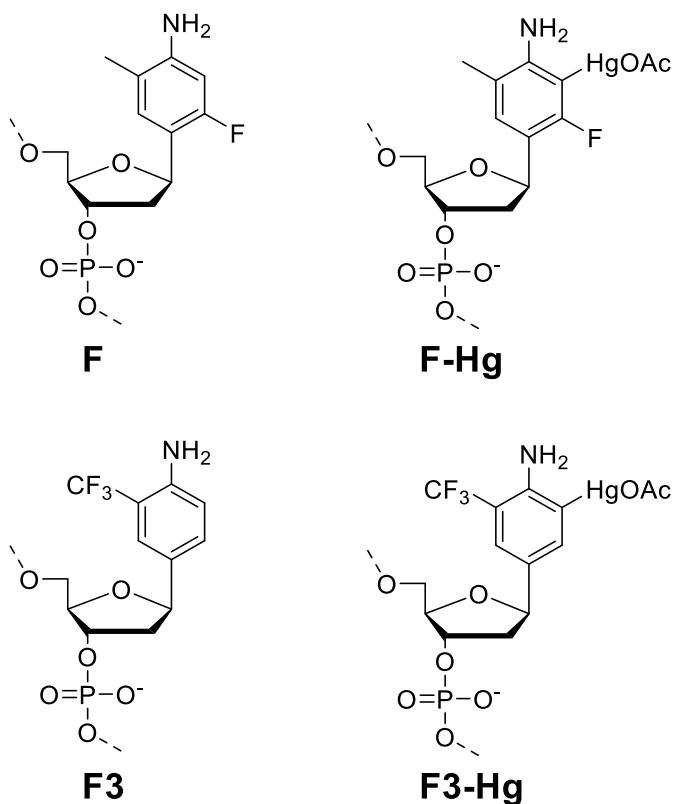
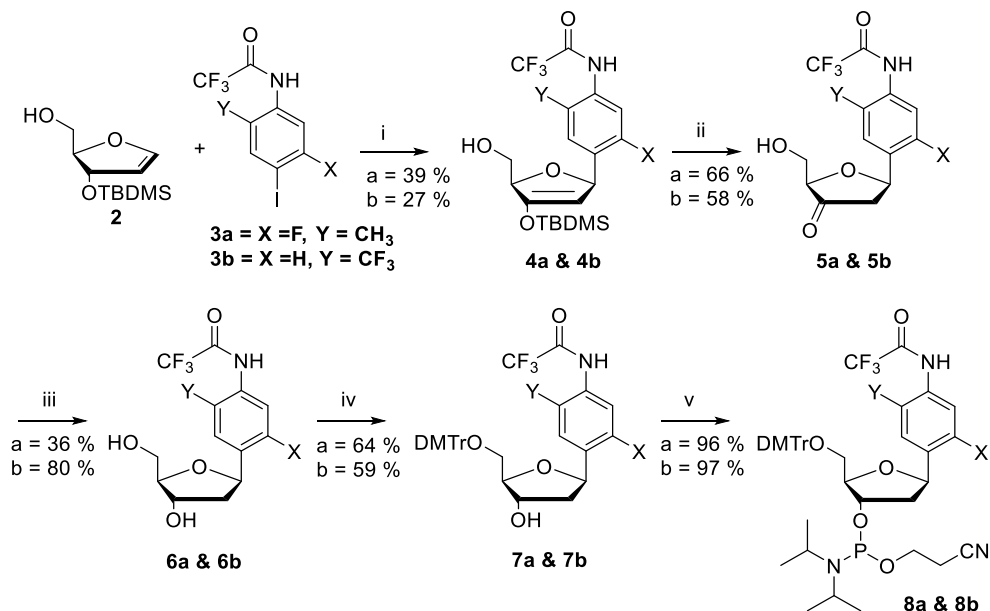


Figure 21. Structures of 3-fluoro-6-methylanilinenucleotide, its mercurated analog, 2-trifluoromethylanilinenucleotide and its mercurated analog.

3.2.1 Synthesis of the mercurated oligonucleotides



Scheme 2. Synthesis of Phosphoramidate Building Block **x**. Conditions: (i) Pd[(*t*-Bu)₃P]₂, *N,N*-dicyclohexylmethylamine, dioxane, 70 °C; (ii) Et₃N·3HF, THF, 0 °C; (iii) NaBH(OAc)₃, MeCN, AcOH; (iv) DMTrCl, pyridine; (v) 2-cyanoethyl *N,N*-diisopropylchlorophosphoramidite, Et₃N, CH₂Cl₂.

3.2.1.1 Synthesis of the Phosphoramidite building block **F** and **F3**

Syntheses of the phosphoramidite building blocks (**8a** and **8b**) are presented in Scheme 2. Heck reaction was used for the coupling of {(2*R*,3*S*)-3-[(*tert*-butyldimethylsilyl)oxy]-2,3-dihydrofuran-2-yl}methanol (**2**)^[247] and trifluoroacetylated 3-fluoro-4-iodo-6-methylaniline (**3a**) or trifluoroacetylated 2-trifluoroaniline (**3b**), yielding 39 % and 27 % desired β-anomers **4**, respectively.^[248] Desilylation and reduction steps were conducted as previously reported.^[152] 5'-O was 4,4'-dimethoxytritylated, and 3'-O was phosphitylated by conventional methods to give phosphoramidites **8a** and **8b**.

3.2.1.2 Oligonucleotide synthesis

The synthesized phosphoramidites **8a** and **8b** were incorporated into oligonucleotides. Oligonucleotides **ON(F)** and **ON(F3)** (Table 2) were synthesized by an automated DNA/RNA synthesizer at 1.0 μM scale. Standard phosphoramidite coupling cycles were used, except that capping was not used to prevent acetylation

of the amino group of **8** with **ON(F)**, and more labile capping with phenoxyacetic anhydride was used with **ON(F3)**. Also, a longer coupling time (300 s) was used in the case of **8**. Cleavage of the oligonucleotides from the solid support was done by standard ammonolysis. Crude oligonucleotides were purified by RP-HPLC and characterized by ESI-TOF.

Mercuration of **ON(F)** was conducted using an excess of mercury acetate (4 equiv.) in aq. 0.1 M NaOAc solution at 55 °C overnight. Mercuration of **ON(F3)** was more complicated, and a higher (30 equiv.) excess of $\text{Hg}(\text{OAc})_2$ was used in aq. 5 mM NaOAc solution at 55 °C overnight. To prevent off-target mercuration, 5-methylcytosines were used instead of cytosines.^[138] The mercuration reaction of **ON(F)** was monitored by ^{19}F NMR spectroscopy, and after disappearance of the ^{19}F NMR resonance signal of starting material, the mixture was purified by RP-HPLC and the authenticity of the product verified by ESI-MS. Mercuration of **F** proceeded smoothly as expected due to the ortho/para directing activating amino- and o/p directing fluoro substituents. In the chromatogram of **ON(F-Hg)**, two major signals with different retention times were observed and separated, both corresponding to the correct product. Reinjection of the purified fractions resulted in HPLC chromatograms containing both earlier and later eluting peaks of **ON(F-Hg)** (Figure 22). Slowly equilibrating inter-/intramolecular secondary structures might be formed between/within the mercurated oligonucleotides.

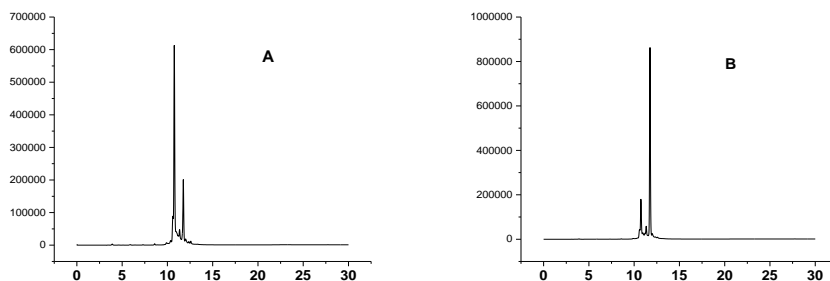


Figure 22. HPLC chromatograms of reinjected **ON(F-Hg)** peaks (**A**= first eluting fraction and **B**=later eluting fraction). Oligonucleotides were eluted with a linear gradient from 5 to 35% of acetonitrile in aq. 0.1 M triethylammonium acetate over 25 min, flow rate 1 mL min^{-1} .

Mercuration of **F3** proved to be much more sluggish, likely because of the deactivating nature of the CF_3 group.^[141,249] Apparently, the activating nature of the amino substituent was not enough to fully compensate for the deactivating nature of CF_3 . Longer reaction times did not increase the yield due to the simultaneous fragmentation of oligonucleotides, so the reaction time had to be kept moderate. For

the **ON(F3)**, the huge excess of Hg^{II} ions broadened HPLC signals a lot, presumably through nonspecific coordination to the oligonucleotide. To overcome this problem, 0.1 M EDTA in 0.01 M Tris-HCl was added just before the purification. Much sharper peaks in the chromatogram were observed, indicating the soundness of this approach. As with the mercuration of **ON(F)**, two different peaks were collected and found to be the correct product (Figure 23). However, the ratio of the two peaks was different, and the first eluted peak was much smaller. Despite these challenges, a sufficient amount of **ON(F3-Hg)** was collected for hybridization studies. The mercuration site was confirmed by enzymatic digestion, exposing a small amount of **ON(F-Hg)** and **ON(F3-Hg)** to P1 nuclease, which cleaves single-stranded oligonucleotides to corresponding nucleoside-5'-monophosphates. Mercuration seemed to retard the digestion, and the mercurated dimers of **F** and **F3** with methylcytosine monophosphates were the smallest mercurated fragments observed. In addition, only mercurated fragments containing **F** or **F3** were observed, confirming a selective mercuration of the modified nucleotide. Mild conditions favoured mercuration into the C2 in **F** and C6 in **F3** because of the directing properties of the substituents of the aniline rings. Due to the small quantity, we did not try NMR characterization to verify further the site specificity of the mercuration (mercuration of C2/C6 of the aniline rings). In previous studies, the site of the mercuration was verified in monomer level by ^{13}C NMR.^[148] However, the site of mercuration in monomer level does not predict well the behaviour in oligonucleotide stage.

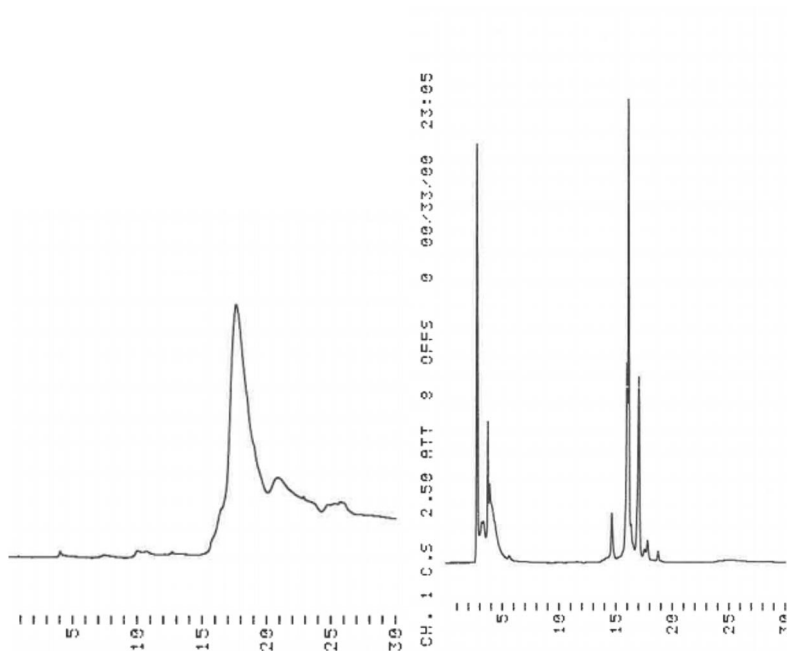


Figure 23. Chromatograms of the mercuration reactions of **ON(F3)** without and with the added EDTA solution before injection. Oligonucleotides were eluted with a linear gradient from 5 to 35% of acetonitrile in aq. 0.1 M triethylammonium acetate over 25 min, flow rate 1 mL min⁻¹.

Mercuration of **ON(F)** and **ON(F3)** was monitored by ¹⁹F NMR spectroscopy until the starting material had disappeared. After purification of the product mixture of **ON(F)**, an extreme, approximately 20 ppm downfield shift of signal was observed, whereas the resonance signal of **ON(F3)** barely shifted at all (Figure 24). The ¹⁹F resonance signal of **ON(F-Hg)** was observed as two broad humps at -98.38 and -100.30 ppm, whereas the resonance signal of **ON(F3)** at -62.28 ppm was diminished, and a broad hump appeared in the same region. After purification, a resonance signal was observed at -62.26 ppm. Broader humps might correspond to slowly equilibrating secondary structures, such as self-folding and/or dimerization, promoted by Hg^{II}-mediated base pairing.^[96] Increasing temperature sharpened resonance signals in the case of **ON(F-Hg)**, presumably by denaturing such secondary structures. Also, a double peak of the desired product was observed in HPLC chromatogram. In the case of **ON(F3-Hg)** and **ON(F3)**, temperature ramp was conducted, where **ON(F3)** showed a linear temperature-dependent passive shift (Figure 25). Instead, **ON(F3-Hg)** showed a non-linear, slightly sigmoidal profile, consistent with intramolecular Hg^{II}-mediated pairing. These observations support the hypothesis of self-folding or dimeric structures of **ON(F-Hg)** and **ON(F3-Hg)**.

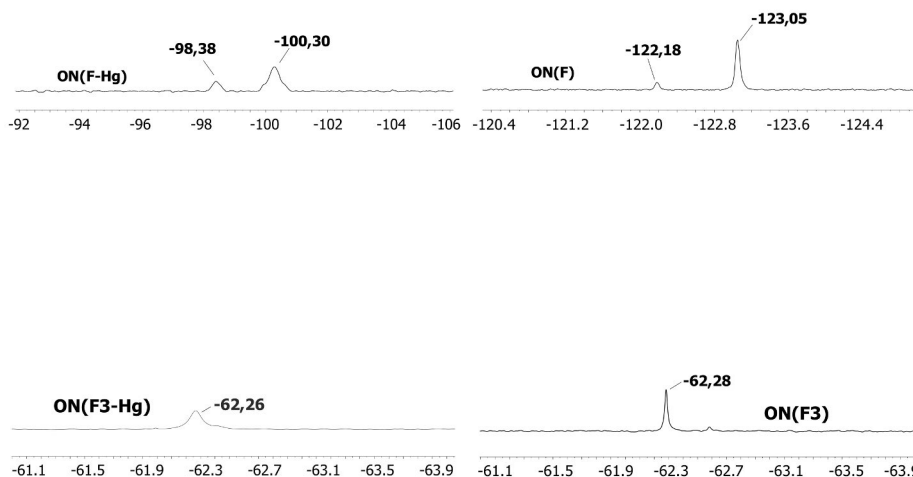


Figure 24. ^{19}F NMR spectra of mercurated and umercurated single-stranded oligonucleotides. Sample composition: [oligonucleotides] = $20\ \mu\text{M}$ for **ON(F-Hg)** and $10\ \mu\text{M}$ for **ON(F3-Hg)**; pH = 7.0 (10 mM cacodylate buffer, $\text{D}_2\text{O-H}_2\text{O}$, 1:9, v/v.); $I(\text{NaCl}) = 0.1\ \text{M}$.

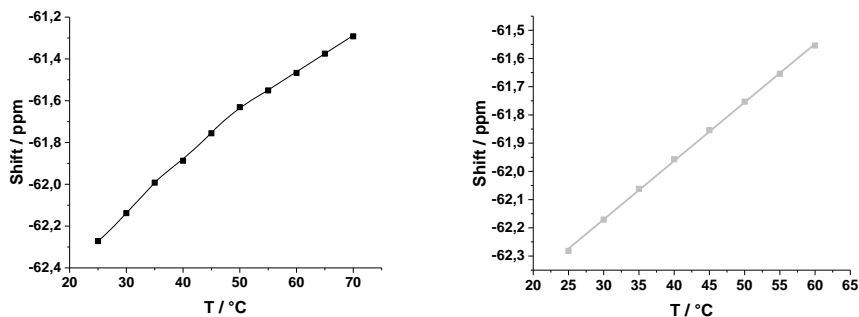


Figure 25. ^{19}F NMR shifts of **ON(F3-Hg)**(left) and **ON(F3)** as a function of temperature. Sample composition: [oligonucleotides] = $10\ \mu\text{M}$; pH = 7.0 (10 mM cacodylate buffer, $\text{D}_2\text{O-H}_2\text{O}$, 1:9, v/v.); $I(\text{NaCl}) = 0.1\ \text{M}$.

3.2.2 Hybridization studies of the mercurated oligonucleotides

3.2.2.1 Melting temperature analysis of ON(F-Hg) and ON(F3-Hg)

The hybridization properties of **ON(F-Hg)** were first studied by UV melting temperature measurements. Samples of **ON(F-Hg)** and **ON(F)** ($2.0 \mu\text{mol L}^{-1}$) in 10 mmol L^{-1} cacodylate buffer ($\text{pH} = 7.0$, $I = 0.10 \text{ M}$ adjusted with NaCl) were prepared, including 1 equiv. of a complementary oligonucleotide, either **ON(A)**, **ON(C)**, **ON(G)** or **ON(T)** (Table 2). Melting profiles were acquired by recording the absorbance at 260 nm over a temperature range of 10–80 °C. Sigmoidal and monophasic melting profiles were observed except for **ON(F-Hg)•ON(T)**, in which case the profile was biphasic (Figure 26 & Figure 27). All melting temperatures are presented in Figure 28. In the case of **ON(F-Hg)**, all mercurated double helices were much more stable than the corresponding unmercurated duplexes except for **ON(F-Hg)•ON(A)**. In the case of **ON(F-Hg)•ON(A)**, the stabilization was modest, only 2 °C relative to **ON(F)•ON(A)**. Stability of **ON(F-Hg)•ON(C)** ($51.9 \pm 0.4 \text{ °C}$) was comparable to stability on natural 11mer duplex containing a C-G pair. The highest stabilities were observed with **ON(F-Hg)•ON(G)** ($59.0 \pm 0.1 \text{ °C}$) and **ON(F-Hg)•ON(T)** ($66.7 \pm 0.2 \text{ °C}$), ~25 and ~28 °C higher than with their unmetallated counterparts, respectively. Melting temperatures of duplexes formed by **ON(F-Hg)** with different complementary strands **ON(X)** ($X = \text{A, C, G or T}$) were separated clearly from each other by at least 6 °C, which is enough to allow applications in the detection of single nucleotide polymorphisms.^[84]

In the case of duplexes formed by **ON(F3-Hg)**, the melting temperature of **ON(F3-Hg)•ON(A)** ($40.4 \pm 0.5 \text{ °C}$) was only ~2 °C higher than that of corresponding unmercurated duplex. In all other cases, T_m values of the mercurated duplexes were much higher, $47.2 \pm 0.3 \text{ °C}$ for **ON(F3-Hg)•ON(C)**, $58.0 \pm 0.9 \text{ °C}$ for **ON(F3-Hg)•ON(G)** and $61.0 \pm 0.4 \text{ °C}$ for **ON(F3-Hg)•ON(T)**. The melting temperatures were well separated (by ~17 °C for **C**, ~28 °C for **G** and ~26 °C for **T**) compared to those of the corresponding unmercurated duplexes.

Both mercurated oligonucleotides showed similar T_m values for duplexes with a given complementary strand, except for a small difference between **ON(F3-Hg)•ON(G)** and **ON(F3-Hg)•ON(T)**. Also, the order of the affinities for the complementary oligonucleotides (**ON(T>G>C>A)**) were similar for both mercurated oligonucleotides. The hybridization results are in line with the previous reports of the stabilizing effect of Hg^{II} -mediated base pairing with 5-mercuricytosine.^[96] The role of the mercury ion in the stabilization of **ON(F-Hg)•ON(X)** duplexes was also verified by repeating the experiments in the presence of 2-mercaptoethanol, a strongly Hg^{II} coordinating agent. After adding an excess of

2-mercaptoethanol, the melting temperatures dropped back to the level of the unmercurated duplexes. The thiol group of the 2-mercaptoethanol has been observed to bind tightly to mercury, and it can outcompete the nitrogen donors of nucleobases.^[151] On the other hand, demercuration in the presence of 2-mercaptoethanol has also been observed in previous reports but only after several heating and cooling cycles.^[148] Both cases will lead to the destabilization of the duplexes stabilized by Hg^{II}-mediated base pairs. Finally, melting profiles of the **ON(F)•ON(X)** duplexes were also recorded in the presence of 1 equiv. of Hg(ClO₄)₂ on to exclude effects on duplex stability by nonspecific coordination of Hg^{II}. The results showed hardly any difference to unmercurated **ON(F)•ON(X)** duplexes, which highlights the importance of fixing the Hg^{II} ion covalently to the predetermined site.

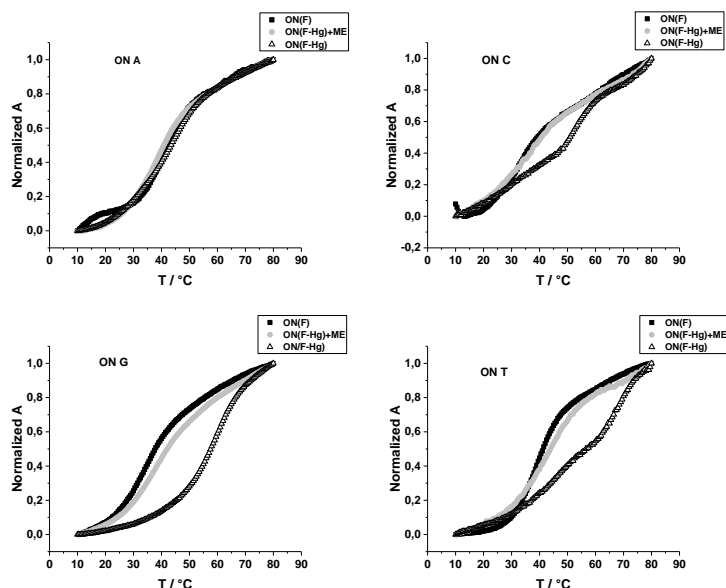


Figure 26. Melting profiles of **ON(F-Hg)•ON(X)**, **ON(F)•ON(X)**, **ON(F-Hg)•ON(X)+ME**. X = A (upleft), C (upright), G (downleft) and T (downright). Sample conditions: [oligonucleotides] = 2.0 μ M; pH = 7.0 (10 mM cacodylate buffer); $I(\text{NaCl}) = 0.1$ M; [2-mercaptoethanol] = 0/30 μ M.

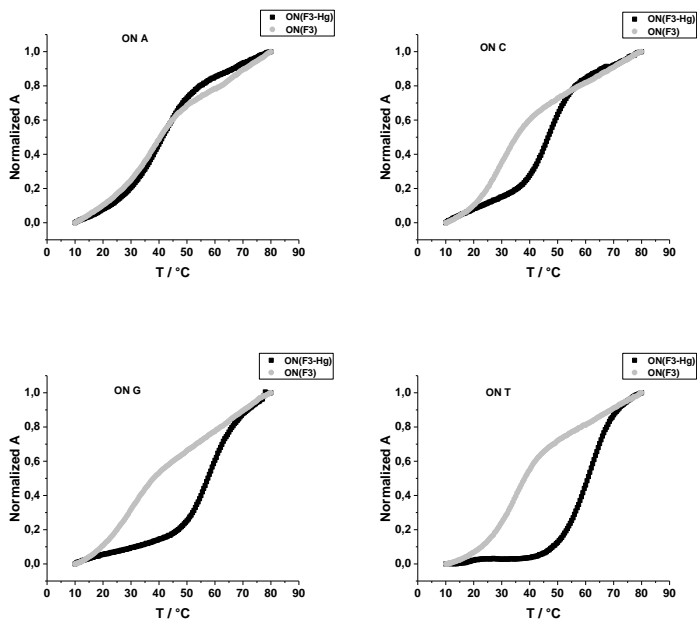


Figure 27. Melting profiles of **ON(F3–Hg)•ON(X)**, **ON(F3)•ON(X)**. X = A (upleft), C (upright), G (downleft) and T (downright). Sample conditions: [oligonucleotides] = 2.0 μM; pH = 7.0 (10 mM cacodylate buffer); I(NaCl) = 0.1 M.

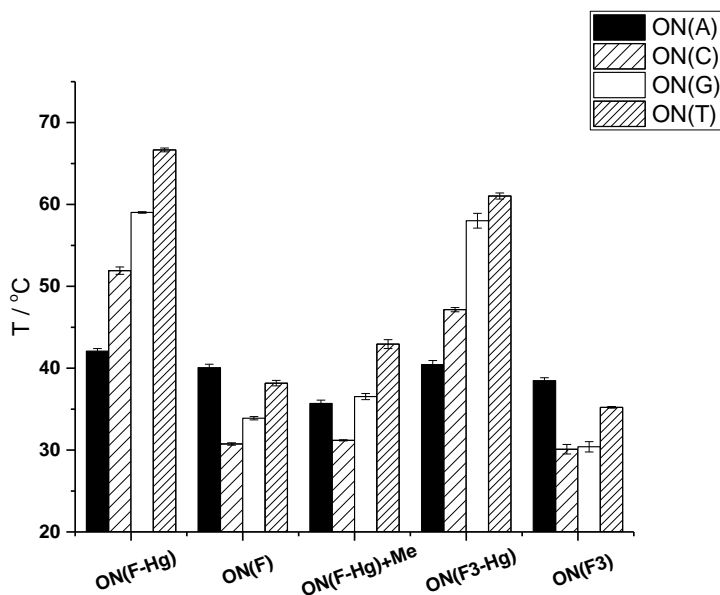


Figure 28. Melting temperatures of **ON(F–Hg)**, **ON(F)**, **ON(F3–Hg)** and **ON(F3)** with the complementary oligonucleotides **ON(A)**, **ON(C)**, **ON(G)**, and **ON(T)**. In case of **ON(F–Hg)**, melting temperatures were also determined in the presence of 2-mercaptoethanol (ME).

3.2.2.2 Evaluation of thermodynamic parameters

The enthalpy and entropy of hybridization have been usually reported to be significantly less negative for oligonucleotides including Hg^{II}-mediated base pairs, because of desolvation of the mercury ion and fewer bonds formed compared to Watson-Crick base pairing.^[47,55,56,96] To evaluate these parameters in the **ON(F-Hg)•ON(X)** and **ON(F3-Hg)•ON(X)** duplexes, van't Hoff plots for hybridization of all the duplexes were constructed from the UV melting temperature data.^[250] Less negative enthalpies and entropies of hybridization were observed for all **ON(F-Hg)•ON(X)** duplexes, as expected (Table 3 & Table 4). Less negative values compared to unmercurated duplexes support the hypothesis of the stabilizing effect of mercury-mediated base pairing being largely attributable to desolvation of the Hg^{II} ion. However, in the case of the **ON(F3-Hg)•ON(X)** duplexes, where the only difference is the bulky trifluoromethane substituent at C6 instead of fluorine at C3, more negative enthalpies and entropies were obtained compared to **ON(F3)•ON(X)** duplexes. The difference was particularly pronounced when the organomercury nucleobase was paired with pyrimidines. The bulky trifluoromethyl group could increase hydrophobic interactions^[251–253], but different bond lengths of metal-mediated base pairs (4 Å)^[48] compared to hydrogen-bonded Watson-Crick base pairs (3 Å) might also explain the results. When pairing with a pyrimidine base, 2-mercuri-6-trifluoroaniline might position itself deeper in the base stack, restricting rotation of the trifluoromethane substituent, which decreases entropy. When pairing with the longer purine bases, the trifluoromethane substituent would be positioned closer to the major groove, allowing rotation. Restricted rotation could also assist the formation of a F—H—N hydrogen bond between the amino and trifluoromethyl groups, previously observed with benzanilidines^[254,255], leading to more favorable enthalpy.

Table 3. Enthalpies of hybridization for oligonucleotide duplexes. Sample conditions: [oligonucleotides] = 2.0 μM; pH = 7.0 (10 mM cacodylate buffer); I(NaCl) = 0.1 M; [2-mercaptoethanol] = 0/30 μM.

	$\Delta H^\circ / \text{KJ Mol}^{-1}$			
	ON(A)	ON(C)	ON(G)	ON(T)
ON(F)	-240 ± 5	-200 ± 5	-185 ± 2	-245 ± 3
ON(F-Hg)	-155 ± 1	-101 ± 1	-156 ± 1	-109 ± 1
ON(F-Hg)+ME	-192 ± 2	-149 ± 1	-159 ± 2	-151 ± 1
ON(F3)	-250 ± 1	-276 ± 3	-251 ± 5	-252 ± 2
ON(F3-Hg)	-260 ± 2	-373 ± 6	-260 ± 6	-310 ± 2

Table 4. Entropies of hybridization for oligonucleotide duplexes. Sample conditions: [oligonucleotides] = 2.0 μM ; pH = 7.0 (10 mM cacodylate buffer); $I(\text{NaCl}) = 0.1 \text{ M}$; [2-mercaptoethanol] = 0/30 μM .

	$\Delta S^\circ / J \text{ Mol}^{-1}$			
	ON(A)	ON(C)	ON(G)	ON(T)
ON(F)	-640 \pm 20	-520 \pm 20	-480 \pm 10	-660 \pm 10
ON(F-Hg)	-380 \pm 10	-200 \pm 10	-360 \pm 10	-220 \pm 10
ON(F-Hg)+ME	-500 \pm 10	-360 \pm 10	-390 \pm 10	-360 \pm 10
ON(F3)	-694 \pm 4	-798 \pm 9	-717 \pm 15	-704 \pm 6
ON(F3-Hg)	-716 \pm 7	-1050 \pm 18	-662 \pm 19	-813 \pm 8

3.2.3 CD spectropolarimetric analysis of ON(F-Hg) and ON(F3-Hg)

CD spectropolarimetric studies were used to confirm the secondary structure of all duplexes. The measurements were carried out using oligonucleotide concentration of 20 $\mu\text{mol L}^{-1}$ with ON(F-Hg) and 10 $\mu\text{mol L}^{-1}$ with ON(F3-Hg) and 1 equiv. of the complementary strand ON(X) in 10 mM cacodylate buffer, pH 7.0, $I = 0.10 \text{ M}$ adjusted with NaCl). Spectra were recorded between 200 and 400 nm at 10 °C intervals over a temperature range of 10–90 °C. With every oligonucleotide duplex, a minimum at 250 nm and a maximum at 280 nm were observed, characteristic of a typical B-type duplex. The minima and maxima diminished on increasing temperature indicating the loss of helicity of the duplex (Figure 29).

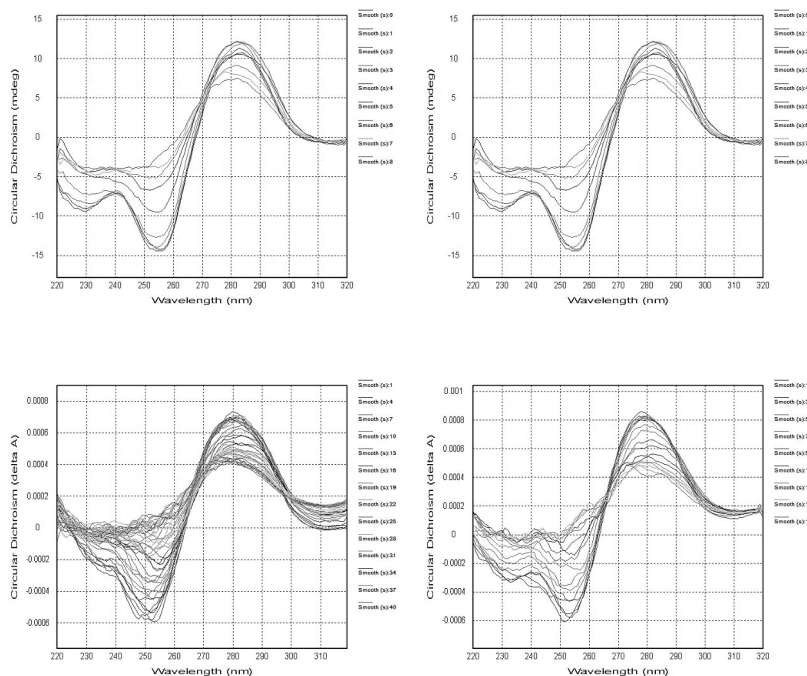


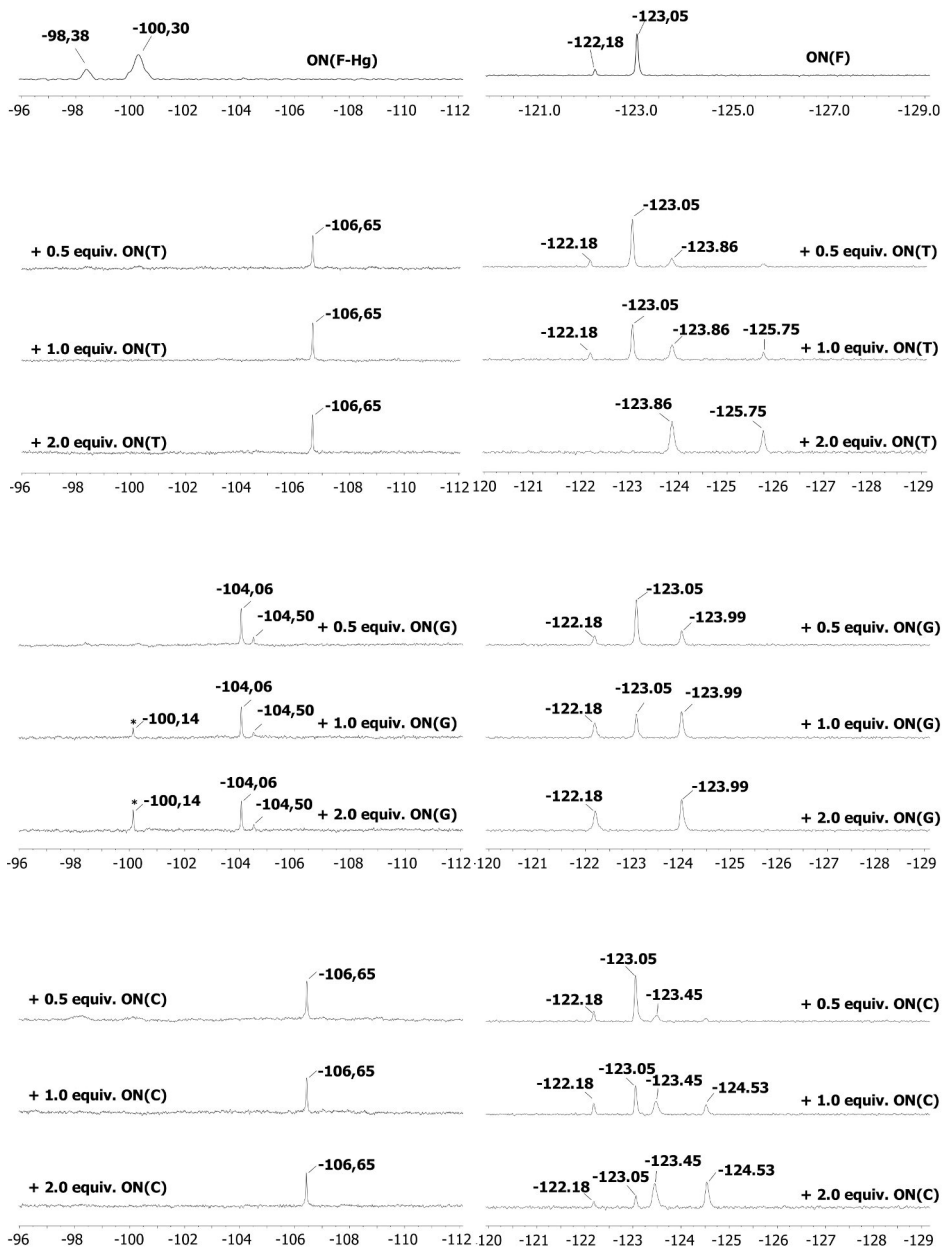
Figure 29. CD profiles of **ON(F-Hg)•ON(T)**, (upleft), **ON(F)•ON(T)** (upright), **ON(F3-Hg)•ON(T)** (downleft) and **ON(F3)•ON(T)** (downright). Sample conditions: [oligonucleotides] = 20, 10 or 10 μM ; pH = 7.0 (10 mM cacodylate buffer); $I(\text{NaCl}) = 0.1 \text{ M}$.

3.2.4 ^{19}F NMR measurements

3.2.4.1 ^{19}F NMR of ON(F-Hg) and ON(F3-Hg) duplexes

^{19}F NMR measurements were conducted using a concentration of 20 μM for **ON(F-Hg)** and **ON(F)**, 10 μM for **ON(F3-Hg)** and 5 μM for **ON(F3)** in 10 mM cacodylate buffer (pH = 7.0, $\text{D}_2\text{O}-\text{H}_2\text{O}$, 1:9, v/v, $I = 0,10 \text{ M}$ adjusted with NaCl) at 25 $^\circ\text{C}$. Both unmercurated single-stranded oligonucleotides showed two signals: at -122,18 ppm (minor) and -123,05 ppm (major) for **ON(F)** and at -62,28 ppm (major) and at -62,59 ppm (minor) for **ON(F3)**. Most likely the two signals correspond to *syn* and *anti* conformers of **F** and **F3**. At first, ^{19}F NMR measurements were conducted using 0.5, 1.0 and 2.0 equiv. of **ON(X)**. After adding **ON(X)** to the **ON(F)** sample, two extra signals appeared with varying intensities and different shifts depending on the complementary nucleobase. Addition of **ON(X)** to the **ON(F3)** sample, on the other hand, caused only one new signal to appear, upfield in the case of **ON(T,G,C)** and downfield in the case of **ON(A)**. Due to the decent affinities of duplexes, multiple signals were observed even in the presence of 2 equiv. of the complementary strand.^[256]

Mercurated oligonucleotides **ON(F-Hg)** and **ON(F3-Hg)** were titrated using 0.5, 1.0 and 2.0 equiv. of complementary **ON(X)**s (Figure 30 & Figure 31). Already after the addition of 0.5 equiv. to the **ON(F-Hg)** samples, sharp signals appeared upfield, indicating the formation of double-helical structures **ON(F-Hg)•ON(X)**. **ON(G)** also gave a minor signal at -104.50 ppm, which might refer to another binding mode, *i.e.* coordination to the N7 of guanine. After the addition of 0.5 equiv. of **ON(G)** and **ON(T)** into the **ON(F3-Hg)** samples, the initial signal decreased, and new clear signals were observed downfield at -62.48 ppm and -62.83 ppm, respectively. The addition of **ON(C)** did not have any visible changes in the ¹⁹F NMR spectrum. However, at elevated temperature two distinct signals were observed, proving that the signals of single-stranded **ON(F3-Hg)** and double-helical **ON(F3-Hg)•ON(C)** are overlapping at 25 °C. Two new signals at -63.43 and -62.55 ppm appeared with **ON(F3-Hg)•ON(A)**, and the **ON(F3-Hg)** signal remained. The signal from the **ON(F3-Hg)** was clearly visible even when 2 equiv. of **ON(A)** was added, suggesting weaker binding. The two new signals might correspond to binding of mercury to N1 and N7 of adenine, but overall the binding was obscure.



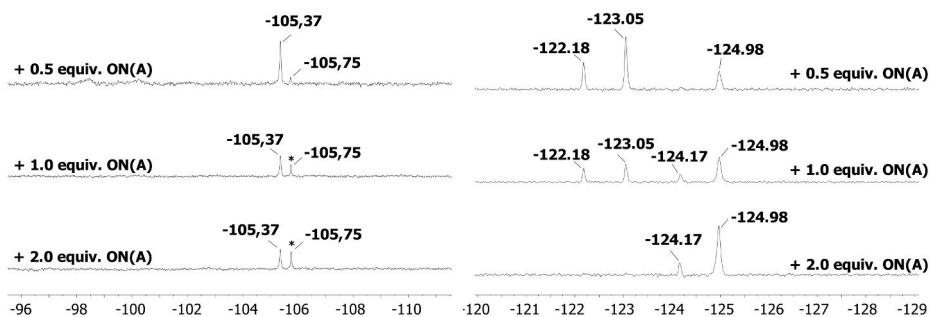
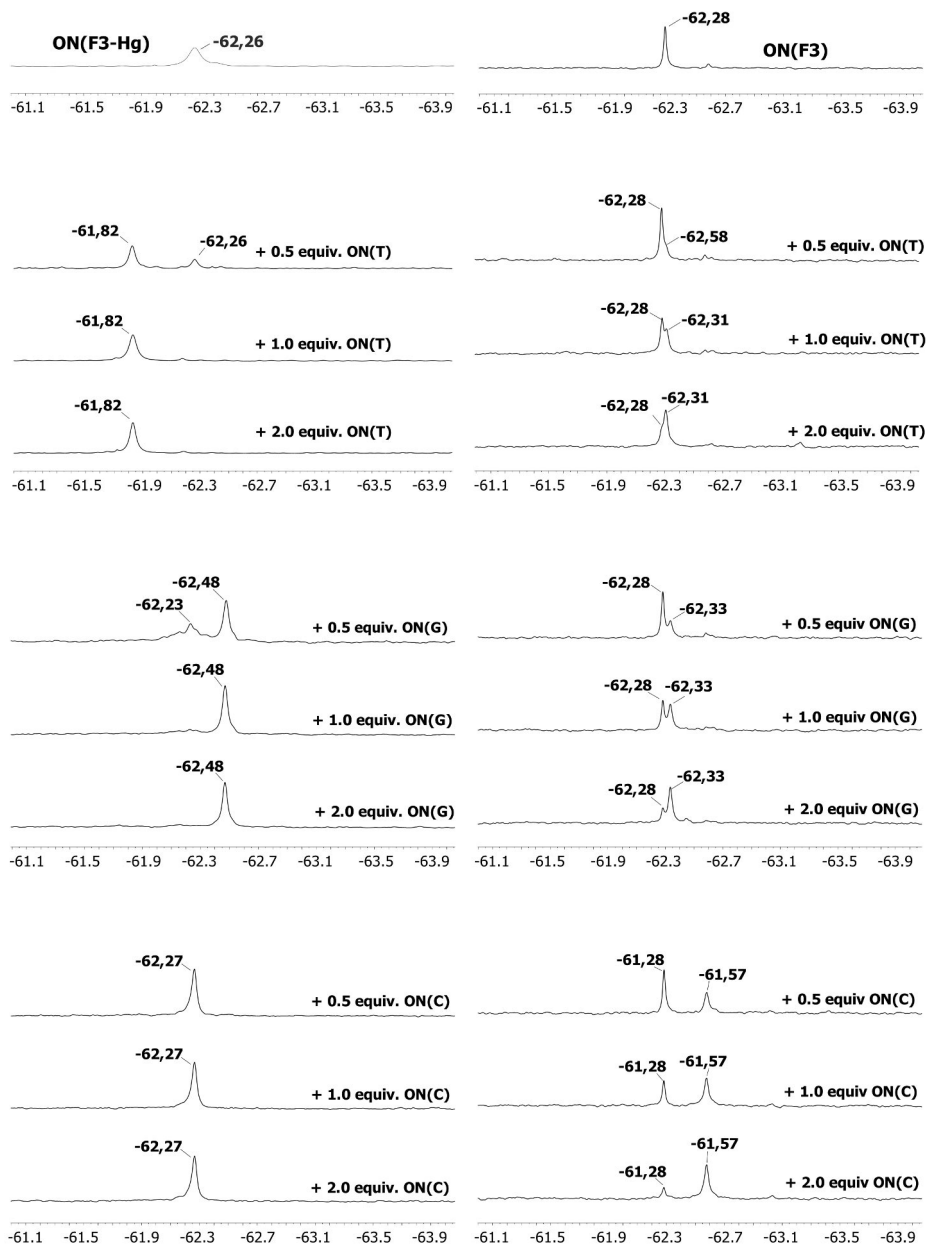


Figure 30. ^{19}F NMR titration of **ON(F-Hg)** and **ON(F)** with 0,5; 1 and 2 equiv of **ON(X)** at 25 °C.

When 1,0 and 2,0 equiv of **ON(X)** was added, the duplex signals strengthened, and the remaining broad signals of the **ON(F-Hg)** and **ON(F3-Hg)** diminished (Figure 30 & Figure 31). Thus, an equimolar amount of **ON(X)** was enough to diminish the signals of the mercurated single-stranded oligonucleotides for every case except **ON(F3-Hg)•ON(A)**. Interestingly, in the case of **ON(F-Hg)•ON(A)** and **ON(F-Hg)•ON(G)**, additional signals (marked with an asterisk) appeared at -105,75 ppm and -100,14 ppm, respectively. As the intensity of these additional signals increased at 2,0 equiv. of the complementary strand, a plausible ternary complex could be formed at low temperature within the tetrapurine tracts of **ON(A)** and **ON(G)**, which are stabilized by Hoogsteen-type Hg^{II} -mediated base pairing. These extra signals disappear when the temperature is increased gradually between the range of 40–45 °C. Similar observations were not detected with **ON(F-Hg)•ON(C or T)**, reference duplexes **ON(F)•ON(A or G)** and all **ON(F3-Hg)•ON(X)**.



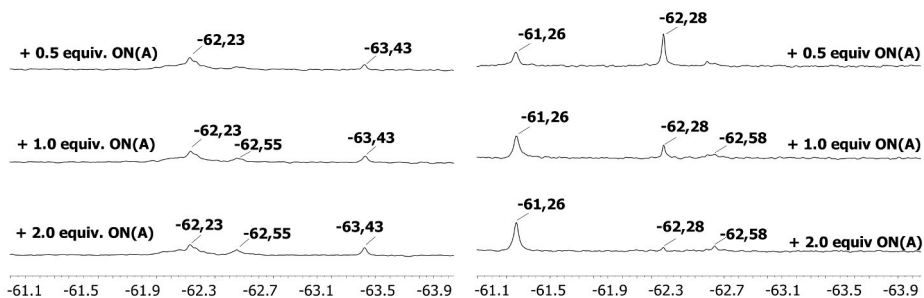


Figure 31. ^{19}F NMR titration of **ON(F3-Hg)** and **ON(F3)** with 0,5; 1 and 2 equiv of **ON(X)** at 25 °C.

3.2.4.2 Temperature elevated measurements

Temperature-elevated ^{19}F NMR measurements were conducted to evaluate the local melting temperatures of duplexes in the vicinity of the putative Hg^{II} -mediated base pairs and clarify the interpretation of the titration experiments, especially in the case of **ON(F3-Hg)•ON(X)**. With **ON(F-Hg)•ON(X)**, the capacity of the probe to detect local dissociation of the Hg^{II} -mediated base pair and its close environment was only evaluated with the two most stable duplexes, **ON(F-Hg)•ON(T)** and **ON(F-Hg)•ON(G)**. Sample compositions were 90 μM **ON(F-Hg)** in 10 mM cacodylate buffer (pH = 7.0, $\text{D}_2\text{O-H}_2\text{O}$, 1:9, v/v, $I = 0.1$ M adjusted with NaCl) and 1 equiv. of **ON(T or G)**. Increasing of the temperature shifted signals downfield (temperature-dependent passive shift of 0.02 ppm K^{-1}) and signals disappeared gradually at 70–85 °C in case of **ON(T)** and 63–78 °C in case of **ON(G)**. The signal areas were compared to an internal standard (4-fluorobenzoic acid) and plotted as a function of temperature. Sigmoidal curves were obtained, and the melting temperature values were determined as inflection points of the curves ($T_m = 76$ °C for **ON(T)** and 69 °C for **ON(G)**).

For the **ON(F3-Hg)•ON(X)** duplexes, more comprehensive evaluations were conducted. Measurements were carried over a range of 25–60 °C for unmercurated and 25–80 °C for mercurated duplexes. For unmercurated duplexes, the signals shifted downfield when the temperature was raised, corresponding to a temperature-dependent passive shift (0.02 ppm K^{-1}). Rough estimations of local melting temperatures were obtained based on areas of the ^{19}F NMR signals. Melting temperatures from ^{19}F NMR were in line with UV melting temperatures of the corresponding duplexes. Mercurated duplexes **ON(F3-Hg)•ON(T)**, **ON(F3-Hg)•ON(G)** and **ON(F3-Hg)•ON(C)** behaved similarly as the unmercurated duplexes (Figure 32). In other words, as the temperature was increased, the duplex signals gradually diminished, and new broader signals appeared corresponding to single-stranded **ON(F3-Hg)**. For **ON(F3-Hg)•ON(T)** and **ON(F3-Hg)•ON(C)**,

melting temperatures were extracted from the relative areas of duplex and single-stranded signals giving 65.5 °C and 54.4 °C, respectively. Determination of the T_m value of **ON(F3-Hg)•ON(A)** was not possible under these conditions as the spectra were unclear and contained multiple signals. In the case of **ON(F3-Hg)•ON(G)** duplex, overlapping signals of duplex and ss**ON(F3-Hg)** near the inflection point precluded reliable determination of T_m . (presented using dashed line in Figure 32B).

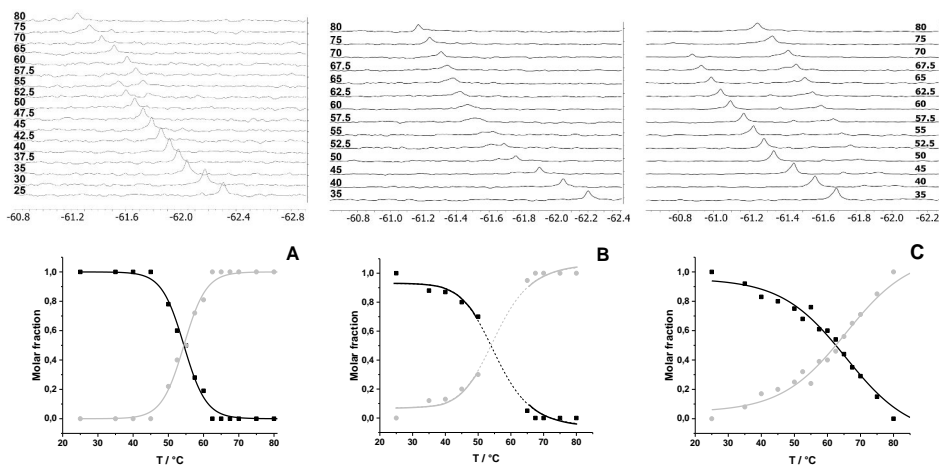


Figure 32. ^{19}F NMR temperature ramps and molar fractions of A) **ON(F3-Hg)•ON(C)**, B) **ON(F3-Hg)•ON(G)** and **ON(F3-Hg)•ON(T)**.

The melting profiles of **ON(F-Hg)•ON(G)** and **ON(F-Hg)•ON(T)** were also extracted from CD spectra using the same samples, allowing comparison of T_m values determined by independent methods (UV, CD and ^{19}F NMR) (Figure 33). UV melting is based on the loss of hydrogen bonding and base stacking, and CD melting on the loss of helicity, both related to the overall denaturation of the oligonucleotide duplex. Instead, ^{19}F NMR shows local dissociation in the proximity of the ^{19}F probe (**F-Hg**). UV melting profiles usually have a broader shift, and a clear inflection point is harder to detect, which may lead to different results between these measurements. In addition, the T_m -values extracted from UV results were higher than values extracted from ^{19}F NMR. However, due to broader UV profiles, partial hyperchromicity with **ON(F-Hg)•ON(T)** and **ON(F-Hg)•ON(G)** may be observed before the dissociation of the Hg^{II} -mediated base pair. All in all, the UV- and ^{19}F NMR melting temperatures were close to each other, indicating co-operative Hg^{II} -mediated base pairing and hybridization in the rest of the strands.

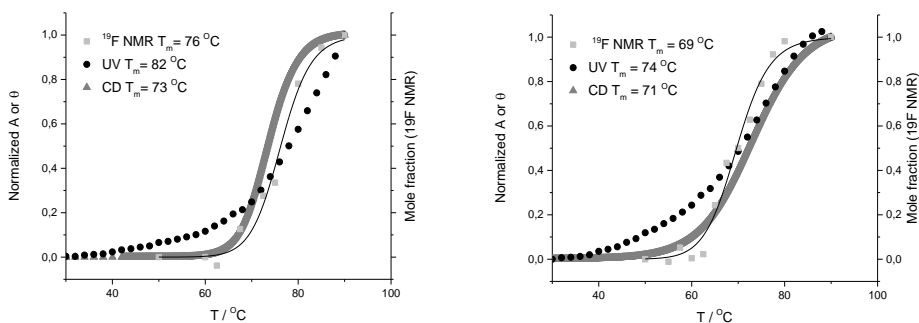


Figure 33. ^{19}F NMR melting curves of **ON(F-Hg)** versus UV and CD melting profiles with **ON(T)** (left) and **ON(G)** (right). Sample composition: 90 μM **ON** in 10 mM cacodylate buffer (pH = 7.0, $\text{D}_2\text{O-H}_2\text{O}$, 1:9, v/v, $I = 0.1$ M adjusted with NaCl).

3.3 Recognition of SNPs by F-Hg

In the third part of this thesis, the potential of **F-Hg** to discriminate nucleobases was evaluated in a molecular beacon system. As discussed in previous chapters, promising results on discrimination the canonical nucleobases by **F-Hg** were obtained with UV melting studies. This kind of discrimination could be applied to the identification of single nucleotide polymorphisms, as discussed in chapter 1.4.2.

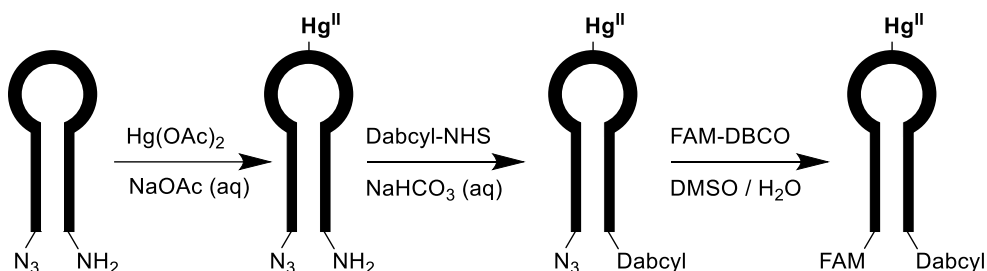
3.3.1 Synthesis of Beacon(F)

For this use, a hairpin-forming 27-mer oligonucleotide **B(F)** (Table 5) was synthesized by an automated DNA/RNA synthesizer following a standard phosphoramidite coupling cycle except that a more labile capping with phenoxyacetic anhydride was used. The sequence contained a six base pair stem and a 15mer loop region. Cytosines were replaced with 5-methylcytosines, as previously explained.^[138] At first, the synthesized oligonucleotide contained a 6-bromoalkyl group in the 5'-end and an amino group in the 3'-end for post-synthetic coupling of a fluorophore (fluorescein) and a quencher (dabcyl). Post-synthetic conjugation protocols were needed to prevent mercuration of the fluorescein and dabcyl moieties.

Table 5. Oligonucleotide sequences used in the study.

OLIGONUCLEOTIDE	SEQUENCE
B(F)	6-Fam-C ^m C ^m TAGC ^m TTC ^m GAGC ^m FC ^m TGGC ^m TTGC ^m TAGG-dabcyI
B(F-Hg)	6-Fam-C ^m C ^m TAGC ^m TTC ^m GAGC ^m F ^{Hg} C ^m TGGC ^m TTGC ^m TAGG-dabcyI
B(X)	6-FAM-CCTAGCTTGCCAGXGCTCGTTGCTAGG-dabcyI
ON(Y)	AAGCCAGYGCTCGAA
ON(F)	5'-C ^m GAGC ^m FC ^m TGGC ^m -3'
ON(F-Hg)	5'-C ^m GAGC ^m F ^{Hg} C ^m TGGC ^m -3'

[a] **F** refers to 5-fluoro-2-methylaniline, **F^{Hg}** to 3-fluoro-2-mercuri-6-methylaniline and **C^m** to 5-methylcytosine. **X** and **Y** refer to A,C,G,T



Scheme 3. Post-synthetic modifications of the molecular beacon.

Before the cleavage of oligonucleotides from support, the 5'-bromo group was converted to an azide by treating with an excess of tetramethylguanidium azide and NaI in dry DMF for 1.5 h at 60 °C. The crude oligonucleotide was purified by RP-HPLC and characterized by ESI-MS. A small amount of a phenoxyacetylated oligonucleotide was observed, which was converted to the desired product by treatment with aqueous methylamine: ammonia mixture (1:1, v/v). N₃-B(F)-NH₂ was mercurated by treatment with an excess of Hg(OAc)₂ (10 equiv.) in aqueous 5 mM NaOAc at 55 °C for 24 h (Scheme 3). The mixture was purified by RP-HPLC and identity of the purified product confirmed by ESI-MS. In contrast to the previously discussed 11mer oligonucleotides, the longer mercurated and unmercurated sequences, proved inseparable by a similar HPLC system^[249]. Nevertheless, mercuration proceeded smoothly, and only mercurated oligonucleotides were collected. DabcyI-NHS ester was coupled to the 3'-terminal amino group in 0.1 M aqueous NaHCO₃ (pH = 8.4), adding aliquots of ester in DMF and vortexing the reaction mixture. The reaction was monitored by RP-HPLC and purified after starting material had been depleted. After this, fluorescein-DBCO was coupled to the 5'-terminal azide group using strain-promoted azide-alkyne cycloaddition

(SPAAC). A DMF solution of FAM-DBCO and an aqueous solution of **ON** were mixed and vortexed overnight. The reaction mixture was purified RP-HPLC and identity of the purified product verified by ESI-MS. An unmercurated reference beacon **B(F)** was prepared in a similar way.

3.3.2 Evaluating the potential of F-Hg as an SNP probe

Before synthesis of **B(F-Hg)**, the potential of the mercurated oligonucleotide **ON(F-Hg)** to recognize opposite nucleobase in molecular beacon system was evaluated by fluorescence measurements with four commercial beacons **B(X)** (where **X** is either A,C,G,T), containing only canonical nucleobases. All beacons were complementary to **ON(F-Hg)** and only the nucleobase opposite to **F-Hg** varied. All samples containing one of the four beacons **B(X)** and 1 equiv. of **ON(F-Hg)** were excited with 495 nm wavelength, and fluorescence emission spectra were measured between 500–600 nm as a function of time (Figure 34). Fluorescence intensity slowly increased over time, and $t_{1/2}$ varied between 170 and 240 min depending on **X**. Commonly in molecular beacon systems, binding of the target strand (conformational changes of target strand to adapt the geometry of loop region) and dissociation of beacon stem section (formed duplex must overcome the energy barrier of dissociation of the stem) are the rate-limiting steps. For this reason, in the current beacon system, a short loop (15 nucleotides) and a relatively long stem (6 base pairs) retard hybridization.^[236] Also, the aforementioned tendency of **ON(F-Hg)** to exist as various secondary structures^[249] might affect the kinetics of hybridization. Also, slower hybridization kinetics has been observed with T-Hg^{II}-T pairs^[40,239] compared to hydrogen-bonded base pairs, so metal-mediated base pairing might be the actual reason for slower hybridization.

Apparent differences in the fluorescence intensities of **B(X)•ON(F-Hg)** having different nucleobase opposite to **F-Hg** were observed. At equilibrium, the order of intensities was **B(T)>B(G)>B(C)≥B(A)**, which is in line with our previous observation of affinities in **ON(F-Hg)•ON(X)** duplexes based on the UV melting temperatures. When the reference beacons **B(X)** were treated with 1 equiv. of **ON(F)**, no significant fluorescence increase was observed, indicating low affinity as expected based on the UV melting temperatures of the **ON(F)•ON(X)** duplexes.^[249] In other words, the equilibrium favors the initial state (the hairpin form). Overall, covalently bound mercury seems crucial for the beacon system because fluorescence increased dramatically only with the mercurated oligonucleotides.

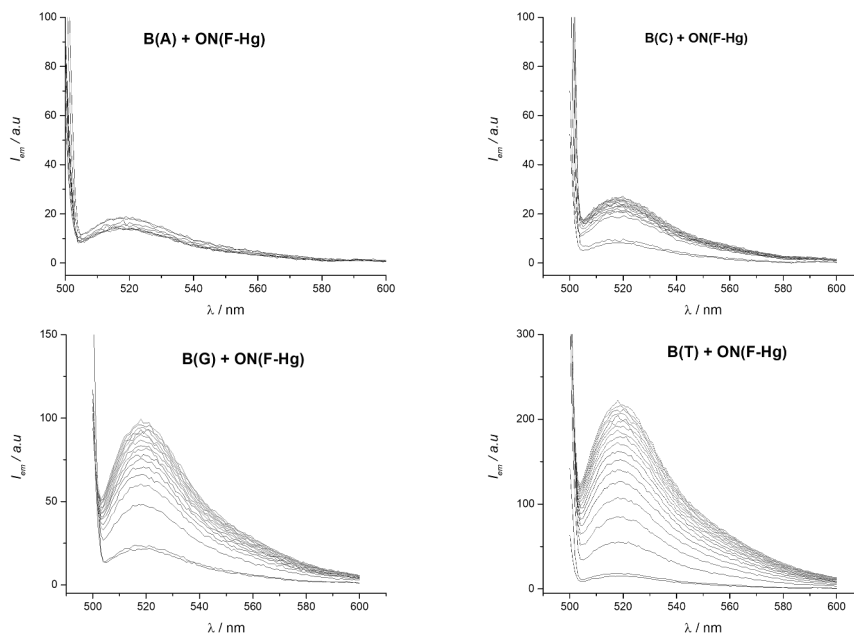


Figure 34. Preliminary fluorescence measurements with **B(X)•ON(F-Hg)**. Sample composition: 50 nM oligonucleotides, 50 mM NaClO₄, 2,5 mM Mg(ClO₄)₂ and 20 mM cacodylate buffer (pH = 7.4).

3.3.3 Fluorescence measurements of B(F-Hg)

The applicability of the organomercury beacon **B(F-Hg)** for detecting single nucleotide polymorphisms was evaluated with a similar fluorescence experiment as with the reference beacons **B(X)**. Fluorescence measurements of samples containing 50 nM **B(F-Hg)** and 5 equiv. of **ON(Y)** were conducted (Figure 35). Higher target sequence concentration (250 nM) was used to speed up the hairpin opening by hybridization. Also, target sequences were extended to 15mer to adjust the equilibrium to favor the duplex over the hairpin and possibly allow separation of cytosine and adenine. Fluorescences of the **B(F-Hg)•ON(Y)** duplexes were monitored until fluorescence intensities remained stable for at least 2 half-lives. The hybridization process of **B(F-Hg)•ON(Y)** was faster compared to **B(X)•ON(F-Hg)** ($t_{1/2} = 20\text{--}80$ min depending on **X** and **Y**), but still much slower compared to beacon-target complexes containing only canonical nucleosides.^[236] After longer times, fluorescence decreasing was observed, suggesting formation of more complicated structures at low temperatures.^[235] After the addition of different target strands **ON(X)**, fluorescence increased eightfold in the case of **ON(T)** and ninefold in the case of **ON(G)** compared to the initial fluorescence of **B(F-Hg)** before addition. When **ON(C)** or **ON(A)** were added, fluorescence intensity increase was mediocre. The order of intensities between different opposite nucleobases was **G>T>>C>A**,

and the differences were enough for robust separation of purine and pyrimidine nucleobases from each other. A more detailed examination of intensities allowed the discrimination of all canonical nucleobases. Reference measurements were carried out with unmercurated **B(F)** to highlight the effect of the covalently bound mercury. Fluorescence intensities were not changed at all after adding complementary strands, indicating a low affinity between **F** and canonical nucleobases. Also, after the addition of free Hg^{II} ions, intensities were more likely to decrease than increase. Hg^{II} ions might bind between thymines forming T- Hg^{II} -T base pairs at the beginning of the loop section, which would lengthen the stem by two base pairs and thus make the hairpin even more stable. The initial fluorescence level of **B(F)** was much higher than that of **B(F-Hg)**, in line with previous observations.^[171,240]

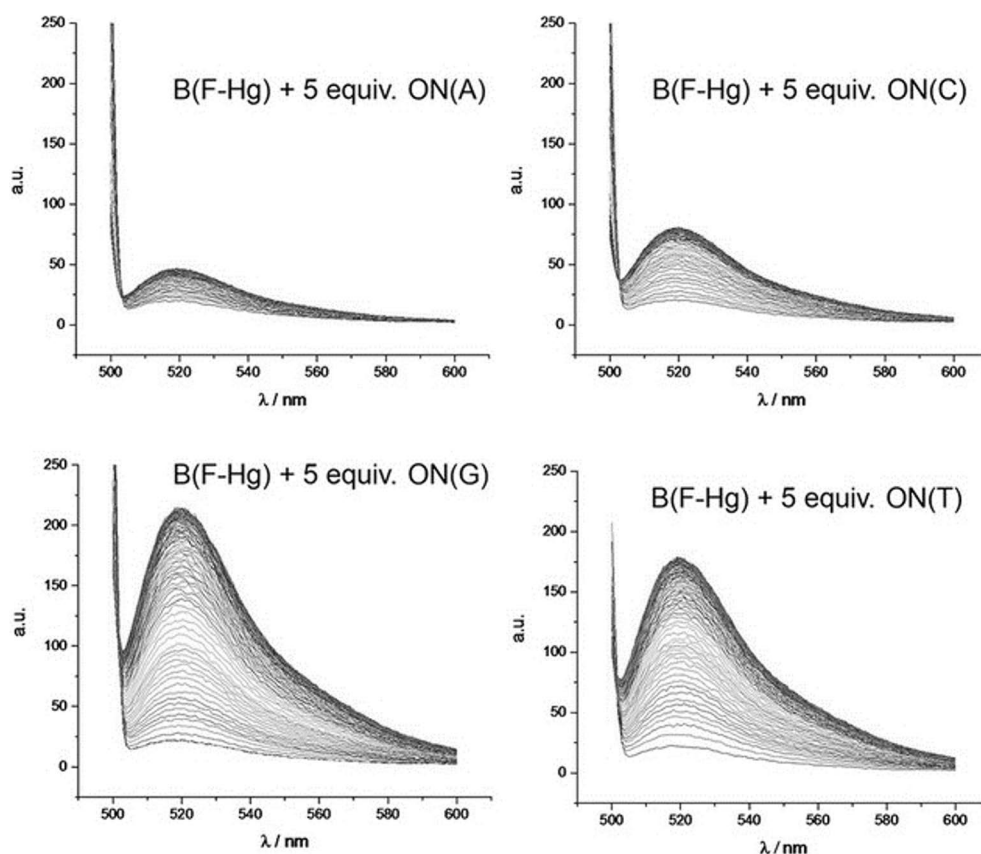


Figure 35. Fluorescence intensities of B(F-Hg)+5 equiv. **ON(Y)**. Measuring times: 0, 1, 3, 5, 7, 10, 13, 16, 20 min, then every 5 min until 60 min, then every 10 min up to 16 h at 25 °C. Sample composition: 50 nM beacon, 250 nM complementary strand, 50 mM NaClO_4 , 2,5 mM $\text{Mg}(\text{ClO}_4)_2$ and 20 mM cacodylate buffer (pH = 7.4).

3.3.4 Temperature-elevated fluorescence measurements

Temperature-elevated measurements were carried out to assess the behavior of the beacon with different target strands at different temperatures. Fluorescence intensities were measured with every **B(F-Hg)•ON(Y)** combination at 5 °C intervals over a 25–80 °C temperature range. Intensities at 520 nm were plotted as a function of temperature and normalized between the initial fluorescence and the highest measured fluorescence of each sample (Figure 36). In Scheme 4, the behavior of the beacon target complex is presented, and with all **ON(Y)** targets, the behavior of the beacon was quite similar. At the beginning of the heating cycle at low temperatures, the increased intensity might be caused by partial intra- or intermolecular hybridization of the beacon stems.^[235] Both of these effects decrease the fluorescence since some amount of the beacon is quenched. The top-level fluorescence at low temperatures indicates dissociation of the more complicated structures, leaving the duplex as the main form present. Next, dissociation of the duplex and concomitant formation of the hairpin structure causes a significant decrease in the fluorescence intensity, and eventually, denaturation of the hairpin into a random coil structure restores the fluorescence. The cooling cycle follows a different profile, where fluorescence stays low even at the low end of the temperature range, which is consistent with the slow hybridization of the metal-mediated duplex.

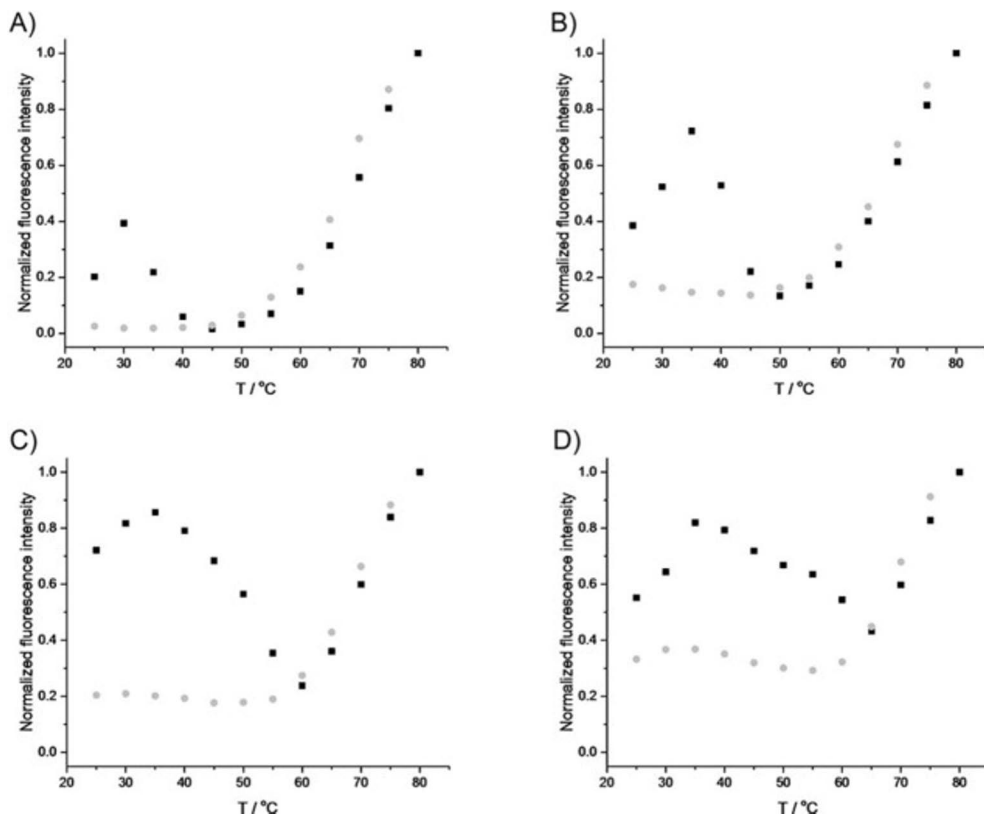
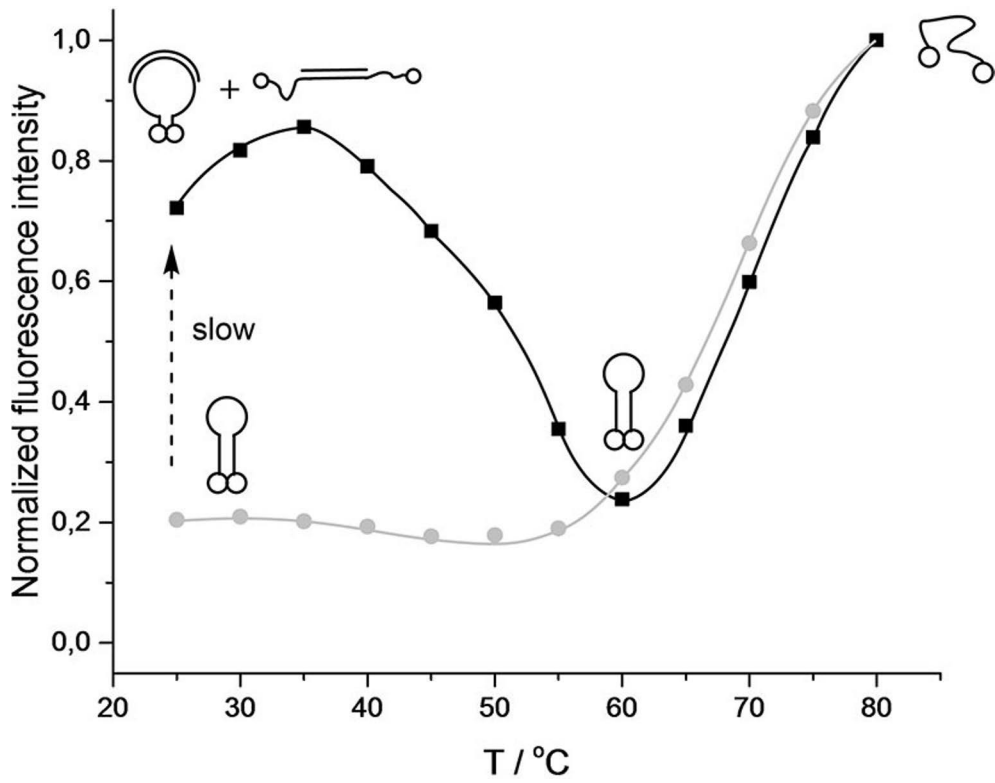


Figure 36. Normalized intensities of **B(F-Hg)•ON(Y)** as a function of temperature.

The lowest point of fluorescence is observed at different temperatures with each **ON(Y)**, at 45 °C for **A**, at 50 °C for **C**, at 60 °C for **G** and at 65 °C for **T**. These temperatures reflect the stability of duplexes with different **Y** in order of $T > G > C > A$, which is in line with the duplex studies on 11mer **ON(F-Hg)**. The fluorescence level in the turning point was above the initial fluorescence with **ON(C, G)** and even higher with **ON(T)**. This behavior might be caused by simultaneous denaturation of the duplex and hairpin forms or partial transition directly from the duplex to the random coil. In conclusion, discrimination of the canonical nucleobases is possible, especially when measurements are carried out at multiple temperatures. As an example, at 35 °C, the maximum fluorescence of **ON(A)** was ~20 % versus 70–85 % with the other **ON(Y)**s. At 45 °C, fluorescence intensities are ~0 % for **ON(A)**, 20 % for **ON(C)** and ~70 % for **ON(G)** and **ON(T)**. Finally, at 60 °C, fluorescence intensity of **ON(T)** is ~50 % compared to ~25 % with all other **ON(Y)**s.



Scheme 4. The behavior of beacon-target strand complex as a function of temperature.

4 Conclusions

As the first goal of the thesis work, fluorescent probes for screening suitable moieties for metal-mediated base pairing were developed. The method was based on a double hairpin forming oligonucleotide structure, where one nucleotide gap was left on structure neighboring a fluorescent nucleoside analog, pyrrolo C. Fluorescence of pyrrolo C is sensitive to changes in the nearby environment such as base stacking and base pairing. Four different probes were synthesized to allow the evaluation of nucleobase selectivity of molecule candidates. Previously studied dipicolinamide Pd^{II}-chelates, were used as model compounds to evaluate the binding in the oligonucleotide stage. Fluorescence titrations showed decreasing fluorescence intensities, indicating the binding of monomer most likely into the gap in the double-hairpin structure. Model compounds in the order of steric hindrance from the smallest to largest hindrance showed decreased fluorescence intensity as a function of chelate concentration. Fluorescence intensities at a wavelength of 520 nm were plotted as a function of chelate concentration, and association and dissociation constants were extracted. Compared to monomer studies, overall affinities were much higher with every Pd-chelate, underlining the effect of base stacking or hydrophobic effects. The probes proved to be sensitive to molecules binding into the gap, and they would be valuable for the screening of nucleobase analogs capable of metal-mediated base pairing.

As the second goal, fluorine-containing nucleoside analogs were synthesized to evaluate affinities towards each natural nucleobase and to collect information on the local environment of the metal-mediated base pair by ¹⁹F NMR. Two different nucleoside **F-Hg** and **F3-Hg** analogs were successfully synthesized, one where fluorine substituent is in the binding side of the nucleobase analog, and another where the trifluoromethane substituent is in the non-binding face, pointing towards the major groove. Compared to corresponding unmercurated counterparts, both mercurated oligonucleotides showed highly increased thermal stability of the double-helical oligonucleotide in order of T>G>C>A. Thermal stabilities were high when pairing with thymine or guanine and lower towards cytosine and adenine. Discrimination between different nucleobases based on UV-melting temperatures was surprisingly clear. Indeed, melting temperatures were clearly separated at least

by 6 °C in the case of **ON(F-Hg)** duplexes. Similarly, with **ON(F3-Hg)** duplexes, separation was clear except for a small difference between **ON(F3-Hg)•ON(T)** and **ON(F3-Hg)•ON(G)**. ¹⁹F NMR spectroscopy was used to evaluate local base-pairing properties. The mercuriation of the probe affected the ¹⁹F resonance signal of **ON(F-Hg)**, shifting it downfield ~20 ppm, whereas with **ON(F3-Hg)**, only broadening of the signal was observed. Discrimination of opposite nucleobases using ¹⁹F NMR was also possible with **ON(F-Hg)**, showing different shifts for every canonical nucleobase. Similarly, the separation of nucleobases with **ON(F3-Hg)** was possible, even though **ON(F3-Hg)•ON(C)** did not impact the ¹⁹F NMR shift at 25 °C and binding with **ON(A)** was obscure. Local melting temperatures were extracted from the results of temperature elevated ¹⁹F NMR measurements. The results were concerted with UV melting temperatures. Increased temperatures revealed overlapping signals of **ON(F3-Hg)** and **ON(F3-Hg)•ON(C)** and plausible intramolecular structures within **ON(F3-Hg)**.

Finally, the discrimination power of the **F-Hg** was applied to a well-known molecular beacon system. Hairpin-forming oligonucleotides were synthesized and mercurated, and fluorophore and quencher were post-synthetically coupled to the terminuses of the oligonucleotide to form the molecular beacon. Fluorescence measurements were conducted at 25 °C and at elevated temperatures to achieve fluorescence intensity versus temperature profiles. Fluorescence intensities increased differently with nucleobases in order of G>T>>C>A at room temperature, allowing robust discrimination between purines and pyrimidines. Temperature-elevated fluorescence results correspond to the transitions of the duplex to the hairpin, and the hairpin to a random coil structure. The heating and the cooling cycle showed different profiles, where the duplex formation was retarded in the latter case indicating the slow formation of the duplex. The discrimination of nucleobases increased at higher temperatures, and a few chosen temperatures allowed clear discrimination of all canonical nucleobases.

5 Experimental methods

5.1 General methods

Reagents for the syntheses were commercial products and were used as received. Oligonucleotides **ON(X)**, **ON(Y)** and **B(X)** were also purchased from commercial sources. All solvents used in organic synthesis and silica gel column chromatography were of reagent grade. Solvents used for moisture-sensitive reactions were dried using either 3Å or 4Å molecular sieves. Solvents for HPLC chromatography were analytical grade, and triethylamine used for TEAA buffer preparation was freshly distilled before use. Organic reactions were followed by thin-layer chromatography (Merck 60 silica gel F254 plates) and the plates were visualized by exposure to UV light (254 nm). For column chromatography, 230–400 mesh silica gel was used. NMR spectra were acquired by Bruker Avance III 500 and 600 MHz spectrometers. Mass spectra were recorded on a Bruker Daltonics micrOTOF-Q or a Thermo Fisher Scientific hybrid quadrupole Orbitrap mass spectrometer using direct infusion.

5.2 Oligonucleotide synthesis

All oligonucleotides except the commercially available ones were synthesized by an Applied Biosystems 3400 DNA/RNA synthesizer using conventional phosphoramidite chemistry. Coupling times for the modified nucleoside analogs were prolonged (300s). In the **ON(F)** and **ON(F3)** and **B(F)** oligonucleotide synthesis, instead of capping with Ac₂O, either the capping step was omitted, or acetic anhydride was replaced with phenoxyacetic anhydride to allow deprotection of the amino group by treatment with ammonia. Couplings were followed by monitoring the trityl response and proceeded with typical efficiency. Cleavage of the oligonucleotides from solid support was conducted by a treatment with aqueous ammonia at 55 °C. In the case of **B(F)**, an aqueous mixture of methylamine and ammonia (1:1, v/v) was used to get rid of the small amount of phenoxyacetyl protection, which had replaced trifluoroacetyl protection of the amino group of the modified bases **F** and **F3**. Purification of oligonucleotides was carried out by RP-HPLC using either a semi-preparative column (Clarity Oligo-RP, 250 mm × 10,0 mm, 5 μm) or an analytical column (Hypersil ODS C18, 250 mm × 4,6 mm, 5

μm). Oligonucleotides were eluted with a linear gradient from 5 to 35 or 40 % of acetonitrile in 100 mM triethylammonium acetate buffer (TEAA, pH = 7.0) over 25 min. The flow rate was 3.0 ml min^{-1} with the semi-preparative column and 1.0 ml min^{-1} with the analytical column. In the case of **P(X)**s, purifying was conducted using a linear gradient from 5–35% of MeCN over 15 min in 50 mM TEAA buffer. The column was thermostated to $70 \text{ }^\circ\text{C}$ to prevent the hybridization of these long oligonucleotides during purification. Detection wavelength was 350 nm (excitation wavelength of pyrrolo-C). **B(F)** and **B(F-Hg)** were also detected by excitation wavelengths of dabcyI (479 nm) and fluorescein (495 nm)

Oligonucleotides were mercurated by treatment with $\text{Hg}(\text{OAc})_2$. Different reaction conditions were used for different nucleoside analogs. Mercurated oligonucleotides were purified by RP-HPLC using an analytical column (Hypersil ODS C18, $250 \text{ mm} \times 4.6 \text{ mm}$, $5 \mu\text{m}$) eluting with a linear acetonitrile gradient (5–35 or 40 % over 25 min) in 100 mM TEAA buffer. In the case of **ON(F3-Hg)**, 0.1 M EDTA in 0.01M Tris-HCl solution was added just before purification to chelate the excess Hg^{2+} ions. Post-synthetic couplings for **B(F-Hg)** and **B(F)** were proceeded after mercuration to avoid mercuration of fluorophore and quencher. DabcyI-NHS ester was coupled to the primary amino group at the 3' terminus of the oligonucleotide, and fluorescein-DBCO was coupled to the azide group at the 5' terminus of the oligonucleotide. The crude products were purified by RP-HPLC using an analytical column (Hypersil ODS C18, $250 \text{ mm} \times 4.6 \text{ mm}$, $5 \mu\text{m}$) with a flow rate of 1.0 ml min^{-1} . After the dabcyI coupling reaction, the reaction mixture was eluted with a linear gradient of acetonitrile in TEAA buffer (5–95%), and after the fluorescein coupling reaction, with 10–50% MeCN in TEAA buffer.

5.3 UV melting temperature studies

UV melting curves were measured at 260 nm on a PerkinElmer Lambda 35 UV-vis spectrophotometer equipped with an integrated Peltier temperature controller unit. Measurements were carried out using 10 mm optical path length, and the temperature was changed at a rate of $0.5 \text{ }^\circ\text{C min}^{-1}$ from 10 to $80 \text{ }^\circ\text{C}$. Sample concentration was $2 \mu\text{M}$ in 10 mmol L^{-1} cacodylate buffer (pH = 7.0, $I = 0.10 \text{ M}$ adjusted with NaCl). The melting temperatures of oligonucleotides duplexes (T_m) were determined as inflection points of the UV melting curves.

5.4 ^{19}F NMR measurements

^{19}F NMR measurements were conducted using 5, 10, 20 or $90 \mu\text{M}$ **ON** concentration in 10 mM cacodylate buffer (pH = 7.0, $\text{D}_2\text{O-H}_2\text{O}$, 1:9, v/v, $I = 0.10 \text{ M}$ adjusted with NaCl). All samples were heated to $90 \text{ }^\circ\text{C}$ and allowed slowly to cool

to room temperature before measurements. Titration measurements were carried out at 25 °C and variable temperature measurements between 25–80 °C. Temperature intervals were 2.5 or 5 °C. The number of scans used was typically 2048 or 4096, but for single-stranded **ON(F-Hg)**, 20000 scans were used. For **ON(F-Hg)** duplexes, a 4-fluorobenzoic acid was used as an internal standard for the temperature-elevated experiments. For **ON(F3-Hg)**, relative areas of double-helical and single-stranded oligonucleotide were used instead. Mole fractions of duplexes versus temperature were plotted, and T_m values were determined as the inflection point of the curves thus obtained.

5.5 CD spectropolarimetric measurements

CD spectra were recorded on an Applied Photophysics Chirascan Spectropolarimeter with integrated Peltier temperature control unit between 220–320 nm over a temperature range of 10–90 °C at 2 or 10 °C intervals. The UV melting temperature and ^{19}F NMR samples were used as such.

5.6 Fluorescence measurements

Fluorescence emission spectra were recorded on a Cary Varian Eclipse fluorescence spectrometer or a Tecan Spark plate reader. The temperature was controlled by a Varian Cary single-cell Peltier accessory. The emission spectra were measured over a range of 500–600 or 420–480 nm, and the excitation wavelength was 495 or 350 nm. The same measurement parameters were used (PMT voltage 800 V, slit 1 nm, scan rate 120 nm/min, cuvette dimensions 10×10 mm) in all cases. Sample concentrations were 3.0 μM ON in 20 mM cacodylate buffer (pH = 7.4, $I(\text{NaClO}_4)$ = 50 mM) for **P(X)** measurements or 50 nM in 20 mM cacodylate buffer (pH = 7.4, 50 mM NaClO_4 and 2.5 mM $\text{Mg}(\text{ClO}_4)_2$) for **B(F-Hg)** measurements. All samples were heated to 90 °C and allowed slowly to cool to room temperature before measurements.

5.7 Enzymatic digestion

The site of the mercuration of **ON(F-Hg)** and **ON(F3-Hg)** was confirmed by enzymatic digestion with P1 nuclease enzyme. Oligonucleotides were treated with P1 nuclease (approximately 0.2 μg) for 6 hours at 37 °C in 25 mM TEAA or TRIS-HCl buffer. **ON(F-Hg)** was first desalted by HPLC, while **ON(F3-Hg)** was only diluted and filtered before analysis of the digestion fragments by ESI-TOF-MS.

Acknowledgements

This thesis is based on experimental work performed in the Laboratory of Organic Chemistry and Chemical Biology at the Department of Chemistry, University of Turku. The financial support from the University of Turku Graduate School: Doctoral Programme in Physical and Chemical Sciences (UTUGS:PCS), Finnish Cultural Foundation and Department of Chemistry are gratefully acknowledged.

First, I would like to express my deepest gratitude to my two awesome supervisors professor Pasi Virta and associate professor Tuomas Lönnberg for giving me the opportunity to pursue PhD research. I honestly think that I got the best pair of supervisors for this work, true experts of oligonucleotide chemistry. Pasi, a man with million ideas, and Tuomas, a man with million answers. You gave me enough freedom to do the research and to learn many things by trial and error, but supported me with your knowledge and encouragement when needed. I am also very grateful to my collaborators Antti Äärelä and Assi Lepistö for helping with the time-consuming synthesis for the paper IV.

I would like to thank professor Michal Hocek and professor Frank Seela for reviewing my thesis and giving valuable comments, and most of all professor Ronald Micura for accepting to be my opponent.

I want to thank all the people in the Bioorganic Chemistry Group, with whom I have had pleasure to work with during my studies: Aapo Aho, Antti Äärelä, Dr. Dattatraya Ukale, Dr. Emilia Kiuru, Dr Heidi Korhonen, Dr. Jianwei Li, Jinghui Yang, Lange Saleh, Dr. Lotta Granqvist, Dr Madhuri Hande, Mark Afari, Dr. Mikko Ora, Dr. Petja Rosenqvist, Petteri Lepistö, Dr. Sajal Maity, Dr. Satu Mikkola, Dr. Tharun Kotammagari, Tommi Österlund, Toni Laine, Vijay Gulumkar, Dr. Ville Tähtinen, Yonglei Lyu and Dr. Yu Cao. Thank you for your help and for providing a pleasant working atmosphere. Special thanks to Aapo, Antti, Petja and Ville for creating a relaxed atmosphere in the lab. It was a great joy and very therapeutic to laugh together at each other's mistakes and failures, and for the reality of organic chemistry when nothing works as planned in the paper. I would like to thank the Instrument Centre crew: Dr. Jani Rahkila for helping with NMR instruments, and Dr. Tuomas Karskela and Dr. Alex Dickens for helping with MS instruments, really appreciated it. Huge thanks to the support team of the department Kirsi Laaksonen,

Tiina Buss, Kari Loikas and Mauri Nauma for providing valuable help with chemicals, instruments and IT systems.

I would like to thank the people of our lunch group including Dr. Jorma Kim, Dr. Ville Eskonen, Dr. Pasi Salonen, Tapio Lempiäinen and Dr. Ville Tähtinen (in order of eating pace) and other unranked eaters Markus Saive and Dr. Milla Suominen. Despite the many questionable eating manners and slow eating pace, you're a big reason why time here was the most enjoyable. Also, the darts club including Petteri Vainikka, Pasi and Ville supported my mental health and provided time to relax. It was always a pleasure to play a few rounds with you guys and beat you completely. Outside the university I want to address thanks to my Eurajoki friends Hugo, Ossi, Petteri, Juha, Joni, Topias, Anniina, Enni, Elviira ja Maija. It has been always fun to see you and to spend time with you.

A big reason for completing this achievement is my family. First and foremost, I want to thank my father Vesa. Unfortunately, you are not here to share this milestone, but I am very grateful for your constant support during my life. You shared a passion for natural sciences and always encouraged me to study and reach for my dreams. Also huge thanks to my mom Anna-Liisa for your support and continuous messages "Miten väikkäri edistyy?" and my brother Antti for many science related discussions and help with mathematical problems.

Last, deepest thanks to Marianna, my dance partner for life, for your patience and continuous help and support during the PhD studies. Thank you for reading and revising my articles and thesis. I'm grateful that I had possibility to share the ups and downs of this journey with you.

Turku, February 2022



Asmo Aro-Heinilä

References

- [1] A. Sigel, H. Sigel, *Metal Ions in Biological Systems: Volume 32: Interactions of Metal Ions with Nucleotides: Nucleic Acids, and Their Constituents*, CRC Press, **1996**.
- [2] S. I. Nakano, M. Fujimoto, H. Hara, N. Sugimoto, *Nucleic Acids Res.* **1999**, *27*, 2957–2965.
- [3] J. D. Watson, F. H. C. Crick, *Nature* **1953**, *171*, 737–738.
- [4] S. Katz, *J. Am. Chem. Soc.* **1952**, *74*, 2238–2245.
- [5] C. A. Thomas, *J. Am. Chem. Soc.* **1954**, *76*, 6032–6034.
- [6] S. Katz, *BBA - Biochim. Biophys. Acta* **1963**, *68*, 240–253.
- [7] G. L. Eichhorn, J. J. Butzow, P. Clark, E. Tarien, *Biopolymers* **1967**, *5*, 283–296.
- [8] R. H. Jensen, N. Davidson, *Biopolymers* **1966**, *4*, 17–32.
- [9] G. L. Eichhorn, *Nature* **1962**, *194*, 474–475.
- [10] G. L. Eichhorn, P. Clark, *Proc. Natl. Acad. Sci. United States* **1965**, *53*, 586–593.
- [11] H. Sigel, *Chem. Soc. Rev.* **1993**, *22*, 255–267.
- [12] S. A. Kazakov, S. M. Hecht, *Nucleic Acid-Metal Ion Interactions*, **2006**.
- [13] J. Müller, *Metallomics* **2010**, *2*, 318–327.
- [14] R. B. Martin, *Acc. Chem. Res.* **1985**, *18*, 32–38.
- [15] W. Zhou, R. Saran, J. Liu, *Chem. Rev.* **2017**, *117*, 8272–8325.
- [16] R. K. O. Sigel, H. Sigel, *Acc. Chem. Res.* **2010**, *43*, 974–984.
- [17] R. M. Izatt, J. J. Christensen, J. H. Rytting, *Chem. Rev.* **1971**, *71*, 439–481.
- [18] R. M. K. Dale, E. Martin, D. C. Livingston, D. C. Ward, *Biochemistry* **1975**, *14*, 2447–2457.
- [19] D. W. Gruenwedel, *Biophys. Chem.* **1994**, *52*, 115–123.
- [20] D. W. Gruenwedel, *J. Inorg. Biochem.* **1994**, *56*, 201–212.
- [21] E. Buncel, C. Boone, H. Joly, *Inorganica Chim. Acta* **1986**, *125*, 167–172.
- [22] E. Buncel, C. Boone, H. Joly, R. Kumar, A. R. Norris, *J. Inorg. Biochem.* **1985**, *25*, 61–73.
- [23] P. R. Young, U. S. Nandi, N. R. Kallenbach, *Biochemistry* **1982**, *21*, 62–66.
- [24] D. W. Gruenwedel, M. K. Cruikshank, G. M. Smith, *J. Inorg. Biochem.* **1993**, *52*, 251–261.
- [25] Y. Tanaka, S. Oda, H. Yamaguchi, Y. Kondo, C. Kojima, A. Ono, *J. Am. Chem. Soc.* **2007**, *129*, 244–245.
- [26] S. Naskar, R. Guha, J. Müller, *Angew. Chemie - Int. Ed.* **2020**, *59*, 1397–1406.
- [27] B. Lippert, P. J. Sanz Miguel, *Acc. Chem. Res.* **2016**, *49*, 1537–1545.
- [28] P. Scharf, J. Müller, *Chempluschem* **2013**, *78*, 20–34.
- [29] Y. Tanaka, J. Kondo, V. Sychrovský, J. Šebera, T. Dairaku, H. Saneyoshi, H. Urata, H. Torigoe, A. Ono, *Chem. Commun.* **2015**, *51*, 17343–17360.
- [30] Y. Takezawa, M. Shionoya, *Acc. Chem. Res.* **2012**, *45*, 2066–2076.
- [31] A. Ono, H. Torigoe, Y. Tanaka, I. Okamoto, *Chem. Soc. Rev.* **2011**, *40*, 5855–5866.
- [32] B. Jash, J. Müller, *Chem. - A Eur. J.* **2017**, *23*, 17166–17178.
- [33] Y. Takezawa, J. Müller, M. Shionoya, *Chem. Lett.* **2017**, *46*, 622–633.
- [34] J. Müller, *Coord. Chem. Rev.* **2019**, *393*, 37–47.
- [35] J. Müller, *Eur. J. Inorg. Chem.* **2008**, 3749–3763.
- [36] G. H. Clever, M. Shionoya, *Coord. Chem. Rev.* **2010**, *254*, 2391–2402.

- [37] S. L. Müller, X. Zhou, P. Leonard, O. Korzhenko, C. Daniliuc, F. Seela, *Chem. - A Eur. J.* **2019**, *25*, 3077–3090.
- [38] H. Zhao, P. Leonard, X. Guo, H. Yang, F. Seela, *Chem. - A Eur. J.* **2017**, *23*, 5529–5540.
- [39] N. Santamaría-Díaz, J. M. Méndez-Arriaga, J. M. Salas, M. A. Galindo, *Angew. Chemie - Int. Ed.* **2016**, *55*, 6170–6174.
- [40] O. P. Schmidt, G. Mata, N. W. Luedtke, *J. Am. Chem. Soc.* **2016**, *138*, 14733–14739.
- [41] N. Sandmann, D. Defayay, A. Hepp, J. Müller, *J. Inorg. Biochem.* **2019**, *191*, 85–93.
- [42] P. Röthlisberger, F. Levi-Acobas, I. Sarac, P. Marlière, P. Herdewijn, M. Hollenstein, *J. Inorg. Biochem.* **2019**, *191*, 154–163.
- [43] A. Fujii, O. Nakagawa, Y. Kishimoto, T. Okuda, Y. Nakatsuji, N. Nozaki, Y. Kasahara, S. Obika, *Chem. - A Eur. J.* **2019**, *25*, 7443–7448.
- [44] L. D. Kosturko, C. Folzer, R. F. Stewart, *Biochemistry* **1974**, *13*, 3949–3952.
- [45] Y. Tanaka, A. Ono, *Dalt. Trans.* **2008**, 4965–4974.
- [46] T. Uchiyama, T. Miura, H. Takeuchi, T. Dairaku, T. Komuro, T. Kawamura, Y. Kondo, L. Benda, V. Sychrovský, P. Bouř, et al., *Nucleic Acids Res.* **2012**, *40*, 5766–5774.
- [47] H. Yamaguchi, J. Šebera, J. Kondo, S. Oda, T. Komuro, T. Kawamura, T. Dairaku, Y. Kondo, I. Okamoto, A. Ono, et al., *Nucleic Acids Res.* **2014**, *42*, 4094–4099.
- [48] J. Kondo, T. Yamada, C. Hirose, I. Okamoto, Y. Tanaka, A. Ono, *Angew. Chemie - Int. Ed.* **2014**, *53*, 2385–2388.
- [49] L. Benda, M. Straka, Y. Tanaka, V. Sychrovský, *Phys. Chem. Chem. Phys.* **2011**, *13*, 100–103.
- [50] L. Benda, M. Straka, V. Sychrovský, P. Bouř, Y. Tanaka, *J. Phys. Chem. A* **2012**, *116*, 8313–8320.
- [51] H. Miyachi, T. Matsui, Y. Shigeta, K. Hirao, *Phys. Chem. Chem. Phys.* **2010**, *12*, 909–917.
- [52] P. Pyykkö, *Chem. Rev.* **1997**, *97*, 597–636.
- [53] H. Schmidbaur, A. Schier, *Chem. Soc. Rev.* **2008**, *37*, 1931–1951.
- [54] P. Pyykkö, M. Straka, *Phys. Chem. Chem. Phys.* **2000**, *2*, 2489–2493.
- [55] H. Torigoe, A. Ono, T. Kozasa, *Chem. - A Eur. J.* **2010**, *16*, 13218–13225.
- [56] J. Šebera, J. Burda, M. Straka, A. Ono, C. Kojima, Y. Tanaka, V. Sychrovský, *Chem. - A Eur. J.* **2013**, *19*, 9884–9894.
- [57] A. Bagno, G. Saielli, *J. Am. Chem. Soc.* **2007**, *129*, 11360–11361.
- [58] H. Torigoe, Y. Miyakawa, A. Ono, T. Kozasa, *Thermochim. Acta* **2012**, *532*, 28–35.
- [59] H. Liu, C. Cai, P. Haruehanroengra, Q. Yao, Y. Chen, C. Yang, Q. Luo, B. Wu, J. Li, J. Ma, et al., *Nucleic Acids Res.* **2017**, *45*, 2910–2918.
- [60] S. Johannsen, S. Paulus, N. Düpre, J. Müller, R. K. O. Sigel, *J. Inorg. Biochem.* **2008**, *102*, 1141–1151.
- [61] T. Dairaku, K. Furuita, H. Sato, J. Šebera, D. Yamanaka, H. Otaki, S. Kikkawa, Y. Kondo, R. Katahira, F. Matthias Bickelhaupt, et al., *Chem. Commun.* **2015**, *51*, 8488–8491.
- [62] Y. Miyake, H. Togashi, M. Tashiro, H. Yamaguchi, S. Oda, M. Kudo, Y. Tanaka, Y. Kondo, R. Sawa, T. Fujimoto, et al., *J. Am. Chem. Soc.* **2006**, *128*, 2172–2173.
- [63] I. Okamoto, K. Iwamoto, Y. Watanabe, Y. Miyake, A. Ono, *Angew. Chemie - Int. Ed.* **2009**, *48*, 1648–1651.
- [64] A. Ono, H. Togashi, *Angew. Chemie - Int. Ed.* **2004**, *43*, 4300–4302.
- [65] N. A. Froeystein, E. Sletten, *J. Am. Chem. Soc.* **1994**, *116*, 3240–3250.
- [66] Y. Li, Y. L. Xia, Y. Jiang, X. P. Yan, *Electrophoresis* **2008**, *29*, 1173–1179.
- [67] A. A. Ouameur, S. Nafisi, N. Mohajerani, H. A. Tajmir-Riahi, *J. Biomol. Struct. Dyn.* **2003**, *20*, 561–565.
- [68] A. A. Ouameur, H. Arakawa, R. Ahmad, M. Naoui, H. A. Tajmir-Riahi, *DNA Cell Biol.* **2005**, *24*, 394–401.
- [69] H. Arakawa, R. Ahmad, M. Naoui, H.-A. Tajmir-Riahi, *J. Biol. Chem.* **2000**, *275*, 10150–10153.
- [70] K. Tanaka, Y. Yamada, M. Shionoya, *J. Am. Chem. Soc.* **2002**, *124*, 8802–8803.

- [71] A. Ono, S. Cao, H. Togashi, M. Tashiro, T. Fujimoto, T. MacHinami, S. Oda, Y. Miyake, I. Okamoto, Y. Tanaka, *Chem. Commun.* **2008**, 4825–4827.
- [72] H. Torigoe, Y. Miyakawa, A. Ono, T. Kozasa, *Nucleosides, Nucleotides and Nucleic Acids* **2011**, *30*, 149–167.
- [73] H. Torigoe, I. Okamoto, T. Dairaku, Y. Tanaka, A. Ono, T. Kozasa, *Biochimie* **2012**, *94*, 2431–2440.
- [74] J. Kondo, Y. Tada, T. Dairaku, H. Saneyoshi, I. Okamoto, Y. Tanaka, A. Ono, *Angew. Chemie - Int. Ed.* **2015**, *54*, 13323–13326.
- [75] T. Dairaku, K. Furuuta, H. Sato, J. Šebera, K. Nakashima, J. Kondo, D. Yamanaka, Y. Kondo, I. Okamoto, A. Ono, et al., *Chem. - A Eur. J.* **2016**, *22*, 13028–13031.
- [76] Y. Tanaka, C. Kojima, E. H. Morita, Y. Kasai, K. Yamasaki, A. Ono, M. Kainosho, K. Taira, *J. Am. Chem. Soc.* **2002**, *124*, 4595–4601.
- [77] T. J. Kistenmacher, M. Rossi, L. G. Marzilli, *Inorg. Chem.* **1979**, *18*, 240–244.
- [78] L. G. Marzi, T. J. Kistenmacher, M. Rossi, *J. Am. Chem. Soc.* **1977**, *99*, 2797–2798.
- [79] L. G. Marzilli, T. J. Kistenmacher, M. Rossi, *J. Am. Chem. Soc.* **2002**, *99*, 2797–2798.
- [80] D. E. DiRico, P. B. Keller, K. A. Hartman, *Nucleic Acids Res.* **1985**, *13*, 251–260.
- [81] Y. Wang, B. Q. Luan, Z. Yang, X. Zhang, B. Ritzo, K. Gates, L. Q. Gu, *Sci. Rep.* **2014**, *4*, 1–9.
- [82] Y. Wang, B. Ritzo, L. Q. Gu, *RSC Adv.* **2015**, *5*, 2655–2658.
- [83] S. Johannsen, N. Megger, D. Böhme, R. K. O. Sigel, J. Müller, *Nat. Chem.* **2010**, *2*, 229–234.
- [84] X. Guo, F. Seela, *Chem. - A Eur. J.* **2017**, *23*, 11776–11779.
- [85] M. Fortino, T. Marino, N. Russo, *J. Phys. Chem. A* **2015**, *119*, 5153–5157.
- [86] X. Chen, A. Karpenko, O. Lopez-Acevedo, *ACS Omega* **2017**, *2*, 7343–7348.
- [87] D. A. Megger, C. Fonseca Guerra, F. M. Bickelhaupt, J. Müller, *J. Inorg. Biochem.* **2011**, *105*, 1398–1404.
- [88] J. Kondo, Y. Tada, T. Dairaku, Y. Hattori, H. Saneyoshi, A. Ono, Y. Tanaka, *Nat. Chem.* **2017**, *9*, 956–960.
- [89] L. A. Espinosa Leal, A. Karpenko, S. Swasey, E. G. Gwinn, V. Rojas-Cervellera, C. Rovira, O. Lopez-Acevedo, *J. Phys. Chem. Lett.* **2015**, *6*, 4061–4066.
- [90] E. Stellwagen, Q. Dong, N. C. Stellwagen, *Biochemistry* **2007**, *46*, 2050.
- [91] J. Wu, F. Du, P. Zhang, I. A. Khan, J. Chen, Y. Liang, *J. Inorg. Biochem.* **2005**, *99*, 1145–1154.
- [92] K. Petrovec, B. J. Ravoo, J. Müller, *Chem. Commun.* **2012**, *48*, 11844–11846.
- [93] S. Kumbhar, S. Johannsen, R. K. O. Sigel, M. P. Waller, J. Müller, *J. Inorg. Biochem.* **2013**, *127*, 203–210.
- [94] A. Terrón, B. Moreno-Vachiano, A. Bauzá, A. García-Raso, J. J. Fiol, M. Barceló-Oliver, E. Molins, A. Frontera, *Chem. - A Eur. J.* **2017**, *23*, 2103–2108.
- [95] I. Onyido, A. R. Norris, E. Buncel, *Chem. Rev.* **2004**, *104*, 5911–5929.
- [96] D. Ukale, V. S. Shinde, T. Lönnberg, *Chem. - A Eur. J.* **2016**, *22*, 7917–7923.
- [97] A. Ono, H. Kanazawa, H. Ito, M. Goto, K. Nakamura, H. Saneyoshi, J. Kondo, *Angew. Chemie - Int. Ed.* **2019**, *58*, 16835–16838.
- [98] H. Urata, E. Yamaguchi, Y. Nakamura, S. I. Wada, *Chem. Commun.* **2011**, *47*, 941–943.
- [99] M. M. Rodriguez-Ramos, J. J. Wilker, *JBIC J. Biol. Inorg. Chem.* **2010**, *15*, 629–639.
- [100] C. Hofr, V. Brabec, *J. Biol. Chem.* **2001**, *276*, 9655–9661.
- [101] O. P. Schmidt, A. S. Benz, G. Mata, N. W. Luedtke, *Nucleic Acids Res.* **2018**, *46*, 6470–6479.
- [102] O. P. Schmidt, S. Jurt, S. Johannsen, A. Karimi, R. K. O. Sigel, N. W. Luedtke, *Nat. Commun.* **2019**, *10*, 1–11.
- [103] A. Fujii, O. Nakagawa, Y. Kishimoto, T. Okuda, Y. Nakatsuji, N. Nozaki, Y. Kasahara, S. Obika, *Chem. - A Eur. J.* **2019**, *25*, 7443–7448.
- [104] X. Guo, P. Leonard, S. A. Ingale, J. Liu, H. Mei, M. Sieg, F. Seela, *Chem. - A Eur. J.* **2018**, *24*, 8883–8892.
- [105] T. Funai, M. Aotani, R. Kiriu, J. Nakamura, Y. Miyazaki, O. Nakagawa, S. ichi Wada, H. Torigoe, A. Ono, H. Urata, *ChemBioChem* **2020**, *21*, 517–522.

- [106] H. Yang, F. Seela, *Chem. - A Eur. J.* **2016**, *22*, 13336–13346.
- [107] F. A. Polonius, J. Müller, *Angew. Chemie - Int. Ed.* **2007**, *46*, 5602–5604.
- [108] J. M. Méndez-Arriaga, C. R. Maldonado, J. A. Dobado, M. A. Galindo, *Chem. - A Eur. J.* **2018**, *24*, 4583–4589.
- [109] S. M. Swasey, L. E. Leal, O. Lopez-Acevedo, J. Pavlovich, E. G. Gwinn, *Sci. Rep.* **2015**, *5*, 1–9.
- [110] H. Liu, F. Shen, P. Haruehanroengra, Q. Yao, Y. Cheng, Y. Chen, C. Yang, J. Zhang, B. Wu, Q. Luo, et al., *Angew. Chemie - Int. Ed.* **2017**, *56*, 9430–9434.
- [111] K. Tanaka, G. H. Clever, Y. Takezawa, Y. Yamada, C. Kaul, M. Shionoya, T. Carell, *Nat. Nanotechnol.* **2006**, *1*, 190–194.
- [112] A. A. Tanpure, M. G. Pawar, S. G. Srivatsan, *Isr. J. Chem.* **2013**, *53*, 366–378.
- [113] L. M. Wilhelmsson, *Q. Rev. Biophys.* **2010**, *43*, 159–183.
- [114] S. G. Srivatsan, A. A. Sawant, *Pure Appl. Chem* **2011**, *83*, 213–232.
- [115] L. M. Wilhelmsson, P. Sandin, A. Holmen, B. Albinsson, P. Lincoln, B. Norden, *J. Phys. Chem. B* **2003**, *107*, 9094–9101.
- [116] M. E. Hawkins, *Cell Biochem. Biophys.* **2001**, *34*, 257–281.
- [117] E. L. Rachofsky, R. Osman, J. B. Ross, *Biochemistry* **2001**, *40*, 946–956.
- [118] D. C. Ward, E. Reich, L. Stryer, *J. Biol. Chem.* **1969**, *244*, 1228–1237.
- [119] G. Mata, O. P. Schmidt, N. W. Luedtke, *Chem. Commun.* **2016**, *52*, 4718–4721.
- [120] J. H. Han, S. Hirashima, S. Park, H. Sugiyama, *Chem. Commun.* **2019**, *55*, 10245–10248.
- [121] I. Schönrrath, V. B. Tsvetkov, T. S. Zatsepin, A. V. Aralov, J. Müller, *J. Biol. Inorg. Chem.* **2019**, *24*, 693–702.
- [122] K. S. Park, J. Y. Lee, H. G. Park, *Chem. Commun.* **2012**, *48*, 4549–4551.
- [123] H. Yang, H. Mei, F. Seela, *Chem. - A Eur. J.* **2015**, *21*, 10207–10219.
- [124] H. Mei, S. A. Ingale, F. Seela, *Chem. - A Eur. J.* **2014**, *20*, 16248–16257.
- [125] R. M. Izatt, J. J. Christensen, J. H. Rytting, *Chem. Rev.* **1972**, *72*, 720.
- [126] G. Mata, N. W. Luedtke, *J. Am. Chem. Soc.* **2015**, *137*, 699–707.
- [127] S. Manna, S. G. Srivatsan, *Org. Lett.* **2019**, *21*, 4646–4650.
- [128] F. Wojciechowski, R. H. E. Hudson, *J. Am. Chem. Soc.* **2008**, *130*, 12574–12575.
- [129] C. M. Zhang, C. Liu, T. Christian, H. Gamper, J. Rozenski, D. Pan, J. B. Randolph, E. Wickstrom, B. S. Cooperman, Y. M. Hou, *RNA* **2008**, *14*, 2245–2253.
- [130] C. Liu, C. T. Martin, *J. Mol. Biol.* **2001**, *308*, 465–475.
- [131] A. S. Wahba, A. Esmaeili, M. J. Damha, R. H. E. Hudson, *Nucleic Acids Res.* **2009**, *38*, 1048–1056.
- [132] X. Ming, F. Seela, *Chem. - A Eur. J.* **2012**, *18*, 9590–9600.
- [133] A. S. Wahba, F. Azizi, G. F. Deleavey, C. Brown, F. Robert, M. Carrier, A. Kalota, A. M. Gewirtz, J. Pelletier, R. H. E. Hudson, et al., *ACS Chem. Biol.* **2011**, *6*, 912–919.
- [134] H. Mei, I. Röhl, F. Seela, *J. Org. Chem.* **2013**, *78*, 9457–9463.
- [135] S. Taherpour, T. Lönnberg, *RSC Adv.* **2015**, *5*, 10837–10844.
- [136] F. Seela, V. R. Sirivolu, *Org. Biomol. Chem.* **2008**, *6*, 1674–1687.
- [137] D. U. Ukale, T. Lönnberg, *ChemBioChem* **2018**, *19*, 1096–1101.
- [138] R. M. K. Dale, E. Martin, D. C. Livingston, D. C. Ward, *Biochemistry* **1975**, *14*, 2447–2457.
- [139] R. M. K. Dale, D. C. Ward, *Biochemistry* **1975**, *14*, 2458–2469.
- [140] R. M. K. Dale, D. C. Livingston, D. C. Ward, *Proc. Natl. Acad. Sci. U. S. A.* **1973**, *70*, 2238–2242.
- [141] K. A. Kobe, T. F. Doumanp, *Ind. Eng. Chem.* **1941**, *33*, 170–176.
- [142] J. W. Haught, C. E. Garland, H. A. H. Pray, *J. Am. Chem. Soc.* **1931**, *53*, 2697–2700.
- [143] T. A. Henry, T. M. Sharp, *J. Chem. Soc.* **1930**, 2279–2289.
- [144] T. A. Henry, T. M. Sharp, *J. Chem. Soc.* **1924**, 2432–2440.
- [145] Y. Ogata, M. Tsuchida, *J. Org. Chem.* **1955**, *20*, 1644–1649.
- [146] B. J. R. Chipperfield, G. D. France, D. E. Webster, J. C. S. I. Perkin, **1972**.
- [147] S. Das, S. Sharma, H. B. Singh, R. J. Butcher, *Eur. J. Inorg. Chem.* **2018**, *2018*, 4093–4105.

- [148] D. U. Ukale, T. Lönnberg, *Angew. Chemie - Int. Ed.* **2018**, *57*, 16171–16175.
- [149] D. Ukale, S. Maity, M. Hande, T. Lönnberg, *Synlett* **2019**, *30*, 1733–1737.
- [150] D. U. Ukale, P. Tähtinen, T. Lönnberg, *Chem. – A Eur. J.* **2020**, *26*, 2164–2168.
- [151] G. Schwarzenbach, M. Schellenberg, *Helv. Chim. Acta* **1965**, *48*, 28–46.
- [152] R. A. Dengale, S. R. Thopate, T. Lönnberg, *Chempluschem* **2016**, *81*, 978–984.
- [153] O. Golubev, T. Lönnberg, H. Lönnberg, *J. Inorg. Biochem.* **2014**, *139*, 21–29.
- [154] S. Taherpour, O. Golubev, T. Lönnberg, *J. Org. Chem.* **2014**, *79*, 8990–8999.
- [155] O. Golubev, T. Lönnberg, H. Lönnberg, *Molecules* **2014**, *19*, 16976–16986.
- [156] S. Maity, M. Hande, T. Lönnberg, *ChemBioChem* **2020**, *21*, 2321–2328.
- [157] M. Hande, O. Saher, K. E. Lundin, C. I. Edvard Smith, R. Zain, T. Lönnberg, *Molecules* **2019**, *24*, DOI 10.3390/molecules24061180.
- [158] H. Räisälä, T. Lönnberg, *Chem. - A Eur. J.* **2019**, *25*, 4751–4756.
- [159] S. K. Maity, T. A. Lönnberg, *ACS Omega* **2019**, *4*, 18803–18808.
- [160] M. Hande, S. Maity, T. Lönnberg, *Int. J. Mol. Sci.* **2018**, *19*, DOI 10.3390/ijms19061588.
- [161] S. K. Maity, T. Lönnberg, *Chem. - A Eur. J.* **2018**, *24*, 1274–1277.
- [162] O. Golubev, G. Turc, T. Lönnberg, *J. Inorg. Biochem.* **2016**, *155*, 36–43.
- [163] S. Taherpour, O. Golubev, T. Lönnberg, *Inorganica Chim. Acta* **2016**, *452*, 43–49.
- [164] M. C. Lim, *J. Inorg. Nucl. Chem.* **1981**, *43*, 221–223.
- [165] S. H. Kim, R. B. Martin, *Inorganica Chim. Acta* **1984**, *91*, 11–18.
- [166] N. Cutillas, G. S. Yellol, C. De Haro, C. Vicente, V. Rodríguez, J. Ruiz, *Coord. Chem. Rev.* **2013**, *257*, 2784–2797.
- [167] A. Collado, M. Gómez-Gallego, M. A. Sierra, *European J. Org. Chem.* **2018**, *2018*, 1617–1623.
- [168] B. Jash, J. Müller, *Angew. Chemie - Int. Ed.* **2018**, *57*, 9524–9527.
- [169] B. Jash, J. Müller, *Chem. - A Eur. J.* **2018**, *24*, 10636–10640.
- [170] B. Jash, J. Müller, *J. Biol. Inorg. Chem.* **2020**, *25*, 647–654.
- [171] B. Jash, P. Scharf, N. Sandmann, C. Fonseca Guerra, D. A. Megger, J. Müller, *Chem. Sci.* **2017**, *8*, 1337–1343.
- [172] B. Jash, J. Neugebauer, J. Müller, *Inorganica Chim. Acta* **2016**, *452*, 181–187.
- [173] G. H. Clever, K. Polborn, T. Carell, *Angew. Chemie - Int. Ed.* **2005**, *44*, 7204–7208.
- [174] J. Müller, *Nature* **2006**, *444*, 698–698.
- [175] T. Funai, Y. Miyazaki, M. Aotani, E. Yamaguchi, O. Nakagawa, S. I. Wada, H. Torigoe, A. Ono, H. Urata, *Angew. Chemie - Int. Ed.* **2012**, *51*, 6464–6466.
- [176] M. Flamme, C. Figazzolo, G. Gasser, M. Hollenstein, *Metallomics* **2021**, *13*, 1–20.
- [177] H. Urata, E. Yamaguchi, T. Funai, Y. Matsumura, S. I. Wada, *Angew. Chemie - Int. Ed.* **2010**, *49*, 6516–6519.
- [178] K. M. Guckian, E. T. Kool, *Angew. Chemie Int. Ed. English* **1997**, *36*, 2825–2828.
- [179] K. M. Guckian, T. R. Krugh, E. T. Kool, *Nat. Struct. Biol.* **1998**, *5*, 954–959.
- [180] S. Moran, R. X. F. Ren, S. Rummey IV, E. T. Kool, *J. Am. Chem. Soc.* **1997**, *119*, 2056–2057.
- [181] C. Switzer, S. E. Moroney, S. A. Benner, *J. Am. Chem. Soc.* **2002**, *111*, 8322–8323.
- [182] J. A. Piccirilli, S. A. Benner, T. Krauch, S. E. Moroney, S. A. Benner, *Nat.* **1990**, *343*, 33–37.
- [183] C. Y. Switzer, S. E. Moroney, S. A. Benner, *Biochemistry* **2002**, *32*, 10489–10496.
- [184] J. Horlacher, M. Hottiger, V. N. Podust, U. Hübscher, S. A. Benner, *Proc. Natl. Acad. Sci.* **1995**, *92*, 6329–6333.
- [185] T. Funai, C. Tagawa, O. Nakagawa, S. I. Wada, A. Ono, H. Urata, *Chem. Commun.* **2020**, *56*, 12025–12028.
- [186] T. Carell, *Nature* **2011**, *469*, 45–46.
- [187] K. S. Park, C. Jung, H. G. Park, *Angew. Chemie* **2010**, *49*, 9951–9954.
- [188] T. Funai, J. Nakamura, Y. Miyazaki, R. Kiriu, O. Nakagawa, S. I. Wada, A. Ono, H. Urata, *Angew. Chemie - Int. Ed.* **2014**, *53*, 6624–6627.
- [189] A. M. Kretulskie, T. E. Spratt, *Biochemistry* **2006**, *45*, 3740–3746.

- [190] T. Tian, S. Peng, H. Xiao, Y. Long, B. Fu, X. Zhang, S. Guo, S. Wang, X. Zhou, S. Liu, et al., *Chem. Commun.* **2013**, 49, 10085–10087.
- [191] P. Röthlisberger, F. Levi-Acobas, I. Sarac, P. Marlière, P. Herdewijn, M. Hollenstein, *Org. Biomol. Chem.* **2017**, 15, 4449–4455.
- [192] M. Flamme, P. Röthlisberger, F. Levi-Acobas, M. Chawla, R. Oliva, L. Cavallo, G. Gasser, P. Marlière, P. Herdewijn, M. Hollenstein, *ACS Chem. Biol.* **2020**, 15, 2872–2884.
- [193] W. Saenger, *Principles of Nucleic Acid Structure*, Springer-Verlag, **1984**.
- [194] P. S. Pallan, P. Lubini, M. Bolli, M. Egli, *Nucleic Acids Res.* **2007**, 35, 6611–6624.
- [195] M. W. Germann, N. Zhou, J. H. van de Sande, H. J. Vogel, *Methods Enzymol.* **1995**, 261, 207–225.
- [196] D. Rentzeperis, L. A. Marky, K. Rippe, T. M. Jovin, *J. Am. Chem. Soc.* **1992**, 114, 5926–5928.
- [197] J. H. Van De Sande, N. B. Ramsing, M. W. Germann, W. Elhorst, B. W. Kalisch, E. V. Kitzing, R. T. Pon, R. C. Clegg, T. M. Jovin, *Science (80-.)*. **1988**, 241, 551–557.
- [198] V. R. Parvathy, S. R. Bhaumik, K. V. R. Chary, G. Govil, K. Liu, F. B. Howard, H. T. Miles, *Nucleic Acids Res.* **2002**, 30, 1500–1511.
- [199] C. Otto, G. A. Thomas, K. Rippe, T. M. Jovin, W. L. Peticolas, *Biochemistry* **1991**, 30, 3062–3069.
- [200] T. Ono, K. Yoshida, Y. Saotome, R. Sakabe, I. Okamoto, A. Ono, *Chem. Commun.* **2011**, 47, 1542–1544.
- [201] D. A. Megger, J. Müller, *Nucleosides, Nucleotides and Nucleic Acids* **2010**, 29, 27–38.
- [202] I. Sinha, C. Fonseca Guerra, J. Müller, *Angew. Chemie - Int. Ed.* **2015**, 54, 3603–3606.
- [203] D. A. Megger, C. Fonseca Guerra, J. Hoffmann, B. Brutschy, F. M. Bickelhaupt, J. Müller, *Chem. - A Eur. J.* **2011**, 17, 6533–6544.
- [204] T. Ihara, T. Ishii, N. Araki, A. W. Wilson, A. Jyo, *J. Am. Chem. Soc.* **2009**, 131, 3826–3827.
- [205] C. Paris, F. Geinguenaud, C. Gouyette, J. Liquier, J. Lacoste, *Biophys. J.* **2007**, 92, 2498–2506.
- [206] Y. Takezawa, W. Maeda, K. Tanaka, M. Shionoya, *Angew. Chemie - Int. Ed.* **2009**, 48, 1081–1084.
- [207] D. R. Jayarathna, H. D. Stout, C. Achim, *Inorg. Chem.* **2018**, 57, 6865–6872.
- [208] J. Choi, T. Majima, *Chem. Soc. Rev.* **2011**, 40, 5893–5909.
- [209] H. A. Day, C. Huguin, Z. A. E. Waller, *Chem. Commun.* **2013**, 49, 7696–7698.
- [210] M. A. S. Abdelhamid, L. Fábíán, C. J. Macdonald, M. R. Cheesman, A. J. Gates, Z. A. E. Waller, *Nucleic Acids Res.* **2018**, 46, 5886–5893.
- [211] D. M. Engelhard, J. Nowack, G. H. Clever, *Angew. Chemie - Int. Ed.* **2017**, 56, 11640–11644.
- [212] D. M. Engelhard, R. Pievo, G. H. Clever, *Angew. Chemie - Int. Ed.* **2013**, 52, 12843–12847.
- [213] N. M. Smith, S. Amrane, F. Rosu, V. Gabelica, J.-L. Mergny, *Chem. Commun.* **2012**, 48, 11464–11466.
- [214] K. Tanaka, M. Shionoya, *Coord. Chem. Rev.* **2007**, 251, 2732–2742.
- [215] T. Ehrenschrwender, W. Schmucker, C. Wellner, T. Augenstein, P. Carl, J. Harmer, F. Breher, H. A. Wagenknecht, *Chem. - A Eur. J.* **2013**, 19, 12547–12552.
- [216] S. Liu, G. H. Clever, Y. Takezawa, M. Kaneko, K. Tanaka, X. Guo, M. Shionoya, *Angew. Chemie - Int. Ed.* **2011**, 50, 8886–8890.
- [217] G. H. Clever, S. J. Reitmeier, T. Carell, O. Schiemann, *Angew. Chemie Int. Ed.* **2010**, 49, 4927–4929.
- [218] E. Toomey, J. Xu, S. Vecchioni, L. Rothschild, S. Wind, G. E. Fernandes, *J. Phys. Chem. C* **2016**, 120, 7804–7809.
- [219] T. Kentaro, T. Atsushi, K. Tatsuhisa, T. Namiki, S. Mitsuhiko, *Science (80-.)*. **2003**, 299, 1212–1213.
- [220] K. S. Park, C. Y. Lee, H. G. Park, *Chem. Commun.* **2016**, 52, 4868–4871.
- [221] A. D. Roses, *Nature* **2000**, 405, 857–865.
- [222] C. A. Stewart, R. Horton, R. J. N. Allock, J. L. Ashurst, A. M. Atrazhev, P. Coggill, I. Dunham, S. Forbes, K. Halls, J. M. M. Howson, et al., *Genome Res.* **2004**, 14, 1176–1187.

- [223] J. Wang, G. S.Y. Pang, S. S. Chong, C. G.L. Lee, *Curr. Drug Metab.* **2012**, *13*, 978–990.
- [224] M. Bachtiar, B. N. S. Ooi, J. Wang, Y. Jin, T. W. Tan, S. S. Chong, C. G. L. Lee, *Pharmacogenomics J.* **2019**, *19*, 516–527.
- [225] J. Chen, C. Shi, X. Y. Kang, X. T. Shen, X. Lao, H. Zheng, *Anal. Methods* **2020**, *12*, 884–893.
- [226] A. A. Martí, S. Jockusch, N. Stevens, J. Ju, N. J. Turro, *Acc. Chem. Res.* **2007**, *40*, 402–409.
- [227] D. M. Kolpashchikov, *Chem. Rev.* **2010**, *110*, 4709–4723.
- [228] D. M. Kolpashchikov, *Acc. Chem. Res.* **2019**, *52*, 1949–1956.
- [229] J. Zheng, R. Yang, M. Shi, C. Wu, X. Fang, Y. Li, J. Li, W. Tan, *Chem. Soc. Rev.* **2015**, *44*, 3036–3055.
- [230] S. Tyagi, D. P. Bratu, F. R. Kramer, *Nat. Biotechnol.* **1998**, *16*, 49–53.
- [231] S. Tyagi, F. R. Kramer, *Nat. Publ. Gr.* **1996**, *14*, 303–308.
- [232] P. Schofield, A. N. Pell, D. O. Krause, *Appl. Environ. Microbiol.* **1997**, *63*, 1143–1147.
- [233] A. Tsourkas, *Nucleic Acids Res.* **2002**, *30*, 4208–4215.
- [234] S. Tyagi, S. A. E. Marras, F. R. Kramer, *Nat. Biotechnol.* **2000**, *18*, 1191–1196.
- [235] J. J. Li, W. Tan, *Anal. Biochem.* **2003**, *312*, 251–254.
- [236] A. Tsourkas, M. A. Behlke, S. D. Rose, G. Bao, *Nucleic Acids Res.* **2003**, *31*, 1319–1330.
- [237] V. M. Farzan, M. L. Markelov, A. Y. Skoblov, G. A. Shipulin, T. S. Zatsepin, *Analyst* **2017**, *142*, 945–950.
- [238] H. Torigoe, A. Ono, T. Kozasa, *Transit. Met. Chem.* **2011**, *36*, 131–144.
- [239] R. Yang, J. Jin, L. Long, Y. Wang, H. Wang, W. Tan, *Chem. Commun.* **2009**, 322–324.
- [240] B. Jash, J. Müller, *Eur. J. Inorg. Chem.* **2017**, *2017*, 3857–3861.
- [241] Y. W. Lin, H. T. Ho, C. C. Huang, H. T. Chang, *Nucleic Acids Res.* **2008**, *36*, e123.
- [242] B. Lippert, M. Leng, in *Met. I*, Springer Berlin Heidelberg, Berlin, Heidelberg, **1999**, pp. 117–142.
- [243] D. Graber, H. Moroder, R. Micura, *J. Am. Chem. Soc.* **2008**, *130*, 17230–17231.
- [244] B. Puffer, C. Kreutz, U. Rieder, M. O. Ebert, R. Konrat, R. Micura, *Nucleic Acids Res.* **2009**, *37*, 7728–7740.
- [245] D. A. Berry, K. Y. Jung, D. S. Wise, A. D. Sercel, W. H. Pearson, H. Mackie, J. B. Randolph, R. L. Somers, *Tetrahedron Lett.* **2004**, *45*, 2457–2461.
- [246] R. A. Tinsley, *RNA* **2006**, *12*, 522–529.
- [247] M. Minuth, C. Richert, *Angew. Chemie - Int. Ed.* **2013**, *52*, 10874–10877.
- [248] N. Joubert, R. Pohl, B. Klepetářová, M. Hocek, *J. Org. Chem.* **2007**, *72*, 6797–6805.
- [249] A. Aro-Heinilä, T. Lönnberg, P. Virta, *Bioconjug. Chem.* **2019**, *30*, 2183–2190.
- [250] J.-L. Mergny, L. Lacroix, *Oligonucleotides* **2003**, *13*, 515–537.
- [251] W. H. Gmeiner, J. W. Lown, R. T. Pon, *J. Org. Chem.* **1991**, *56*, 3602–3608.
- [252] Y. Ito, M. Matsuo, T. Osawa, Y. Hari, *Chem. Pharm. Bull.* **2017**, *65*, 982–988.
- [253] I. Luyten, P. Herdewijn, *Eur. J. Med. Chem.* **1998**, *33*, 515–576.
- [254] S. R. Chaudhari, S. Mogurampelly, N. Suryaprakash, *J. Phys. Chem. B* **2013**, *117*, 1123–1129.
- [255] S. K. Mishra, N. Suryaprakash, *Molecules* **2017**, *22*, 423.
- [256] N. Bhuma, V. Tähtinen, P. Virta, *European J. Org. Chem.* **2018**, *2018*, 605–613.



**TURUN
YLIOPISTO**
UNIVERSITY
OF TURKU

ISBN 978-951-29-8783-2 (PRINT)
ISBN 978-951-8784-9 (PDF)
ISSN 0082-7002 (Print)
ISSN 2343-3175 (Online)